Fermilab Experimental
Proposal 570
Spokesperson: Irwin A. Pless
Massachusetts Institute of Technology
Laboratory for Nuclear Science
575 Technology Square, Room 408
Cambridge, Massachusetts 02139
Telephone: (617) 253-6081
8 September 1977

PROPOSAL FOR A STUDY OF PARTICLE PRODUCTION AND DYNAMICS FROM X = 0 TO X = 1 AND THE DEPENDENCE ON INCIDENT QUANTUM NUMBERS

Brown University
Providence, Rhode Island 02912

D. Brick
A. M. Shapiro
M. Widgoff

~~University of Cambridge~~
~~Cambridge, England~~

~~R. E. Ansorge~~
~~J. R. Carter~~
~~W. W. Neale~~
~~J. G. Rushbrooke~~
~~D. R. Ward~~
~~B. A. Webber~~
~~T. O. White~~

CERN
Geneva, Switzerland

F. Bruyant
L. Montanet

~~Fermilab~~
~~Batavia, Illinois 60510~~

~~D. Bogert~~
~~J. Wolfson~~

Illinois Institute of Technology
Chicago, Illinois 60616

R. A. Burnstein
H. A. Rubin

Indiana University
Bloomington, Indiana 47401

E. D. Alyea, Jr.

Johns Hopkins University
Baltimore, Maryland 21218

A. Pevsner
L. Bachman

Massachusetts Institute of Technology
Cambridge, Massachusetts 03139

F. Barreiro
O. Benary
E. S. Hafen
R. I. Hulsizer
V. Kistiakowsky
I. A. Pless
P. Trepagnier
R. K. Yamamoto

University of Mons
Mons, Belgium

P. Gillis
F. Grard
V. Henri
P. Herquet
J. Skura
R. Windmolders

University of Nijmegen Nijmegen, The Netherlands	F. Crijns W. Kittel W. Metzger C. Pols J. Schotanus R. Van de Walle
Oak Ridge National Laboratory Oak Ridge, Tennessee 37830	H. O. Cohn R. D. McCulloch
University of Padova Padova, Italy	A. Bettini M. Cresti M. Mazzucato L. Peruzzo P. Rossi G. Sartori S. Sartori L. Ventura A. Zudori G. Zumerle
University of Pavia Pavia, Italy	S. Alborghetti R. Attendoli E. Calligarich G. Cecchet R. Dolfini L. Mapelli S. Ratti
University of Rome Rome, Italy	L. Barone R. Bizzarri G. Bressi G. Ciapetti D. Dionisi P. F. Loverre D. Zanello L. Zanello
Rutgers University New Brunswick, New Jersey 08903	P. F. Jacques R. J. Plano T. L. Watts
Stevens Institute of Technology Hoboken, New Jersey 07030	E. B. Brucker E. L. Koller P. E. Stamer S. Taylor
Technion Haifa, Israel	S. Dado J. Goldberg S. Toaff

Tel-Aviv University
Tel-Aviv, Israel

G. Alexander
S. Dagan
J. Grunhaus
A. Levy
D. Lissauer
Y. Oren

University of Tennessee
Knoxville, Tennessee 37916

W. M. Bugg
G. T. Condo
T. Handler
E. L. Hart

University of Trieste
Trieste, Italy

E. Castelli
C. Omero
P. Poropat
M. Sessa

Weizmann Institute of Science
Rehovot, Israel

Y. Eisenberg
B. Haber
D. Hochman
U. Karshon
E. E. Ronat
A. Shapira
R. Yaari
G. Yekutieli

Yale University
New Haven, Connecticut 06520

H. Kraybill
D. Ljung
T. Ludlam
H. D. Taft

Summary

We propose a study of the production of π^0, $\pi^{\pm}$, Λ^0, K^0, K^+, K^-, p, $\bar{p}$ in multiparticle final states, with tagged positive and negative beams of 200 GeV/c particles incident on protons. In addition, a new phenomenon in which a large amount of electromagnetic energy is emitted in the forward direction will be investigated. Evidence for this phenomenon was observed in Experiment 154.

This experiment is to be carried out with the advanced hybrid spectrometer system, with the bubble chamber as target, and with the downstream portion of the spectrometer including two powerful new tools, an ISIS system to identify charged particles and a forward gamma detector (FGD) to study the production of electromagnetic energy. The beam momentum and the ISIS design are such as to give high efficiency for identification of particles produced in the central region of x and y, where most particle production takes place. The two instruments will allow us to study for the first time correlations among neutral particles and between neutral and charged particles, and also questions of local conservation of transverse momentum and of quantum numbers.

We wish to achieve a positive beam with 10% K^+, the remainder being equally divided between p and π^+, and a negative beam composition of 20% $\bar{p}$, the remainder π^-. We propose 1×10^6 pictures in each of the two beams. This will allow us to study the details of the production processes as a function of the quantum numbers of the projectile particle under identical experimental conditions, with good statistics.

Introduction

We propose a comprehensive experiment to examine the dynamics of hadronic production utilizing the full analyzing power of the advanced 30-inch hybrid bubble chamber system for a variety of incident beams with downstream instrumentation for the identification of heavy charged particles (ISIS) and for the measurement of electromagnetic decays of forward-going neutral particles (Forward Gamma Detector).

Presently available data, consisting primarily of momentum distributions of charged secondary pions, have revealed a pattern in which short-range phenomena characteristic of asymptotic models coexist with strong fragmentation effects. At Fermilab energies the nature of the beam and target particles is reflected in the major fraction of particle production; not only the diffraction component, but also the high-multiplicity component and the (presumably) deeply inelastic production of J/ψ show a marked dependence on the quantum numbers of the incident channel. In the latter cases the observed effects may be a direct consequence of the kinematic distribution of quarks among the incident particles.

In order to extract new information regarding these features of the strong interaction mechanism, we propose an experiment with the full retinue of charged hadron beams available to the 30-inch chamber for the widest spectrum of incident channel quantum numbers, employing the ISIS detector to isolate heavy charged particles (K's and protons) in the final state, and the forward gamma detector for a more nearly complete accounting of the total energy into pions. These new capabilities will allow a much more complete examination of the generalized charge structure of events than has been possible in the past and in turn will require longer exposures. The physics topics will emphasize multiparticle production in the central region. The parameters of the experiment have been chosen to optimize the effectiveness of the ISIS detector in this range of center-of-mass momenta.

We request 1.0×10^6 pictures with a tagged negative beam and 1.0×10^6 pictures with a tagged positive beam, both at 200 GeV/c momentum. The positive beam will be composed of approximately 10% K^+, with remainder consisting of equal numbers of π^+ and p, while the negative beam will consist of about 20% $\bar{p}$ and 80% π^-. The use of these tagged beams will enable us to study the dependence of the interaction characteristics on the quantum numbers of the incident particle with minimum systematic errors and minimum set-up time. These areas of investigation will include single particle distributions for identified charged and neutral particles, multiplicity studies, and correlation studies, including the question of neutral-charged particle correlations about which little is known. The ω, η^0, $\rho^\pm$ and other resonances which decay into π^0's will now be studied in detail and their connection with clusters will be clarified. Also, local conservation of transverse momentum, strangeness and other quantum numbers will be checked with much more complete information. The forward gamma detector will also permit the investigation of the large amounts of forward going neutral energy observed in low multiplicity events, a new phenomenon which has been observed at Fermilab energies (E154). Four-constraint fits will be extended to events with one, two, and possibly three π^0's, and events with charged K's. In addition, we will engage in more speculative searches: a search for a possibly new phenomenon where both projectile and target end up near x=0; a search for new particles that decay into one or more heavy particles and several pions; a study of four-constraint physics; and a study of pairs of identical heavy particles to compare with the Bose-like behavior seen in identical-pion pairs.

Physics of the Experiment

The primary object of this experiment is the study of the production characteristics of particles and resonances in interactions with target protons, and the dependence of these production characteristics on the quantum numbers of the projectile particle.

We will be able to detect, identify and measure γ, π^0, $\pi^{\pm}$, K^0, $K^{\pm}$, p, $\bar{p}$, Λ^0, with sufficient accuracy to isolate and study the resonances they form.

Figure 1 shows the main features of the downstream spectrometer system which makes these studies possible.

Specific physics topics we will explore are:

1. Study of π^0 Production

In order to study π^0 production, we have built a lead glass shower detector-hodoscope with good energy and spatial resolution. A prototype has been extensively tested and used in E299; the result of these tests as well as a description of the full scale forward gamma detector (FGD) are included in Appendix I.

With this device we will be able to reconstruct π^0 and η^0 mesons and to distinguish up to six gamma rays ($3\pi^0$). Thus, we shall be able to perform a study of the two, four, six, and eight charged prong topologies where one, two and possibly three π^0's are observed, allowing four constraint (4C) fits. There have been no previous studies of these channels. This experiment, together with E154 and E299, also will permit high statistics studies of the four, six, and eight charged prong topologies with no neutral particles, and comparison with the corresponding channels with π^0 mesons should prove extremely fruitful. For example, our E154 study of the four charged-particle 4C sample[1] has shown that more than 92% of the cross section is due to beam and target diffraction dissociation. $\rho^0\pi^-$ events make an important contribution to the beam dissociation cross section in the A_1 and A_2 mass region and there is some evidence for a contribution from $f^0\pi^-$. Higher statistics should permit a resolution of the latter question as well as yielding a better understanding of the three-pion system in all invariant mass regions. In this experiment it will be possible also to obtain results for the four charged-prong, one π^0 channel at a similar level of statistics.

This experiment will also permit an inclusive study of π^0 production as a function of rapidity in the forward hemisphere. Such a study is extremely important in order to verify the previous evidence for the existence of clusters and to determine whether they consist mainly of two pions ("ρ" like) or three pions ("ω" like) and indeed whether clusters are the well-known resonances. Rigorous tests of local transverse momentum conservation will be carried out, whereas with charged-particle rapidity studies only, definitive tests of this sort are not possible.

Another facet of this experiment is the examination of the forward going neutral energy associated with the production of two charged particles. Our interest in this phenomenon stems from our observations in Exp. 154 ($\pi^- p$ at 150 GeV/c). For this experiment we had in our PWC system a crude gamma ray detector consisting of a two-radiation length thick piece of lead followed by three PWC planes. This counter permitted a rough measurement of the intensity of electromagnetic energy incident on the lead converter in each event. In the two-prong inelastic data we found a significant class of events in which most of the incident momentum went into the forward electromagnetic shower [refer to proposal for E393, Appendix III]. Monte Carlo calculations emulating known diffractive processes were not able to reproduce the observed results. We believe that these observations indicate a new phenomenon occurring in the 2-prong events, and that a detailed study of the electromagnetic energy associated with the two-prong events is required. Data from the forward gamma detector in the experiment proposed here will allow us to determine π^0 four-vectors and form relevant invariant mass distributions. If there are narrow structures in this final state, we will be able to detect them. In any event, we will be able to determine the character of this final state in an exclusive manner and determine if there are any new physical phenomena involved.

2. Multi-Particle Production with Charged Particle Identification

In order to identify charged particles which leave the bubble chamber in the forward direction, we will use the Fermilab ISIS system which is described in Appendix II. This is the relativistic rise particle identifier which was first discussed in the September 1975 Bubble Chamber Symposium[2] and which was further specified during a workshop held at Fermilab in May 1976[3]. This device is designed to have good acceptance for particles produced in the central region, near x=0, where most particle production occurs, and is essential to the study of the following questions.

a) Single Particle Inclusive Distributions

K^+, K^-, p, $\bar{p}$ production as functions of t, x and y will be measured. These will be the first complete data of this kind at these energies. K^0 and Λ^0 distributions will also be studied. It is important to determine where in the rapidity chain these heavy particles tend to lie - are they produced in association with either the target or projectile, or does production simply peak in the central region. By comparison of measurements made with the different projectile particles under identical circumstances, it will be possible to see over what range of rapidity the nature of the incident particle affects the production of these particles.

Comparison of $K^{\pm}K^{\mp}$, $K^{\pm}\Lambda^0$, $K^{\pm}K^0$ production for different incident beam particles will allow a search for a strangeness = 0 plateau. The existence of such a plateau would be interesting, in view of the fact that no charge = 0 plateau exists in π^-p interactions.[4]

b) Correlations

Rapidity correlations between pairs of charged pions have yielded much information leading to our current understanding of the nature of multiparticle production. The observed short-range correlations have stimulated great interest in the question of cluster formation and the concept of local quantum number conservation near y = 0[5].

Specific identification of $K^{\pm}$ and $p^{\pm}$ with good efficiency in the central region will greatly extend the correlation information and allow a study of baryon number and strangeness compensation in addition to that of electric charge. Also of prime interest would be the study of π^0 creation near the central rapidity region. Measurements of the π^0 mesons will permit the more complete study of local conservation of transverse momentum. To date, there is very little information regarding the correlation between neutral and charged pions. The distribution of π^0 production and correlations between π^0's have yet to be studied. In addition, identical particle effects which have been studied for charged pion pairs will be investigated for K^+K^+, K^-K^- and $\pi^0\pi^0$ pairs.

This experiment, by virtue of π^0 detection and charged kaon identification, should provide a rich variety of new opportunities for the study of correlations in effective mass of multiparticle systems (e.g., resonance production), and the study of multiparticle correlations treating resonance states as single prompt particles.

c) Braking Collisions

There appears to be some experimental evidence from the ISR that a cross section approaching one millibarn exists for a process where both incident protons stop in the center-of-mass.[6] The number and distribution of the associated particles (presumably mostly pions) is of great interest. No data exist on these questions. There are two speculations about the origin of this phenomenon. The first is that the two protons stop due to a mutually catastrophic bremsstrahlung of pions. This would manifest itself by the emission of two large jets of pions, forward and backward. The second speculation is that the protons stop due to a coherent central collision of the fundamental constituents (quarks, partons), and this type of reaction might yield an isotropic distribution of pions. Establishing that the ISR result is real and measuring the distributions of the outgoing particles would establish a totally new phenomenon which should yield fundamental information on elementary hadronic properties.

d) Resonance Production

The capability for detecting charged K mesons as well as neutral strange particle decays over momentum ranges which encompass the central region, coupled with the π^0 detection capability of the forward gamma detector, will provide the means for a systematic study of the following matrix of inclusive reactions:

$$\begin{bmatrix} \pi^{\pm} \\ K^{+} \\ p^{\pm} \end{bmatrix} + p \longrightarrow \begin{bmatrix} \eta \\ \rho^{\pm}, \rho^{0} \\ K^{*\pm}, K^{*0} \\ \Phi^{0} \\ \omega^{0} \\ \Delta, y^{*} \end{bmatrix} + \text{anything}$$

The initial analysis goal will be to determine the cross sections as functions of the kinematic variables x, y, t, etc. The contribution of resonances, especially the meson resonances, to the whole of multiparticle production is important in its own right, and has obvious implications for the understanding of clustering phenomena. Of the reactions listed above, only those leading to ρ^0 and Δ^{++} have been studied in any detail in collisions at Fermilab energies.

In terms of the generalized charge structure of events, we expect that the kinematic distribution of resonance states will be far more sensitive to the nature of reaction mechanisms than is the distribution of their decay products. The proposed experiment will afford a broad investigation of the kinematic behavior of identifiable resonances in terms of the resonance quantum numbers and the quantum numbers of the incident beam. Existing data for the production of ρ, K*, and J/ψ show a marked dependence on the nature of the incident particles, with central production observed in pp or p-nucleus collisions and forward, beam-like production observed in collisions of mesons with nucleons. This could be the result of the usual hierarchy of coupling

strengths for the various quantum number exchanges in a multiperipheral mechanism, or it could result from the intrinsic constituent structure of beam and target. Although the absolute cross sections for ρ^0 production are nearly equal for π meson and proton beams incident[7], the relative cross sections for J/ψ production are very different[8], and recent measurements of J/ψ induced by meson, proton and anti-proton beams at 40 GeV/c[9] point to a significant contribution from valence quark annihilation. Of particular interest in this context will be a systematic examination of the production of the low-mass meson resonances ρ, ω, Φ, K^* for π, K, p and $\bar{p}$ beams incident.

Data of this sort will be important as well for the emerging phenomenology of hadronic interactions via hard collisions of constituents. While such models emphasize the high-P_T regime beyond the reach of bubble chamber data, it is clear that more complete and precise data on the resonance structure of "normal" events will be of great value in the interpretation of experiments which probe the structure of large transverse momentum phenomena.

e) $\bar{p}p$ Annihilation

Our primary interest in an enriched $\bar{p}$ component of the negative beam arises from our desire to have the widest possible spectrum of incident channel quantum numbers (or valence quark configurations) available for a systematic study of the dynamics of particle production. The importance of a $\bar{p}$ beam in the context of such a program is discussed in the subsections above.

In addition, it would be of great interest to measure the total $\bar{p}p$ annihilation cross section. An attempt will be made to do so in this experiment in spite of the major difficulties involved in estimating the cross section for $\bar{p}p \rightarrow \bar{n}n + X$. While this cross section can be estimated in principle by assuming factorization and applying this assumption to measurements of the channels $\bar{p}p \rightarrow \bar{n}p + X$, $\bar{p}p \rightarrow \bar{p}n + X$, and $\bar{p}p \rightarrow \bar{p}p + X$, meaningful results can only be obtained if the factorization assumption

is reliable to considerably better than 5%. This is because the interesting difference $\sigma_T(\bar{p}p) - \sigma_T(pp)$ is expected to be of the order of 2mb[10], which is 5% of either cross section and the correction for $\bar{n}n$ production must be known considerably better than the difference itself. It is obvious that inefficiencies in measuring any of the three cross sections will reduce the reliability of the estimate of the annihilation cross section. It is clearly important, however, to establish the measurable cross sections as accurately as possible.

Beam and Experimental Apparatus

As has been discussed, the experiment will require the Fermilab hybrid 30-inch bubble chamber - PWC spectrometer, with the addition of an ISIS system and the FGD in the downstream portion of the spectrometer, as shown in Fig. 1. These devices are described in detail in Appendices I and II.

A prototype of the FGD has been intensively and successfully tested in use and its performance is described in Appendix I. Results of these measurements show that we are able to locate the shower centers within a standard deviation of 1.4 mm, and to measure the shower energy with a resolution $\Delta E/E = .27/\sqrt{E}$ where ΔE is the full width at half maximum of the measured energy distribution for incident electrons of nominal energy E. The prototype has been tested with incident electrons of energies ranging from 26 GeV/c to 100 GeV/c. The angular acceptance of the full FGD is 125 mr.

The full scale FGD is now being assembled at Fermilab.

The Fermilab ISIS is well matched to the spectrum of charged particles leaving the bubble chamber, since the beginning of the relativistic rise region for protons is at about 5 GeV/c and that for kaons and pions is lower. The acceptance of the Fermilab ISIS is also quite well matched to the angular spread of the particles leaving the bubble chamber (see Appendix II).

As discussed in Appendix II, the resolution of the Fermilab ISIS decreases above 10 GeV/c with increasing momentum and kaon identification becomes poor above 40 GeV/c. Thus the momentum resolution of the hybrid system ($\Delta p/p = 0.06p\%/GeV/c$) is sufficient so as not to be a limitation on the Fermilab ISIS over the momentum range where it has good resolution, particle identification in this device requiring momenta measured to better than 10%.

A primary interest of this experiment is the study of reactions which yield protons nearly at rest in the center of mass and mesons in the central region of rapidity. As can be seen in Figs. 2 and 3, the corresponding laboratory momenta of these secondary particles fall in a region where the resolution of the Fermilab ISIS is very good.

The first module of the Fermilab ISIS (ISIS-1) is being assembled. After preliminary testing it will be shipped to Fermilab the beginning of October where it is scheduled for a beam test starting October 27.

Preliminary studies have shown that, with an accelerator beam of 400 GeV/c, the desired ratio of 10% K^+ is achievable in the 200 GeV/c positive beam, with the remainder approximately equally divided between π^+ and p. Theoretical calculations indicate that one should be able to achieve the desired $\bar{p}/\pi^-$ ratio of 1/4 in the negative 200 GeV/c beam. Beam tests will have to be made to determine the actual beam compositions. With these beams, enriched in K^+ and $\bar{p}$, an intensity of about 10^{10} particles per ping will yield the desired 8 tracks per picture.

Equipment Costs

New equipment will be required for this experiment. All electronic items shown in fig. 1, i.e., P1, D1, I1, D2, I2, D3, and FGD, will be used for the first time in this experiment. The following list describes these items, their cost and who will furnish them.

Description	Cost	Responsibility
P1 - 3,500 wire PWC system	$125,000 85,000	Universities Fermilab
D1 - 80 channel Drift Chamber system	25,530 45,000	Fermilab Universities
I1 - ISIS 1	40,000 225,000	Fermilab Universities
D2 - 80 channel Drift Chamber system	25,530 49,000	Fermilab Universities
I2 - ISIS 2	146,200 187,000	Fermilab Universities
D3 - 80 channel Drift Chamber system	70,530	Universities
FGD - Forward Gamma Ray Detector	250,000 100,000	Universities Fermilab
Computer		Fermilab

As noted before, the FGD is complete and hence requires no new money. ISIS I is actually under construction and test and does not require new money. ISIS II, the PWC and Drift Chamber systems do require new money. Note that the above figures are approximate. Detailed figures will be furnished and negotiated for the agreement.

REFERENCES

1) "The Exclusive Channel $\pi^- \pi^- \pi^+ p$ in $\pi^- p$ Interactions at 147 GeV/c", D. Fong et al., Nuovo Cim. 34A, 659 (1976).

2) Bubble Chamber Symposium, September 1975. Reported by T. Groves, NALREP, December 1975.

3) Particle Identifiers for Hadron Physics, May 1976. Reported by V. Kistiakowsky, NALREP, July 1976.

4) "Evidence for Charged Cluster Emission in 147 GeV/c $\pi^- p$ Collisions", D. Fong et al., Phys. Lett. 61B, 99 (1976).

5) "Local Quantum-Number Compensation in Multiple Production", C. Quigg, Phys. Rev. D12, 834 (1975).

6) M. Jacob, private communication.

7) "Inclusive and Semi-Inclusive ρ^0 Production in $\pi^- p$ Interaction at 147 GeV/c", D. Fong et al., Phys. Lett, 60B, 124 (1975); "ρ^0 Production in 205 GeV/c pp Production", R. Singer et al., Phys. Lett. 60B, 385 (1976).

8) "Measurement of ψ (3.1) Meson Production by Pions and Protons", G. J. Blanar et al., Phys. Rev. Lett. 35, 346 (1975); "Production of Muon Pairs by 150 GeV/c π^+ and Protons", K. J. Anderson et al., Phys. Rev. Lett. 36, 237 (1976).

9) "Experimental Comparison of j/ψ Production by $\pi^\pm$, $K^\pm$, p and $\bar{p}$ Beams at 39.5 GeV/c", M. J. Corden et al., Phys. Lett. 68B, 96, (1977).

10) "Total Cross Sections of p and $\bar{p}$ on Protons and Deuterons Between 50 and 200 GeV/c", A. S. Carroll et al., Phys. Rev. Lett. 33, 928 (1974).

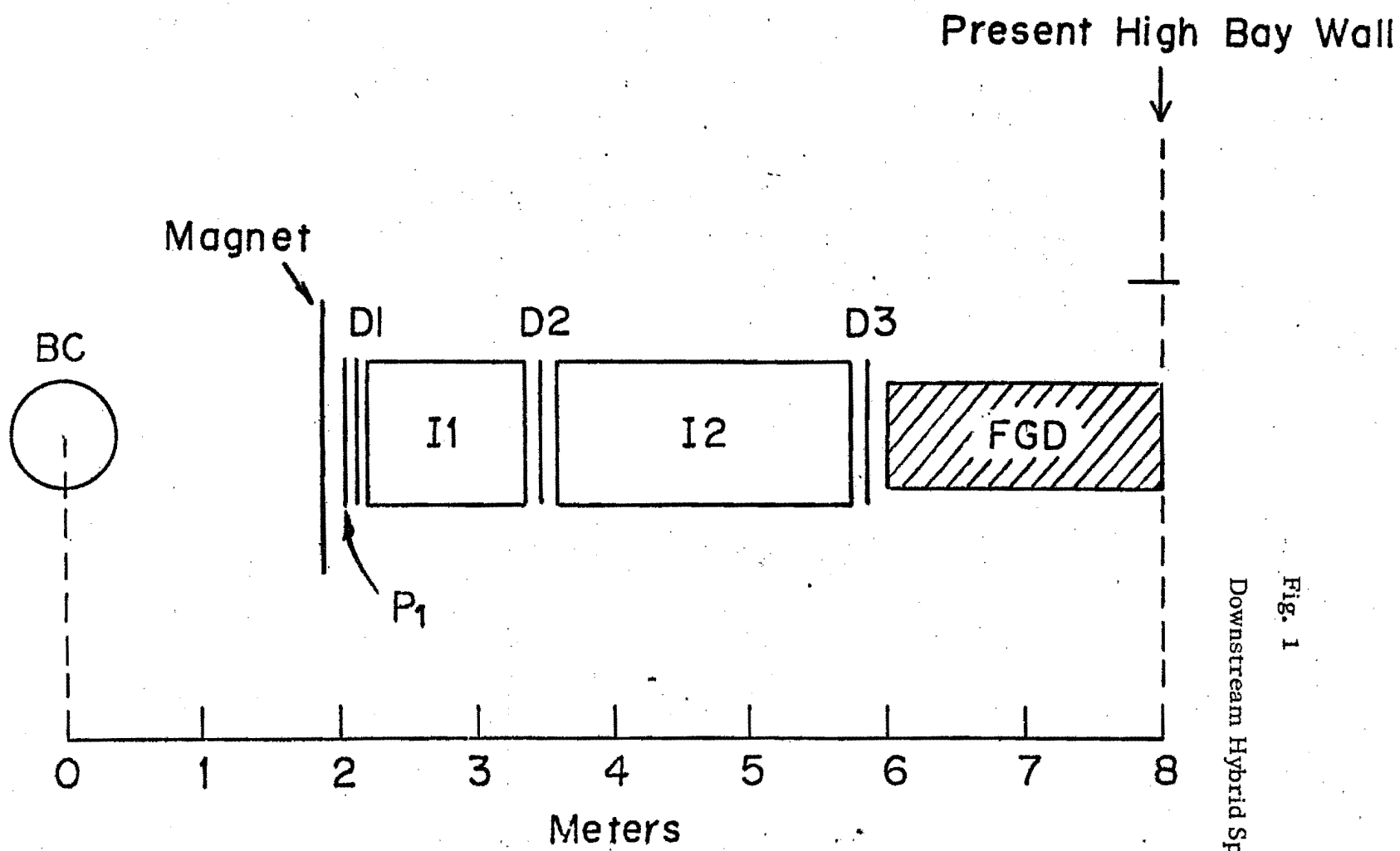

Fig. 1

Downstream Hybrid Spectrometer System

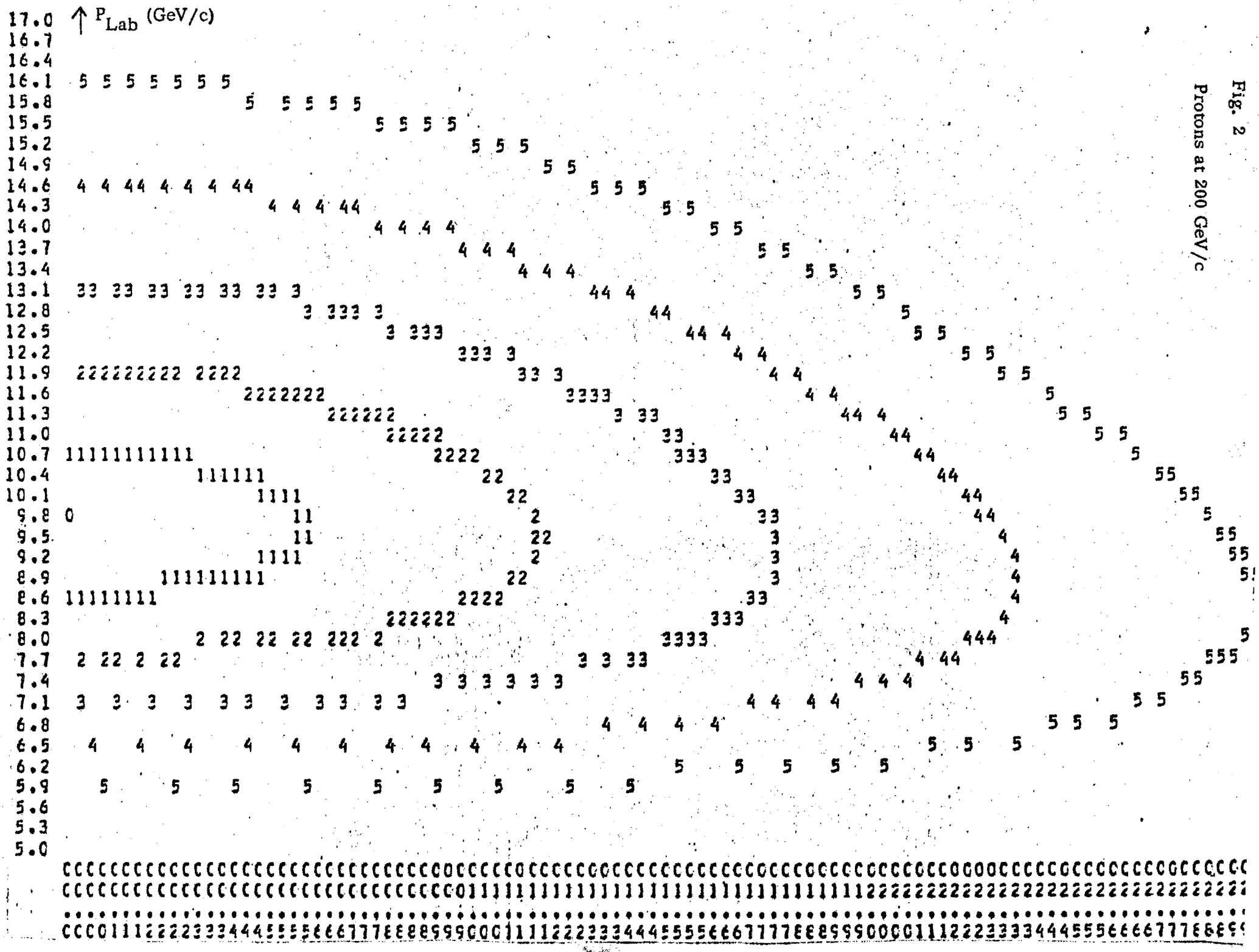

Fig. 2

Protons at 200 GeV/c

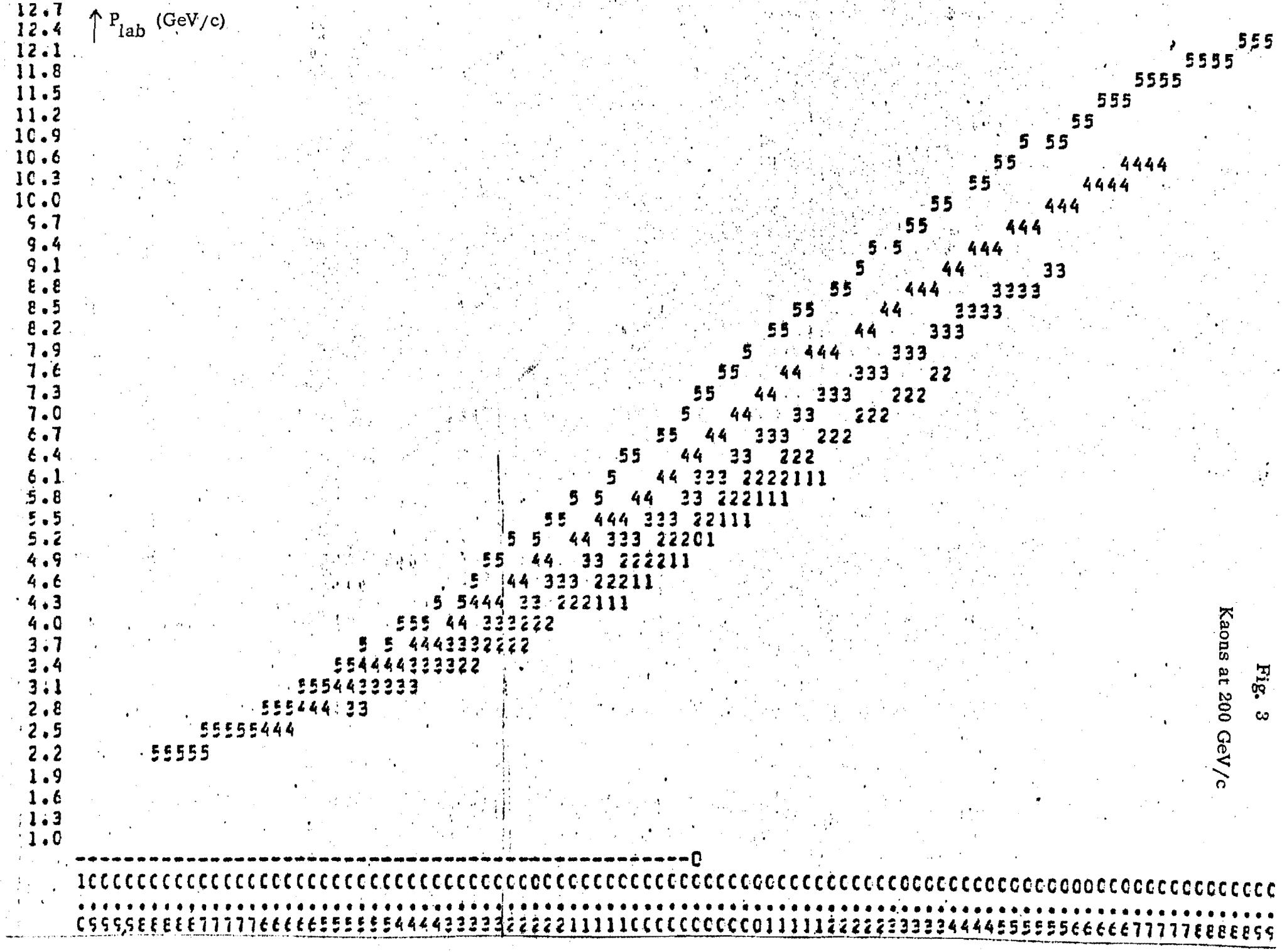

Fig. 3

Kaons at 200 GeV/c

APPENDIX I

Test Results of a 31 cm x 31 cm Lead Glass Electromagnetic Shower Detector

IHSC Consortium

To be Submitted to Nuclear Instruments and Methods

Introduction

Preliminary test runs of a lead-glass Cerenkov electromagnetic shower detector have been carried out using a tagged negative electron beam at the Fermi National Accelerator Laboratory, with nominal beam energies of 30, 40, 50, 60, 75, and 100 GeV. The detector tested here is a reduced scale version of the shower detector to be used with the Hybrid Spectrometer[1] at Fermilab and the Forward Gamma Detector at CERN. Several workers have studied and used various types of lead glass shower detectors[2] and lead-scintillator sandwich detectors.[3,4] The novel feature of this system is that the electromagnetic shower converter, as well as the absorber, consists of active elements, ensuring negligible unobserved energy loss and good energy resolution.

The Detector

The detector (Fig. 1) consists of three sections: (1) converter, (2) shower hodoscope, and (3) absorber. Photons or electrons incident on the converter develop a cascade electromagnetic shower which then passes through the shower hodoscope. The shower hodoscope is then able to measure the profile of the shower allowing for determination of the shower centroid. Finally, the shower is totally absorbed by the absorber and the energy deposited in it is measured along with the energy deposited in the converter.

The converter is constructed of two layers of lead glass bars, each bar being 6.25cm x 6.25cm x 75cm and of type F-2[5]. Each layer consists of five bars with the axes of the bars in the different layers situated at 90^0 to each other and overlapping with an area of 31cm x 31cm (see Fig. 1). There are a total of four radiation lengths presented to the beam (two radiation lengths per layer). These bars are each viewed by an AMPEREX 56 AVP[6] photomultiplier with clear silicone resin wafers[7] used for optical contact.

The bars are wrapped with 1/4 mil. aluminized mylar and the entire coverter unit is housed in a light tight wooden box. The box (Fig. 2) is made of clear pine, notched, glued, and screwed together to afford maximum strength. The interior corners were sealed and all surfaces were painted black to minimize light leaks.

The photomultipliers were spring loaded against the glass to ensure good optical contact between the glass and the encapsulating resin coat on the phototube faces.

The calibration package shown schematically in Fig. 3 is essentially a two-compartment light-tight container. One compartment contains the argon strobe lamp, which is mounted at the center of a spherical support for fiber optic light guides which are illuminated by the strobe. These guides carry light from the strobe to the detector phototubes, and it is this light standard against which the gain stability of the tubes is determined. To monitor the stability of the strobe, one of the light guides is directed into the second compartment of the calibration package and is viewed, together with a collimated Am^{241}-doped NaI(Tl) scintillator source[8], by a reference phototube. The strobe signal is attenuated by a neutral filter to a level comparable to that of the Am^{241}.

The shower hodoscope consists of three plastic scintillator planes, made of "fingers" 1cm thick and 1.5cm wide of type NE100[9]. The central plane has vertical fingers with the other two planes set at $\pm 45^0$ to it. Each scintillator finger is viewed by low cost RCA 931A[10] photomultipliers which are adequate for the large amount of light produced by the high flux electron showers. To increase the light acceptance of the internal photocathode through the lateral window, each finger is equipped with light guide heads of cylindrical shape which focus the light on the photocathode. The 78 photomultipliers (29 for each diagonal plane and 20 for the vertical plane) are enclosed in a single light-tight aluminum box. Figure 4 is a photograph displaying the light guides for the three scintillator planes.

The linearity of the 931A photomultiplier was measured in a separate test and found to be linear within 1% up to 20 mA, and at 40 mA the deviation from linearity was found to be 10%. The output charge from each 931A photomultiplier for the fingers is digitized in order to establish the spatial position of the shower as described in detail below.

In order to equalize the gains of the photomultipliers used with the finger hodoscope, a light diffusing, graded Lucite bar is used for the three planes. Light from a pulsed cold-cathode Krytron (EG&G KN-22)[11] is diffused by a white painted band on the surface of the Lucite bar facing the end of the fingers (see Fig. 5). The pink light from the KN-22 is incident on a scintillator bar, made of the same scintillator plastic as used in the hodoscope, which induces fluorescent light with the same spectrum as the actual scintillations. This induced light is then incident on the diffusing bar which distributes the proper amount of light to each finger. The grading of the shape of the Lucite bar and the variation in width of the painted diffuser band were empirically determined to ensure the uniformity of diffused light accepted by each finger. To compensate for the attenuation of light flux with distance, both the thickness of the Lucite bar and the width of the painted diffusing band were tapered. The result is a "saber" 1.5 meters long with a thickness of 4.5cm at the beginning and 1.5cm at the end with the diffusing band starting with a width of 0.7mm and increasing linearly to 2.0mm. Within a length of 1 meter the variation in the light output is less than 2%.

The shower absorber is made up of 4 lead glass blocks of type SF5[5], each being 15cm x 15cm x 60cm in dimension. These blocks are placed behind the finger hodoscope with their longitudinal axis perpendicular to the plane of the finger hodoscope, thus presenting ~ 25.4 radiation lengths for shower absorption. Each absorber block is equipped with a 5 inch EMI 9530R[12] photomultiplier, coupled to the glass

with optical grease[13]. These blocks are wrapped with aluminized mylar and opaque tape and are not housed, but stacked in the open. The identical scheme for equalizing photomultiplier gains is used for these absorber blocks as for the converter blocks, described earlier.

The Beam Description

The test was carried out in the Fermilab Neutrino Section N5 hadron beam line, which is normally used in conjunction with the 15 foot bubble chamber. A 30cm x 5mm x 5mm Be target having ~ 1 absorption length as well as ~ 1 radiation length was used. A semi-differential gas Cerenkov counter was used to tag electrons in the beam but no attempt was made to incorporate the electron trigger in the gate logic, since the Cerenkov counter was located too far upstream. This being the case, a trigger having reasonably high rejection of π^-'s and μ^-'s was devised by adding the photomultiplier signals from the second layer of the converter with a linear fan-in. The output signal of the fan-in was then discriminated at a level to insure an electron count when registered as such by the Cerenkov counter. This allowed a relatively small amount of high energy hadronic showers to be registered with virtually no loss of electron events. The fraction of good triggers (i.e., electrons) ranged from 60% at 30 GeV/c to 30% at 50 GeV/c and only a few percent at 100 GeV/c due to the decreasing electron content in the beam with increasing energy.

The beam was dispersed over an area of $\sim$ 10cm (horizontal) by 6cm (vertical) at the apparatus, allowing for showers to develop throughout several converter and absorber components. The beam was directed over various regions of the entire active area of the apparatus. A triplet set of proportional wire chamber planes was situated just in front of the detector to enable off-line position determination of each incident particle.

The momentum bite of the beam including systematic uncertainties due to beam monitoring resulted in a $\frac{\Delta p}{p} \approx 1\%$.

Data Acquisition

A master gate was formed by two-fold coincidence between two scintillators separated by 2 meters and situated immediately before the apparatus. This gate was then fanned out to the Proportional Wire Chamber (PWC) gating and storage logic and the Analog to Digital Converter (ADC) units for the lead glass and scintillator hodoscope components. The PWC system is capable of storing information for 16 particles with dead time during storage of ~150 nsec. The ADC units for the lead-glass system were operated with an integrating gate of ~ 400 nsec, during which time the master gate generator was locked out by a latch. Thus the maximum hardware dead time of the system during data storage was ~ 400 nsec. The ADC units used were LeCroy 2249A CAMAC modules[14] with 10 bit digital readout and least count of 1/4 p C. The overall deadtime of the system was dictated by the PDP-11/45 computer[15] which read out the ADC units through direct memory access. Upon completion of the ADC readout, the master gate lockout latch was cleared to allow continuation of data acquisition. This was repeated for a maximum of 16 particles or until the end of spill, whichever came first. Thus, each event consisted of ADC information along with the corresponding PWC information which allowed for off-line determination of beam position, shower-core position and energy, on an event by event basis.

After each beam spill which resulted in the storage of information for up to 16 beam events, up to 16 calibration events originating from the triggering of the various light sources (EG&G KN22 for the scintillator hodoscope, Kerns[16] flash lamps for the lead glass converter and absorber blocks and the Am^{241} doped NaI) were recorded.

Energy Determination

As a shower develops through the system, some of its energy is deposited in the first two layers of lead glass converter blocks and the remainder of energy is deposited in the absorber blocks. The amount of energy deposited in the hodoscope

scintillators is negligible and is not taken into account in this study. Thus there are 14 active components, 10 converters and 4 absorbers, whose photo-multiplier output charge represents energy deposited in the system. The coefficient α_k for each component which relates charge to energy is determined by a least square analysis using the expression:

$$\chi^2 = \sum_i (E_i - \sum_k^{14} \alpha_k C_{ki})^2$$

E_i = energy of the electron for the ith event.

α_k = charge to energy conversion factor to be determined.

C_{ki} = charge from the kth component of the ith event.

The fit was carried out at 50 GeV to determine the α_k coefficients which in turn were used to obtain the shower energy $E_i = \sum \alpha_k C_{ki}$ for the 30, 40, 60, 75, and 100 GeV runs.

In this report, no attempt was made to compensate for photomultiplier (EMI 9530 for absorbers, AMPEREX 56 AVP for converters) gain drifts due to temperature change. The analysis is as elementary as possible.

Figure 6 displays the sum of the energy distribution in the first two converter layers summed for each event whereas fig. 7 shows the distribution of energy deposited in the absorber blocks for the same sample at 50 GeV. Figure 8 displays the distribution of total shower energy determined for each event in the 50 GeV run which includes hadronic as well as electronic showers (no Cerenkov electron tag was imposed). The major portion of hadronic showers was eliminated by selectively setting the threshold of a discriminator into which the OR'ed output of the second layer of converter blocks was fed.

Figure 9 displays the 50 GeV distribution with the Cerenkov electron tag imposed. The remainder of the hadronic shower is then seen to be eliminated.

The entire remaining low energy tail may be due to π's with a delta ray in the Cerenkov counter registering as a beam electron.

Figures 10-14 display the shower energy distributions for 100-30 GeV incoming electrons. In all cases the Cerenkov electron tag was imposed.

Figure 15 is a plot of the actual beam energy versus measured energy. As can be seen, the linearity is good up to the highest energy value. The resolution, in terms of FWHM, for the various energies is shown in fig. 16 and its energy dependence is given by:

$$\frac{\Delta E}{E}\,(\mathrm{FWHM}) = \frac{27 \pm 2\%}{\sqrt{E}}$$

or

$$\sigma = (11.4 \pm 0.8)\, 10^{-2} \sqrt{E}$$

where E is the energy of the shower in units of GeV.

Position Determination

The center of an electron shower whose radial distribution is (closely) exponential and which has a characteristic width of 2.3cm is determined by evaluating the weighted average of the signals from the hodoscope fingers. This method introduces a systematic error due to the exponential behavior of the shower profile and the discrete sampling of the fingers[4]. This systematic shift to the finger center has been corrected by the following function:

$$\Delta x = 0.075 \sin\left[\frac{2\pi}{w}\,(\bar{x} - x_c)\right]$$

w = 1.5cm width of finger.

x_c = coordinate of finger center closest to $\bar{x}$.

$\bar{x}$ = weighted average coordinate.

A plot of the quantity $d = x + y + \sqrt{2}v$ where x, y, and v are the finger coordinates allows us to estimate the resolution of our detector. Elementary geometric considerations dictate d is constant and the standard deviation of its measurement is twice that of each coordinate, assuming x, y, and v are measured with the same accuracy. The final shower position is determined by a least square fit to x and y along with the geometric constraint given by d.

Figure 17 shows the distribution of d at 50 GeV. FWHM is 6.3 mm which leads to the conclusion that each coordinate has a resolution of $\sigma = 2.7$ mm.

Figures 18a and 18b show the x and y distributions of the difference between the shower center determined by the hodoscope fit and the position of the incident electron as given by the PWC. The distributions are consistent with the 1.4 mm hodoscope resolution since the PWC has 2 mm wire spacings.

Conclusion

The results of this test show that an electromagnetic shower detector can be built without the use of inactive components, such as lead. This allows for better shower energy determination and simplifies the overall construction. The plastic scintillator hodoscope is used solely for determining the position and not the energy of the showers and thus does not require extreme measures to insure pulse height integrity. The charge to digital converter units used with the position hodoscope were probably much better than required, only because of their availability. Cheaper units could be substituted for this task. Temperature control and temperature compensation in the electronics were not considered for this test. Although effects due to temperature variation were found to be negligible, the final system will be monitored for temperature variations.

The energy resolution for this prototype system was found to be $\sigma = (11.4 \pm 0.8) \times 10^{-2} \sqrt{E}$ GeV and shower-core positions were determined with $\sigma = 1.4$ mm resolution. By periodically calibrating the phototube gains with a known energy electron beam, it is conceivable that a system such as this could be used with systematic errors known and correctable to better than a percent.

Acknowledgments

We would like to thank Fermilab and its Neutrino Section for their support and use of the N5 beam line and the use of the 15' bubble chamber tagging system. Particular thanks go to J. C. Walker and C. Needles of the Neutrino Section for their help throughout the entire test.

REFERENCES

1) D. G. Fong et al., Nucl. Phys. B102, 386(1976); Phys. Lett. 53B, 290(1974).

2) J. S. Beale et al., NIM 117, 501(1974).

L. M. Lederman and R. A. Vidal, NIM 129, 65(1975).

B. J. Blumenfeld et al., NIM 97, 427(1971).

M. Holder et al., Phys. Lett. 40B, 141(1972).

J. A. Appel et al., NIM 127, 495(1975).

R. G. Astratsaturov et al., NIM 107, 105(1973).

3) A. V. Barnes et al., Phys. Rev. Lett. 37, 76(1976).

G. Donaldson et al., Phys. Rev. Lett. 36, 1110(1976).

4) Yu. Bushnin et al., NIM 106, 493(1973).

Yu. Bushnin et al., NIM 120, 391(1974).

5) Schott Optical Glass Inc.
York Avenue
Duryea, Pennsylvania 18642
U. S. A.

	F-2	SF-5
Radiation Length (cm)	3.06	2.36
Critical Energy (MeV)	18.4	15.8
Density (gr/cm^2)	3.60	4.08
Refractive Index	1.62	1.6727

6) Amperex Electronic Corp.
230 Duffy Avenue
Hicksville, N. Y. 11802

56AVP - 2 inch head-on photomultiplier tube with 14 stages.

7) Dow Corning Corp.
Midland, Michigan 48640
U. S. A.

Sylgard 184, Encapsulating Resin

8) The Harshaw Chemical Company
Crystal-Solid State Division
1945 East 97th Street
Cleveland, Ohio 44106

Am^{241} Doped NaI (Tℓ) Light Pulser ~ 200 counts/sec.

9) Nuclear Enterprises
931 Terminal Way
San Carlos, California 94070

10) RCA Electronic Components
Harrison, N. J. 07029

931A - 1 1/8" Diameter Side-on photomultiplier tube with 9 stages.

11) E G & G Inc.
Electro-Optics Division
35 Congress Street
Salem, Massachusetts 01970

KN-22 Cold Cathode, Gas-filled Krytron

12) EMI Gencom Inc.
80 Express Street
Plainview, New York 11803, U. S. A.

9530R - 5" diameter, "super" S-11 cathode, 11 dynodes

13) Dow Corning Corp.
Midland, Michigan 48640
U. S. A.

Optical Grease

14) LeCroy Research Systems Corp.
Spring Valley, N. Y. 10977
U. S. A.

CAMAC Model 2249A, 12-channel A to D converter

15) Digital Equipment Corp.
Maynard, Massachusetts 01754
U. S. A.

PDP-11/45 Computer

16) Private communication
Kerns, Gordon
Physics Department
Fermilab
P. O. Box 500
Batavia, Illinois 60510, USA

These flash lamps were designed by C. Kerns and loaned to us during the test.

Figure Captions

Figure 1 Schematic of the converter, hodoscope and absorber layout.

Figure 2 Photograph of the converter and its light-tight box.

Figure 3 Schematic of the light calibration package.

Figure 4 Photograph of the light pipes from the scintillator hodoscope.

Figure 5 Schematic of the "saber" light diffusing bar used for the hodoscope calibration.

Figure 6 Energy distributions of the showers in the converter, from 50 GeV/c electrons.

Figure 7 Energy distributions of the showers in the absorber, from 50 GeV/c electrons.

Figure 8 Energy distributions of the showers detected by the entire system from 50 GeV/c negatives. The long tail on the low energy side is due to hadrons.

Figure 9 Energy distributions of the showers detected by the entire system, from 50 GeV/c electrons, with the Cerenkov counter electron tag invoked.

Figure 10a Energy distribution of the showers as detected by the system, from 100 GeV/c negatives. The Cerenkov counter electron tag is not used here since the counter efficiency is low at this energy.

Figure 10b Energy distribution of the same sample as shown in fig. 10a, except the electron tag from the Cerenkov counter is used. Due to the low efficiency, the sample is depreciated.

Figures 11-14 Energy distributions for electrons at 75, 60, 40 and 30 GeV/c, respectively.

Figure 15 Measured shower energy versus actual electron beam energy.

Figure 16 Energy resolution (% FWHM) versus $E^{\frac{1}{2}}$ for the various shower energies.

Figure 17 Distribution of $d = u + v + \sqrt{2}\,x$ for shower cores. See text for definition of d.

Figure 18a Distribution of x coordinate differences between shower core and beam electron positions.

Figure 18b Distribution of y coordinate differences between shower core and beam electron positions.

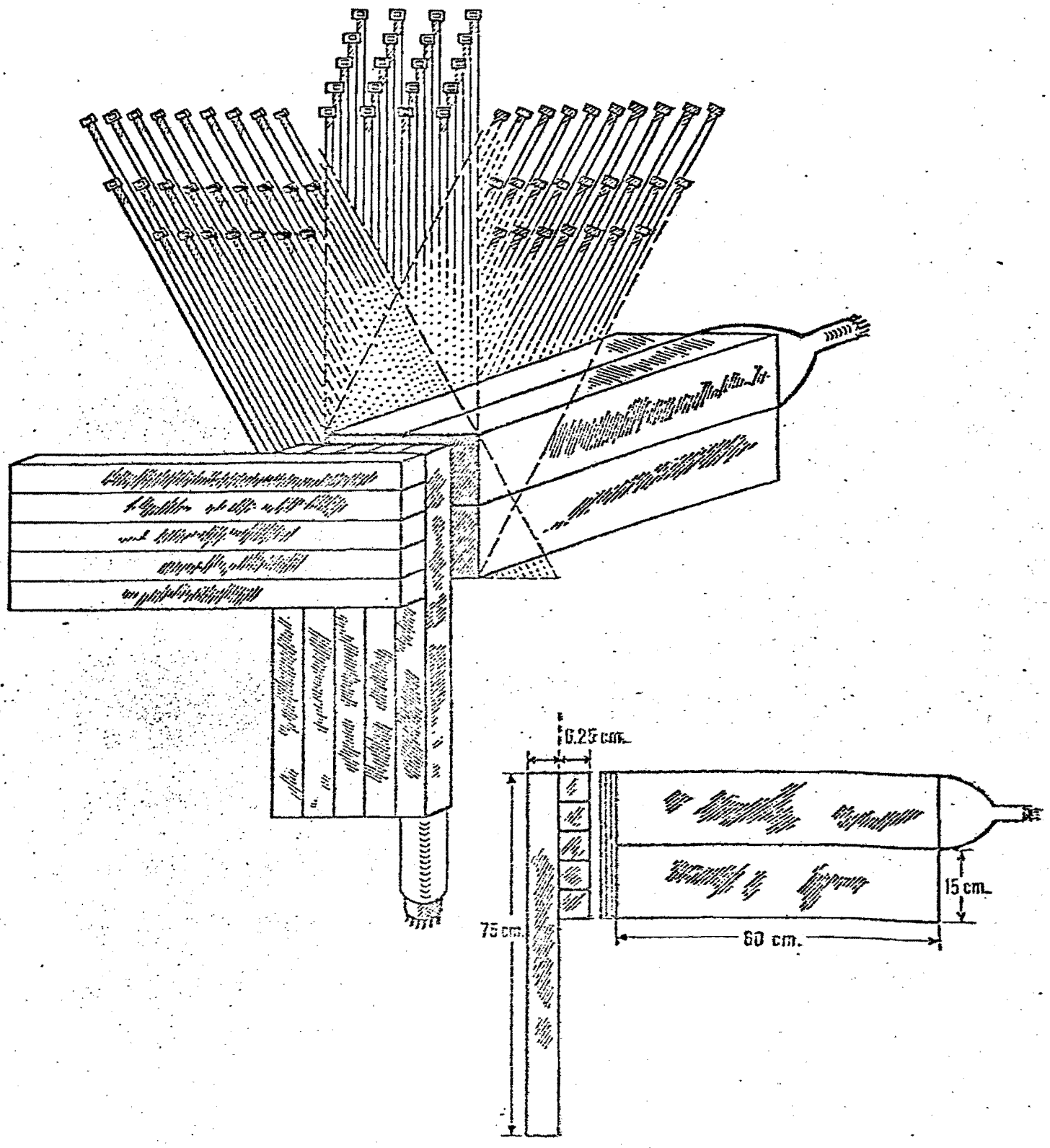

FIG 1

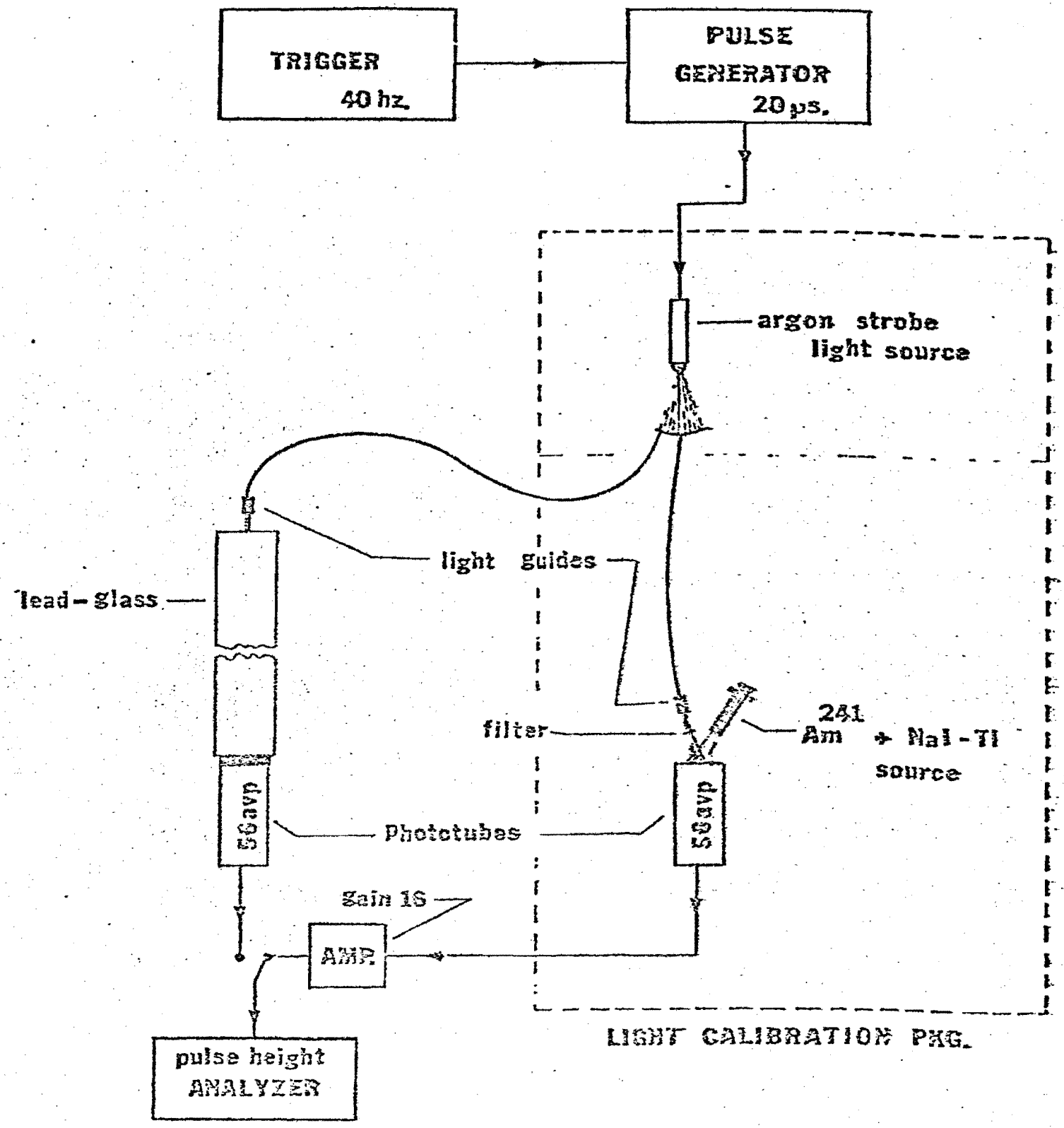
TRIGGER
40 hz.
PULSE
GENERATOR
20 μs.
argon strobe
light source
light guides
lead-glass
filter
241
Am + NaI-Tl
source
Phototubes
Gain 18
AMP.
pulse height
ANALYZER
LIGHT CALIBRATION PKG.

FIG 3

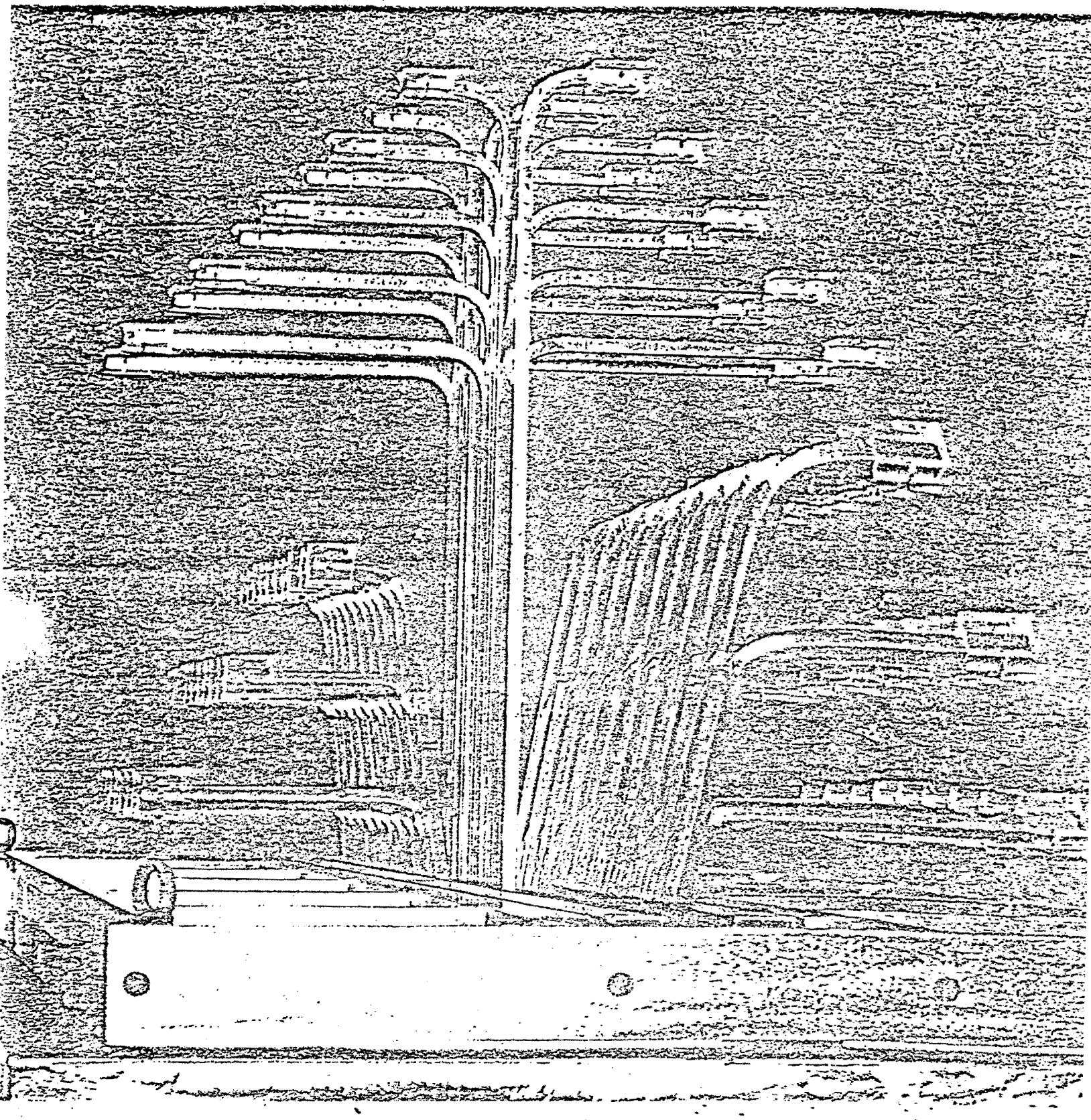

FIG 4

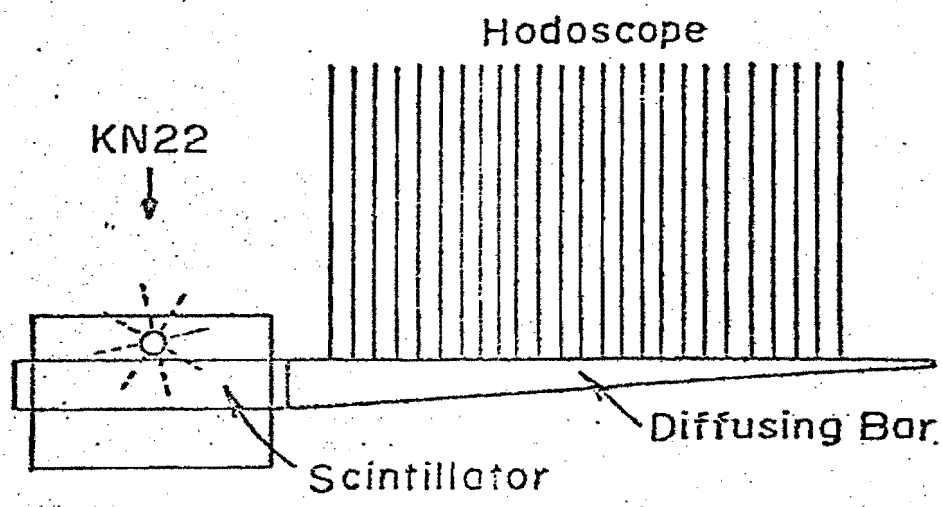

Schematic of Light Calibration System for Hodoscope

FIG. 5

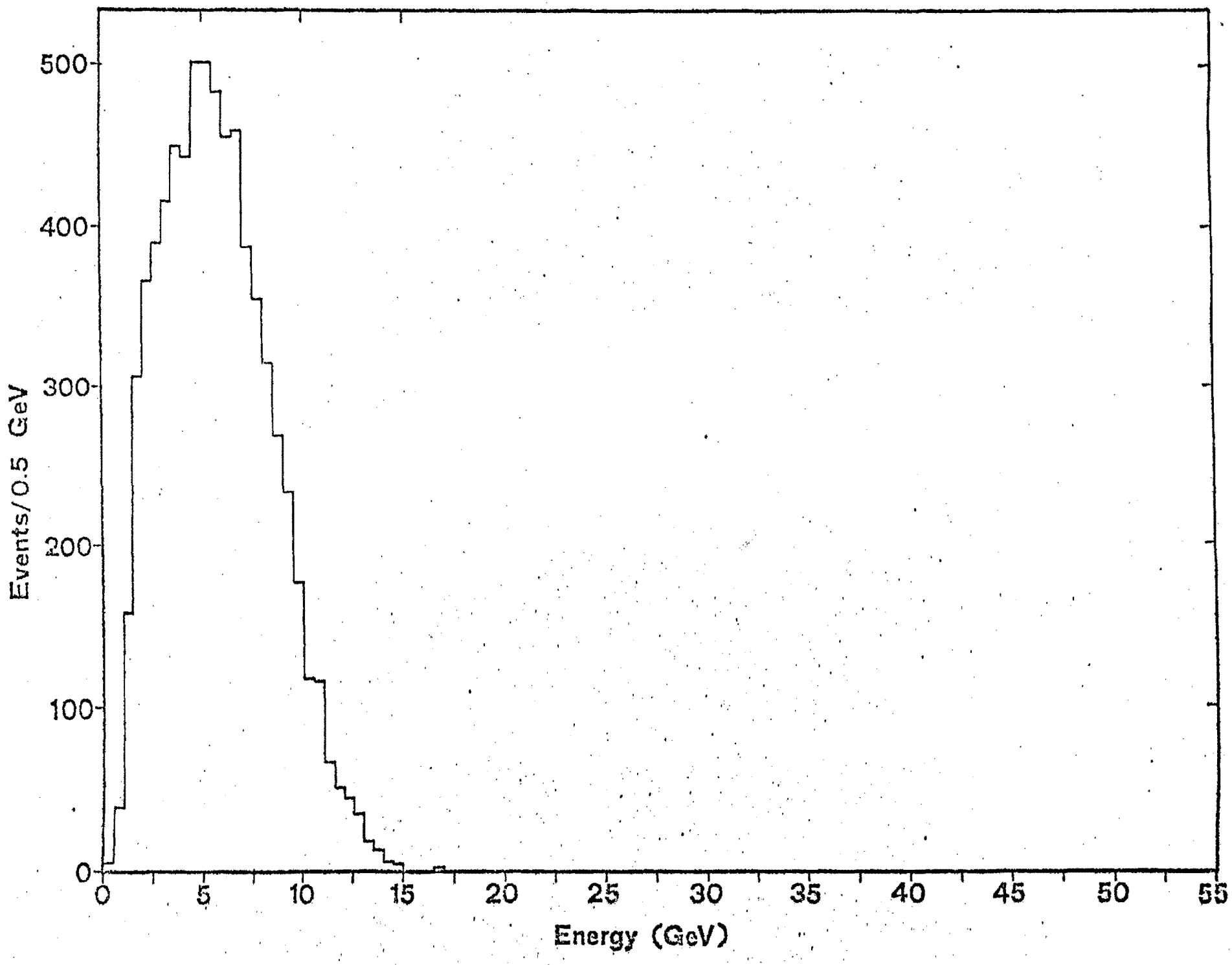
Events/0.5 GeV
500
400
300
200
100
0
0
5
10
15
20
25
30
35
40
45
50
55
Energy (GeV)

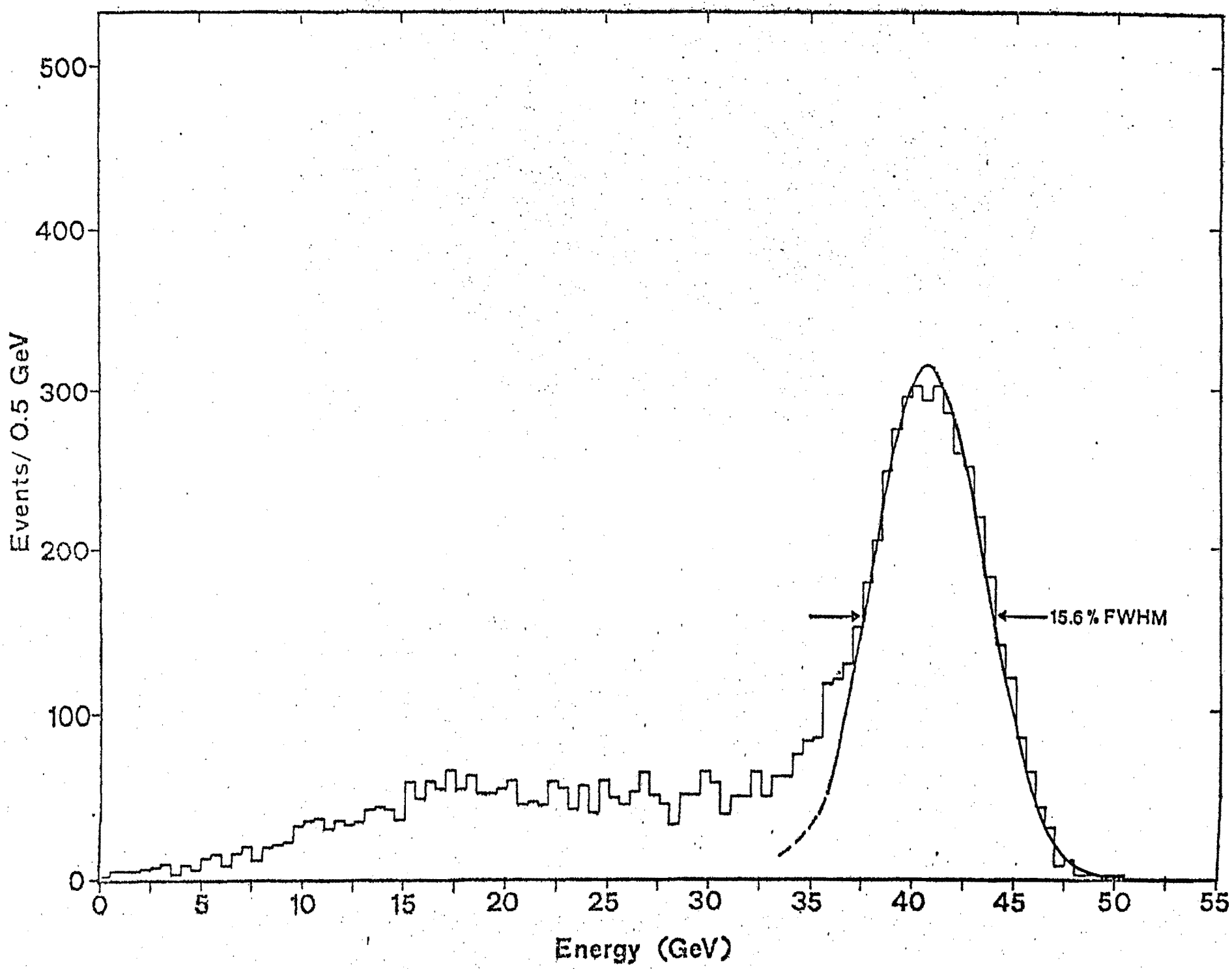
500
400
300
200
100
0
Events/ 0.5 GeV
0
5
10
15
20
25
30
35
40
45
50
55
Energy (GeV)
15.6 % FWHM

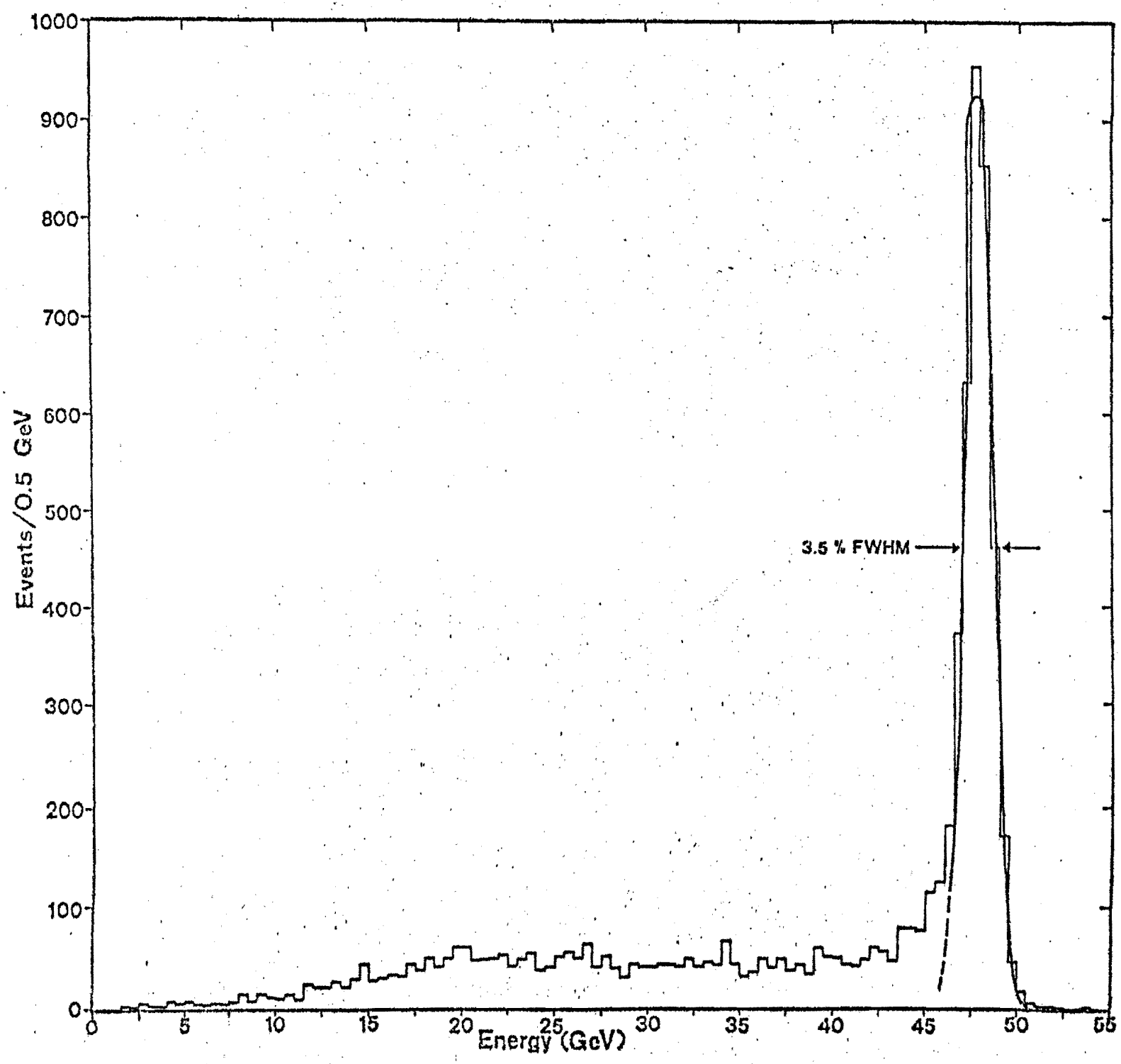
Events/0.5 GeV
Energy (GeV)
3.5 % FWHM
0
100
200
300
400
500
600
700
800
900
1000
0
5
10
15
20
25
30
35
40
45
50
55

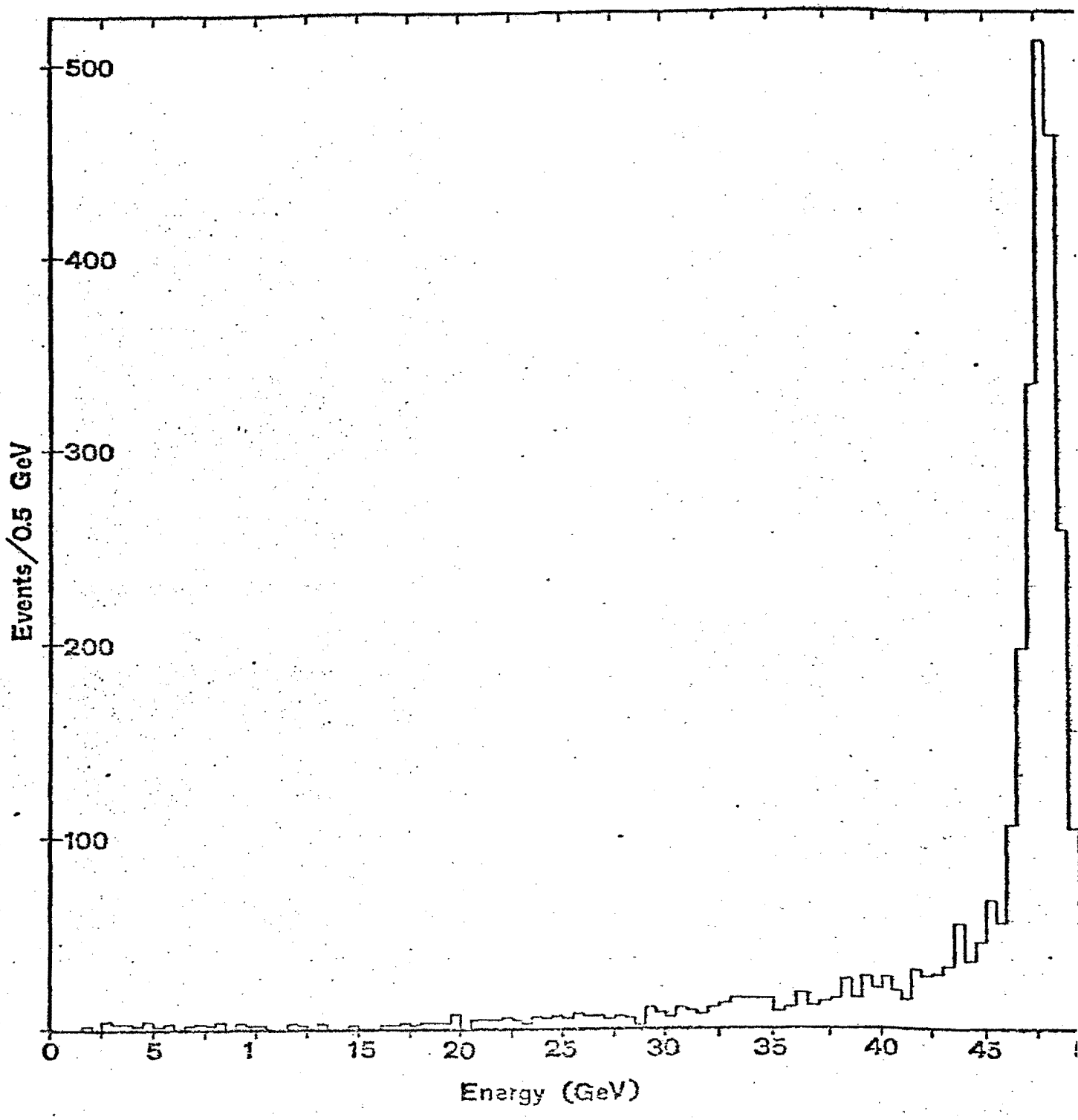
500
400
300
200
100
Events/0.5 GeV
0
5
1
15
20
25
30
35
40
45
Energy (GeV)

FIG 9

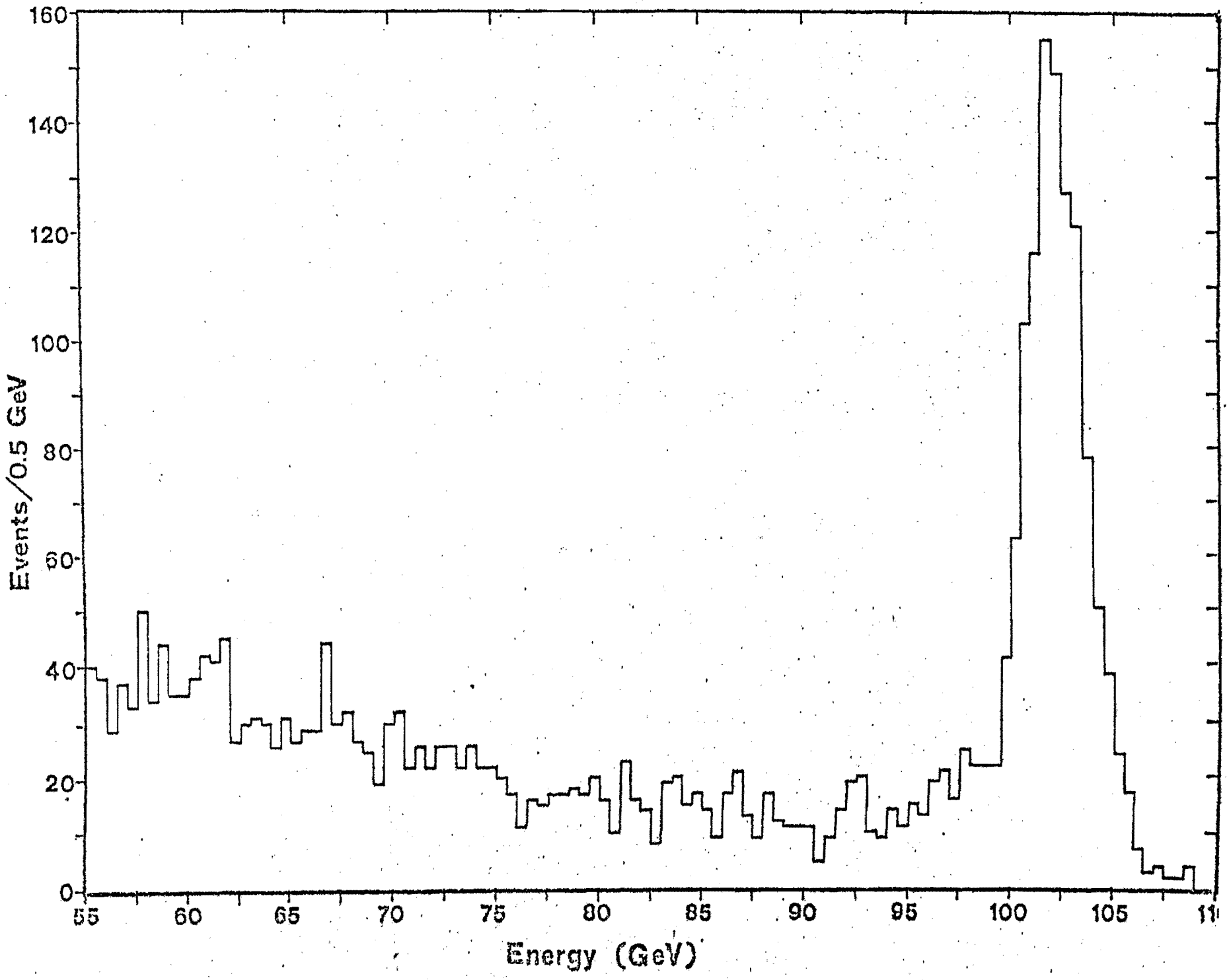
Events/0.5 GeV
Energy (GeV)
0
20
40
60
80
100
120
140
160
55
60
65
70
75
80
85
90
95
100
105

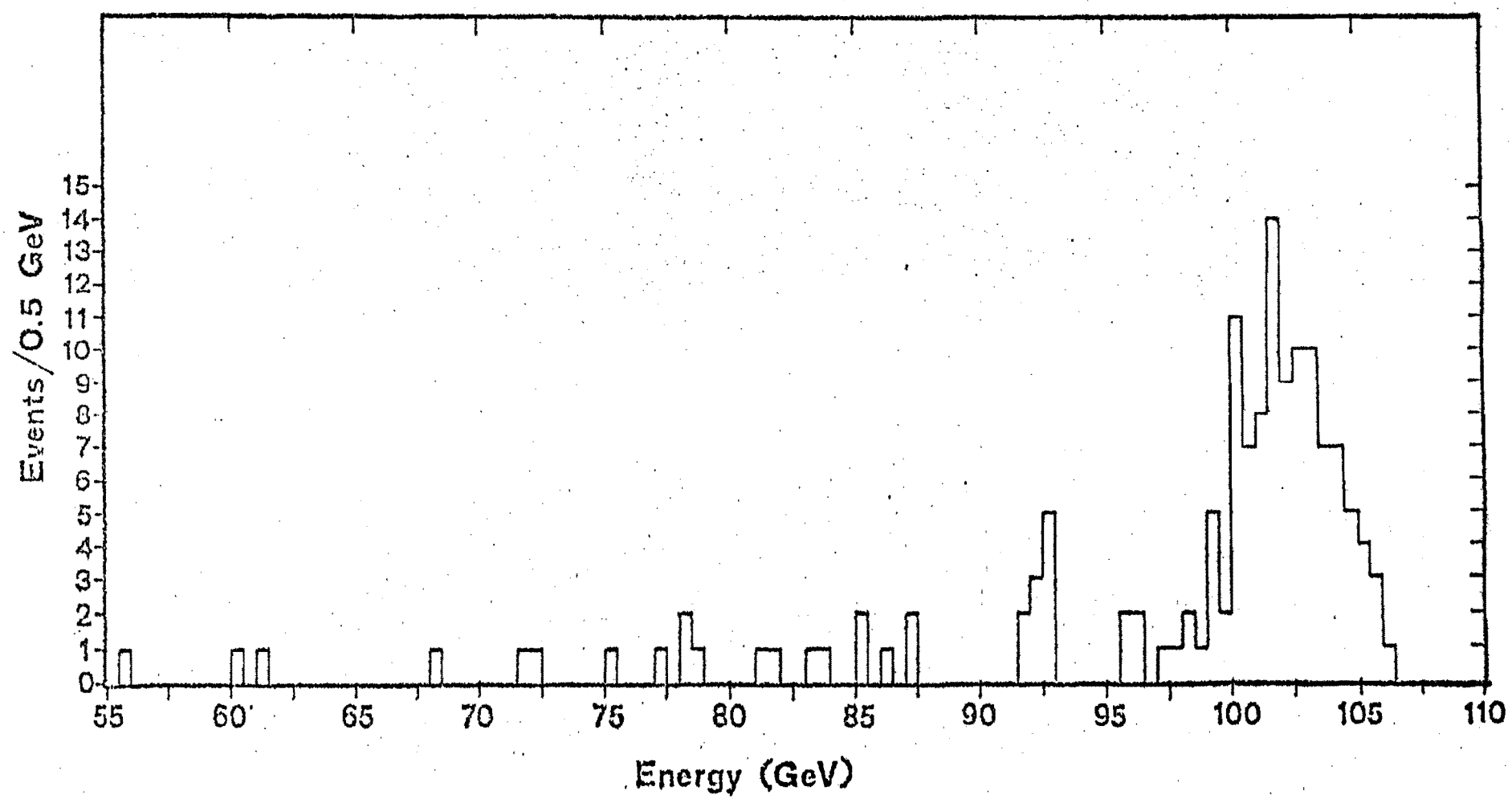
Events/0.5 GeV
0
1
2
3
4
5
6
7
8
9
10
11
12
13
14
15
55
60
65
70
75
80
85
90
95
100
105
110
Energy (GeV)

FIG 10b

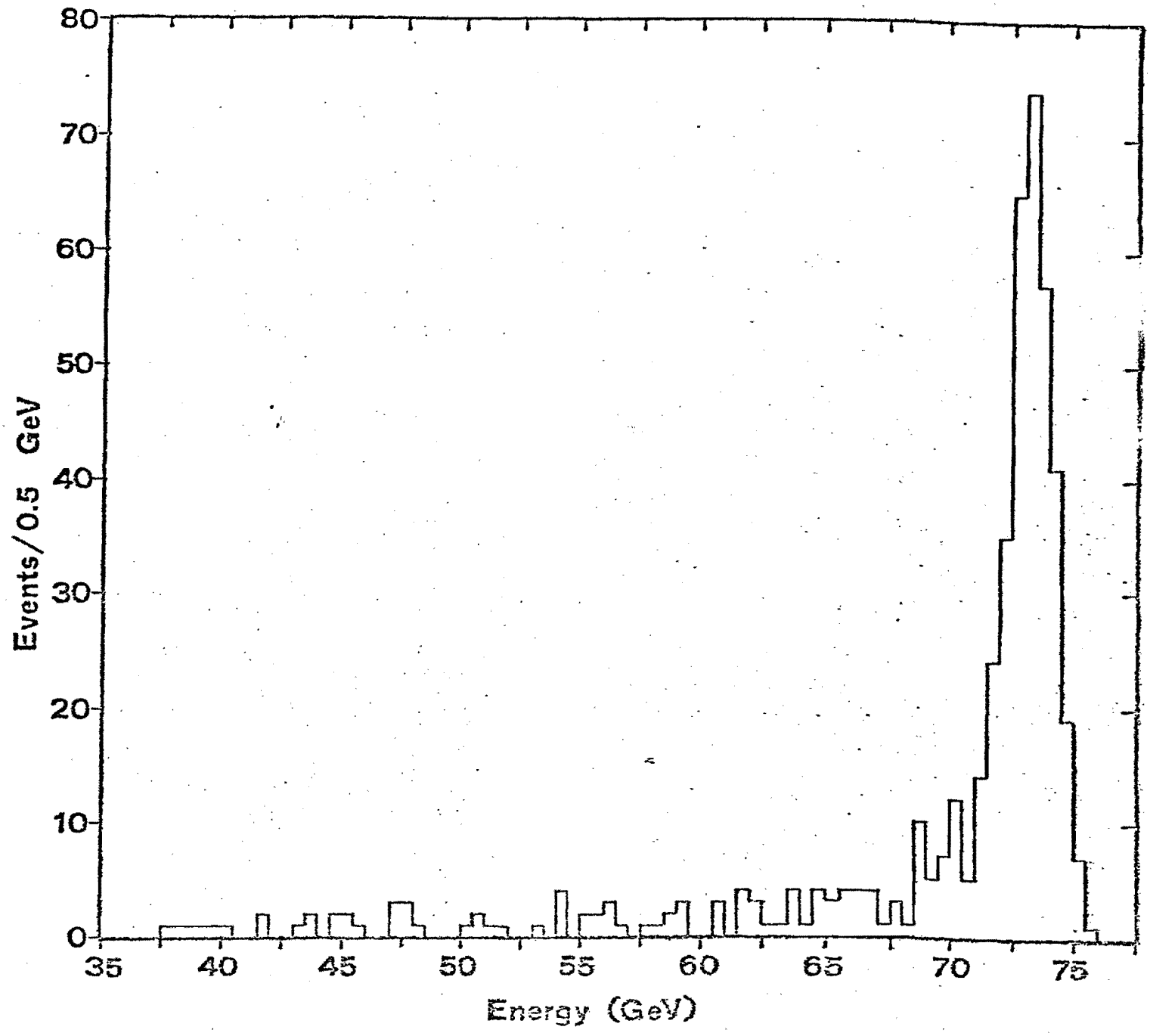
80
70
60
50
40
30
20
10
0
Events/0.5 GeV
35
40
45
50
55
60
65
70
75
Energy (GeV)

FIG 11

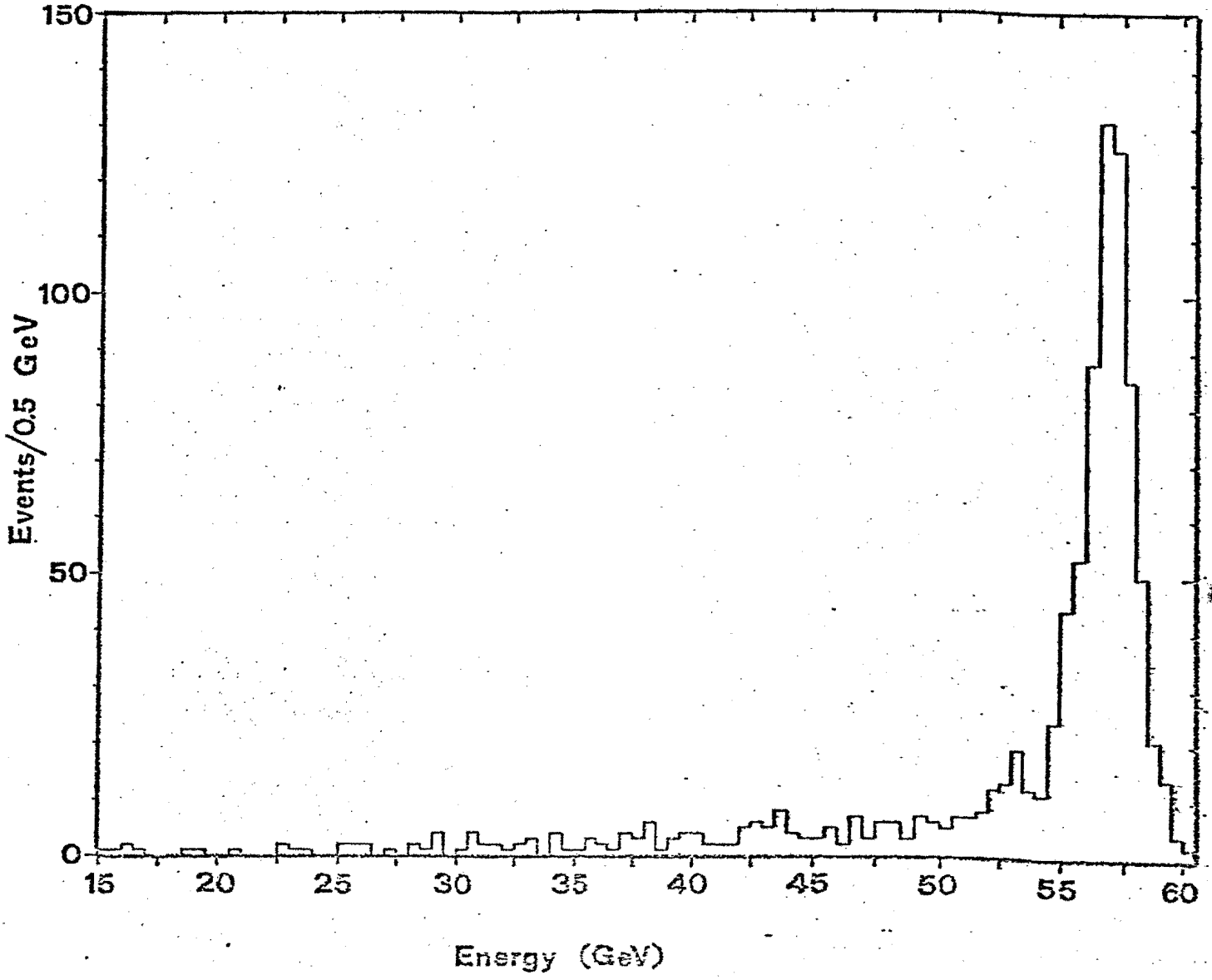

FIG 12

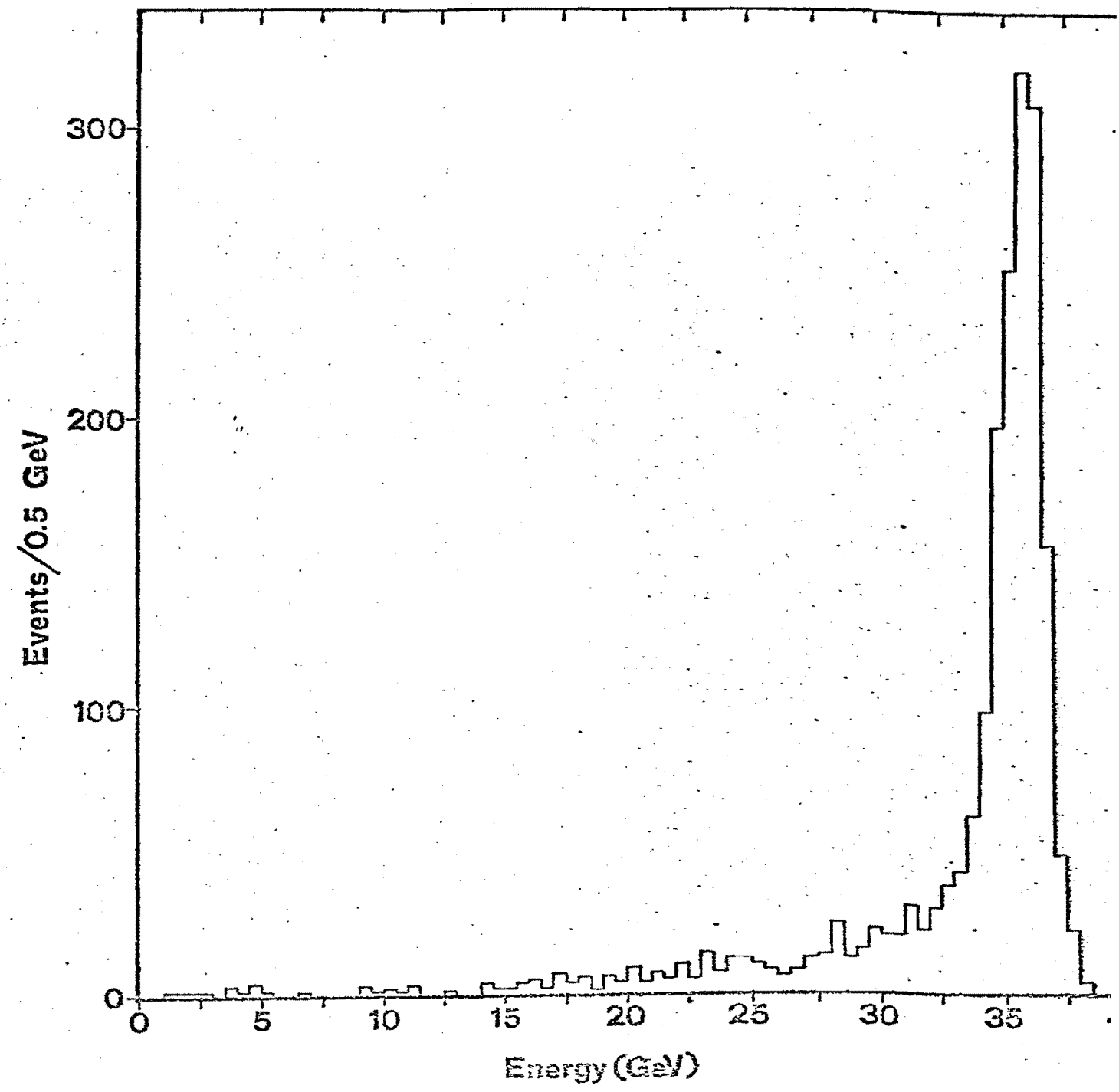

FIG 13

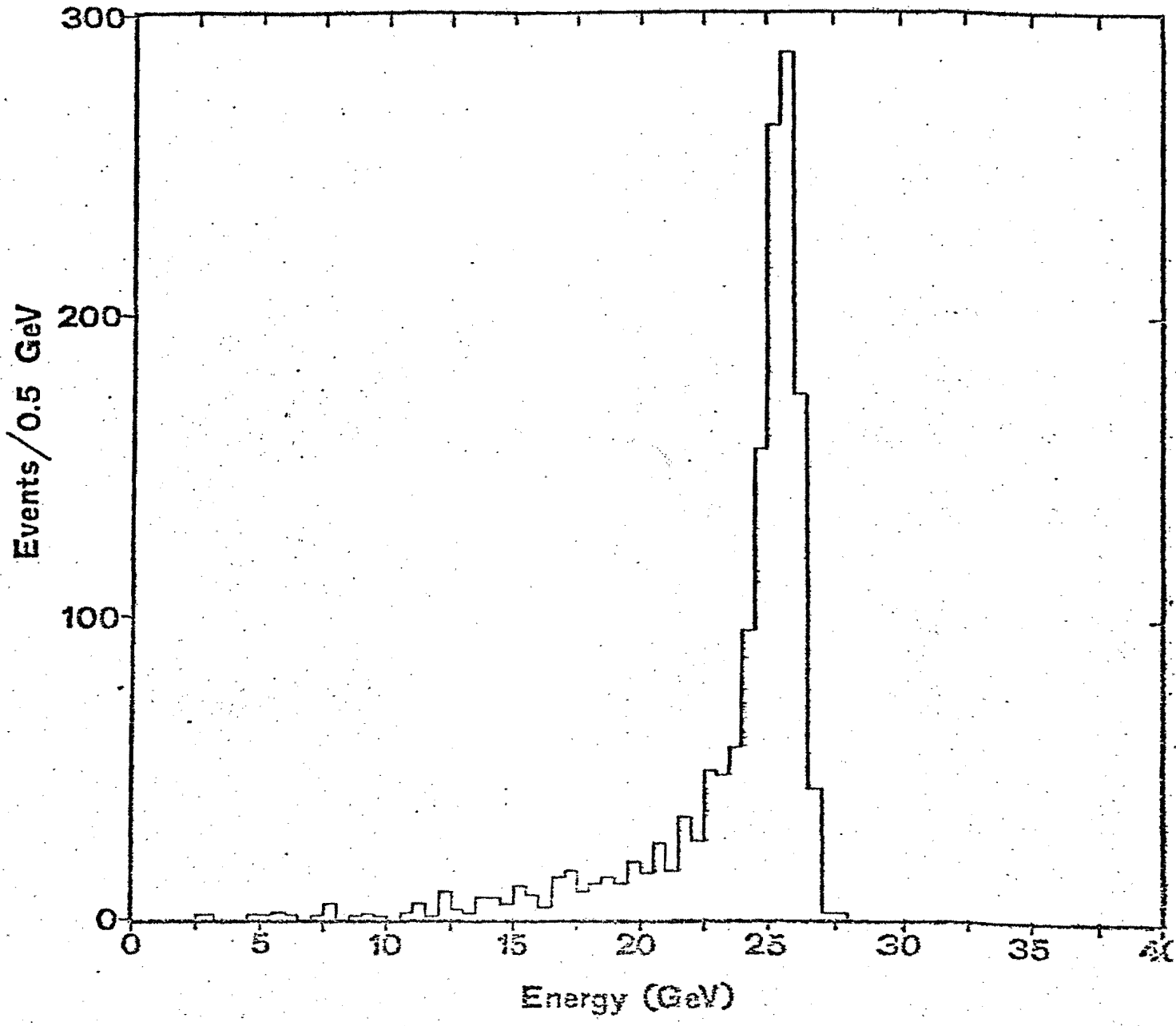

FIG 14

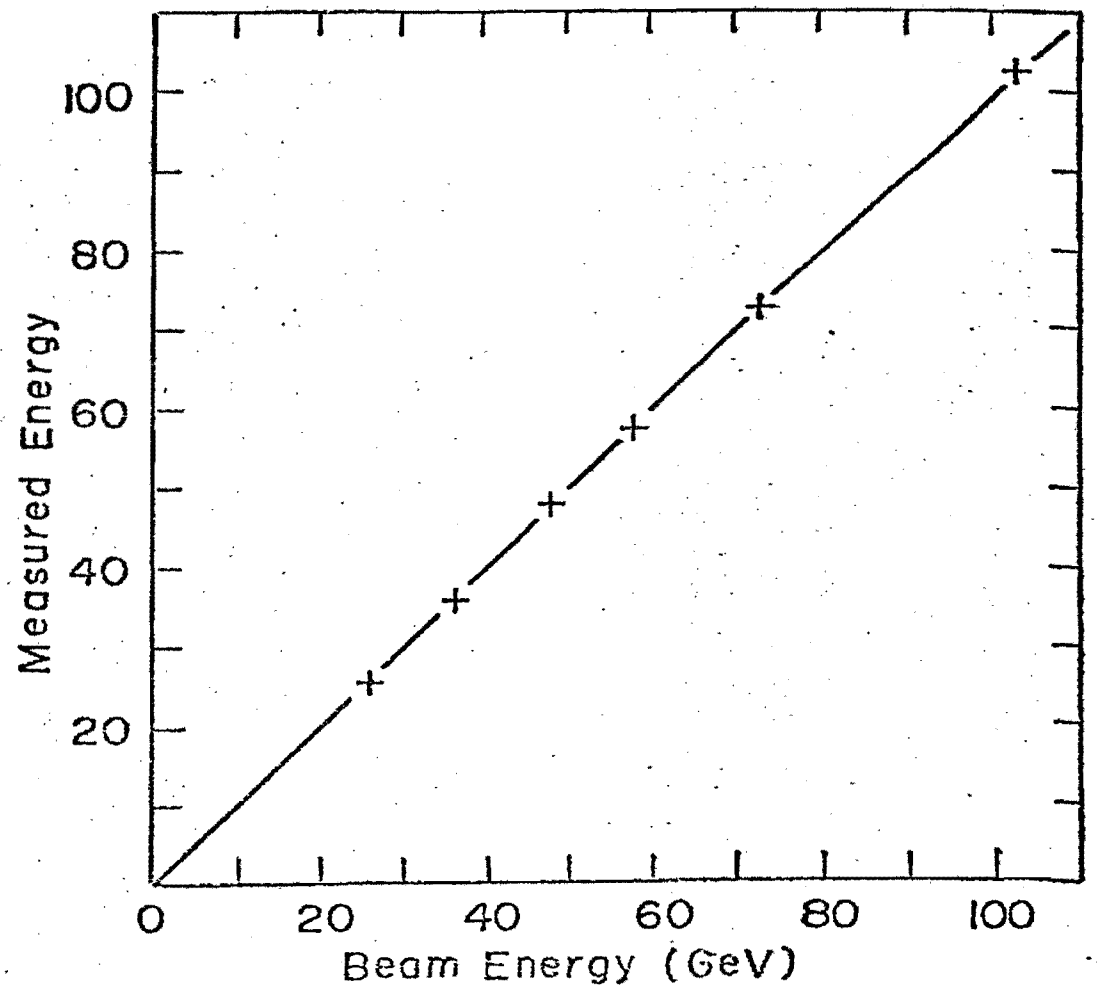
100
80
60
40
20
Measured Energy
0
20
40
60
80
100
Beam Energy (GeV)

FIG 15

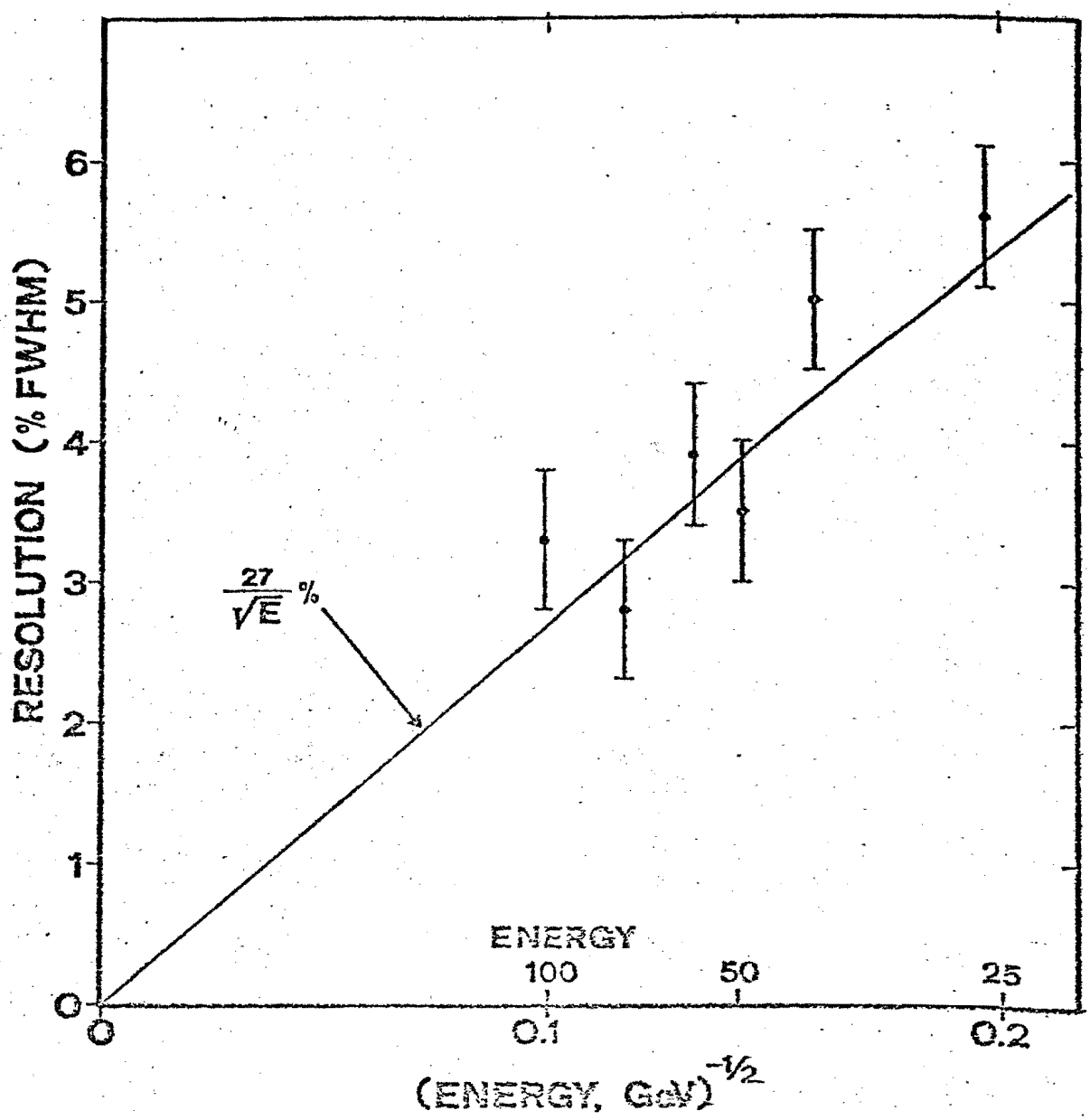
RESOLUTION (% FWHM)
6
5
4
3
2
1
0
$\frac{27}{\sqrt{E}}$ %
ENERGY
100
50
25
0
0.1
0.2
(ENERGY, GeV)$^{-1/2}$

FIG 16

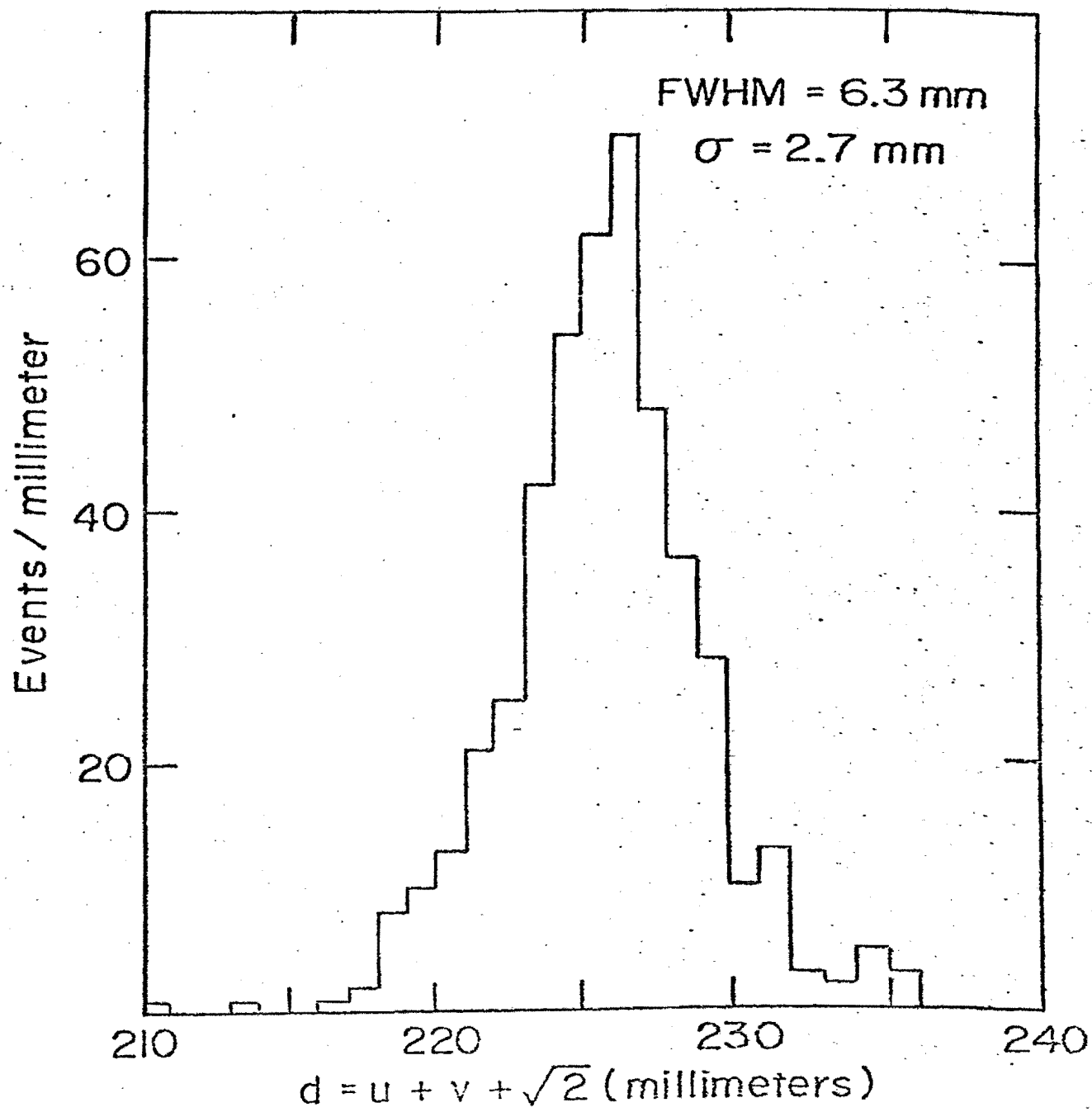
FWHM = 6.3 mm
σ = 2.7 mm
60
40
20
Events / millimeter
210
220
230
240
d = u + v + √2 (millimeters)

FIG 17

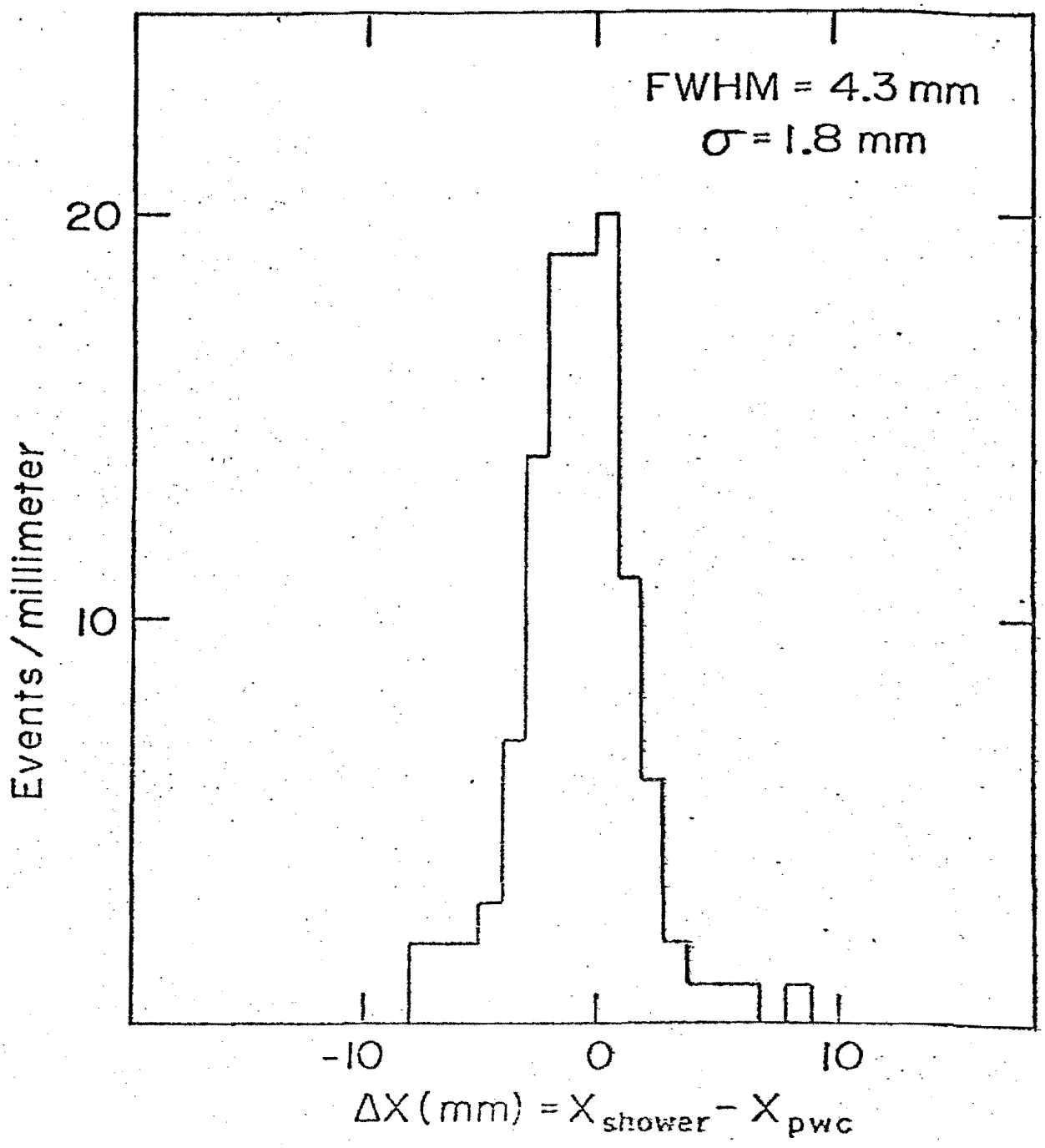
FWHM = 4.3 mm
σ = 1.8 mm
20
10
Events / millimeter
-10
0
10
ΔX (mm) = X shower − X pwc

Fig 18a

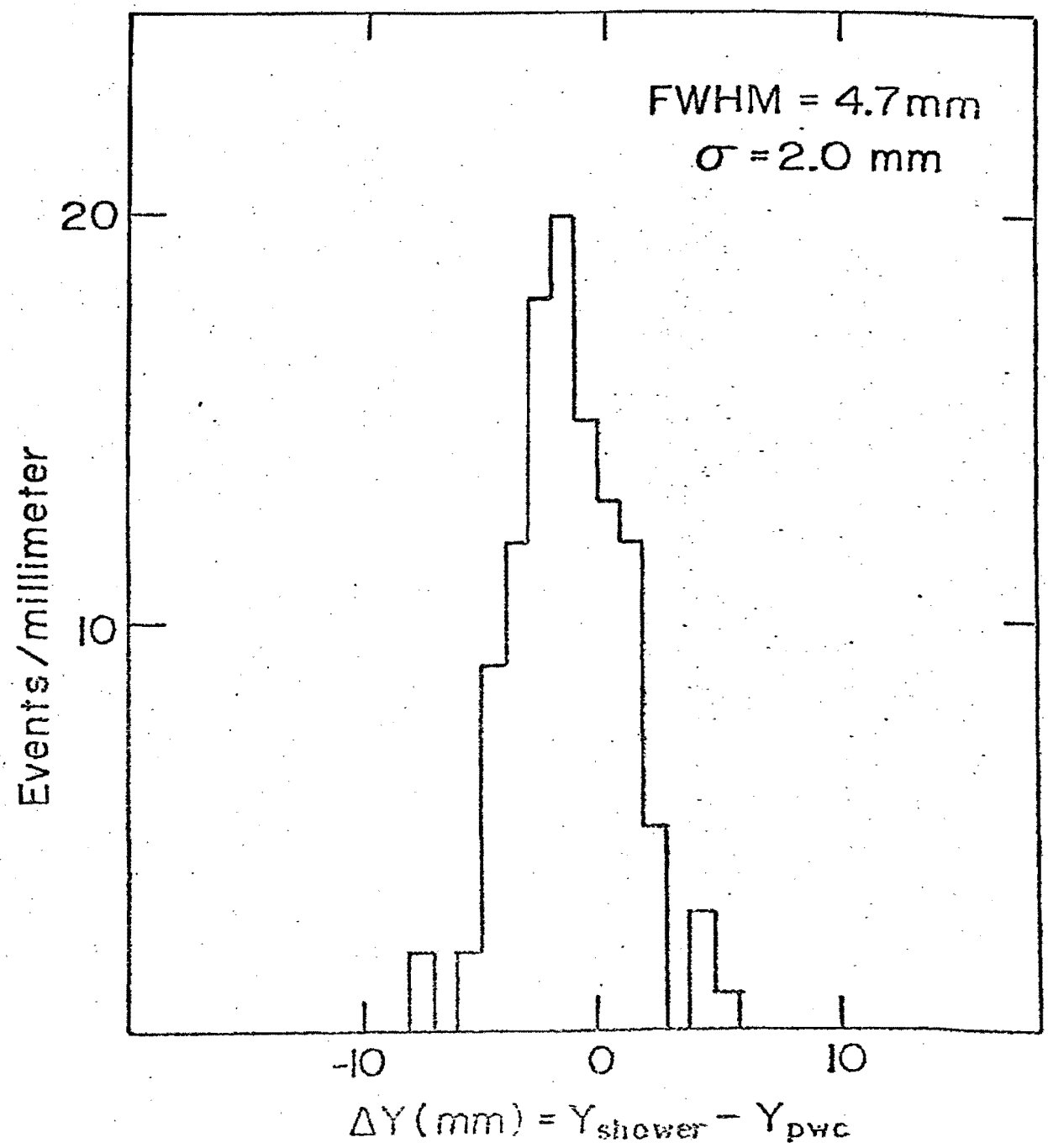
FWHM = 4.7mm
σ = 2.0 mm
20
10
Events/millimeter
-10
0
10
ΔY (mm) = Y_shower − Y_pwc

FIG 18A

DPI Note #5
July 27, 1977

Acceptance and Resolution Studies for the Fermilab ISIS

T. B. Stoughton, T. Ludlam, and V. Kistiakowsky

Introduction

Studies have been carried out previously of the acceptance and resolution anticipated for an ISIS-like device by R. Plano (Rutgers), W. Bugg (Tennessee), and J. Brau and V. Kistiakowsky (MIT). Some of these results were presented at the May 1976 Fermilab Workshop on Particle Identifiers for hadron physics and their consideration was partly the basis for choosing ISIS as a component of the downstream charged particle identifier. Appendix 1 of this note contains results obtained by W. Bugg for 147 GeV/c π^-p interactions (E-154) and references will be made to these figures and tables.

The present study was carried out for 300 GeV/c π^-p interactions because of the proposal to use ISIS for such an experiment (Fermilab proposal, P-488). The study attempts to answer some questions raised during and subsequent to the workshop.

The results given in the following sections are based on a sample of 147 GeV/c π^-p events (E-154) which have been modified to simulate 300 GeV/c events. The analysis was carried out independently at MIT (VK, TS) and at Yale (TL) with somewhat different assumptions and the results were in agreement where direct comparison was possible.

The quasi-300 GeV/c events were obtained from 147 GeV/c events by multiplying the longitudinal component of the center

of mass momentum of every charged particle by $\sqrt{s(300)/s(147)}$ where s(300) and s(147) are the center of mass energy for 300 GeV/c and 147 GeV/c π^-p interactions, respectively. The particles were then transformed into a frame in which the transformed target proton was at rest.

At MIT, the particles were swum downstream from their experimental vertex positions. At Yale, the incident pions were assumed to be parallel to the x-axis and the production vertices were distributed randomly in a volume of the bubble chamber defined as follows in the usual coordinate system:

$$-.20 < x < .10\text{m}$$

$$.035 < y < .085\text{m}$$

$$-.195 < z < -.185\text{m}$$

The accuracy of the swimming program was verified by swimming particles from 147 GeV/c events to the position along the beam-line of a proportional wire plane in the existing hybrid system and comparing the y and z coordinates obtained in this fashion with the experimental positions.

Studies were made both with and without background. Five noninteracting beam tracks were randomly distributed in an area of the bubble chamber defined as follows:

$$.015 < y < .105\text{m}$$

$$.210 < z < -.170\text{m}$$

The event and the five noninteracting beam tracks were randomly distributed in a 250 μsec spill. The effect of this background on the track resolution was negligible. The major source of

background results from the interaction of low momentum event tracks with the magnet and other material. W. Bugg (Tenn.) has measured the event related background for 147 GeV/c and found an average of 7 tracks at the entrance of ISIS-1 and only two tracks at the exit of ISIS-2. It was attempted to simulate this highly divergent background by randomly distributing 147 GeV/c events on the surface of the magnet aperture. This background resulted in an average of 5.5 tracks at ISIS-1 and 4.5 tracks at ISIS-2. Since a slowly diverging background track is more likely to interfere with an event track (also slowly diverging), this simulated background has a very pessimistic effect on track resolution.

Figure 1 gives the momentum distribution for all particles from simulated 300 GeV/c events and for those which escape through the B. C. magnet aperture into the downstream system. These distributions may be compared with figure A-4 (figure 4 in Appendix A). The main effect of the transformation to 300 GeV/c is an understandable shift to higher momenta.

Figure 2 gives the rapidity distribution for A) all particles from the simulated 300 GeV/c events, B) the particles which escape the magnet, C) the particles with $p > 5$ GeV/c which escape the magnet, and D) the particles with $p > 5$ which pass through a 1mx1mx3m long ISIS ending at x=6.125m. These figures may be compared with figures A-10 through A-20 (figures in the appendix) and the main effect of the transformation is seen to be a widening of the rapidity region and as expected a depletion

of the number of events with $y < 0$ and $p > 5$ GeV/c which escape the magnet.

Figure 3 shows the distribution of the number of events which result in a given number of charged particles in ISIS-1 and figure 4 that for ISIS-2. The averaged charged multiplicities are 3.0 for ISIS-1 and 2.6 for ISIS-2. These numbers are obtained from the 147 GeV/c events, scaled up in energy as described, which have a total charge multiplicity of 7.40 ± 0.04.[1] The average total charge multiplicity at 300 GeV/c, obtained by interpolating data at 147, 200, and 360 GeV/c, is 8.5/event. In the studies at Yale, the 360 GeV/c data of Firestone et al.[2] were used for the purpose of summing or averaging over all multiplicities. This multiplicity distribution is reproduced in figure 5. Figure 6 shows the frequency of charged tracks entering ISIS-1 and ISIS-2 as a function of primary multiplicity.

I. Acceptance

Since design considerations seem to dictate that ISIS consist of two modules rather than the three originally proposed, this study was carried out for a 1 meter long ISIS module (ISIS-1) with an entrance plane at x=2.375m and a 2 meter long ISIS module (ISIS-2) with an entrance plane at x=4.125m.

Due to voltage breakdown and gas purity considerations it is undesirable to increase the dimension of ISIS beyond 1 meter in the direction perpendicular to the plane of signal wires. However, the criteria limiting the dimension of ISIS in the direction parallel to the signal wires is less restrictive

so tests were made to determine the fraction of particles gained by extending the dimension of ISIS beyond 1 meter in this direction.

Table I shows the fraction of the tracks which escape the magnet and traverse the entire length of ISIS-1 for various y and z dimensions. Table II shows the same fraction for the second module of ISIS. The tests show that virtually nothing is gained by increasing the dimension of ISIS beyond 1 meter in the z-direction, but a 5% increase in the fraction of tracks which traverse the entire length of ISIS-2 occurs by increasing the dimension in the y-direction by 20cm. The reason for this is that the bubble chamber magnetic field points in the z-direction and so the tracks are more spread out in the y-direction. However, due to the lower density of tracks in the y-direction, track resolution is so much more efficient with the wires parallel to the z-axis (which will be discussed in the next section) that the acceptance gained by having the extended wires perpendicular to the z-axis is negligible compared to the loss in track resolution. Therefore, the wires should be parallel to the z-axis (direction of the B. C. magnetic field) and thus the dimension of ISIS is limited to approximately 1 meter in the y-direction. As Tables I and II show, no significant gain in acceptance is obtained by increasing the dimension of ISIS in the z-direction. Therefore in all further tests ISIS is assumed to be 1 meter in both the y and z-direction.

II. Track Overlap

The effectiveness of ISIS in identifying a given track is determined by the number of cells the track traverses in which it can be resolved from neighboring tracks in the event. Since it is necessary to make an accurate determination of the ionization, it is necessary to integrate the pulse arriving at the wire for a long enough time so that all the charge is collected. W. W. M. Allison et al.[3] have found that this time varies from ~0.25 μsec to ~0.4 μsec, corresponding to spacial resolutions of 1cm to 1.7cm for a drift velocity of 4cm/μsec. The lower limit is for tracks passing close to the sense wire and the upper limit for tracks where the charge has drifted 2m. For this study, two tracks were considered to be unresolvable in those regions where their projections on the x-y plane were within 1cm of each other.

In the studies carried out at Yale, ISIS-1 was divided into 62 cells and ISIS-2 into 125 cells corresponding approximately to the number of data samples from each module. That study determined the average number of "clear" cells for each track and the fraction of tracks with 90% of the track clear. In the MIT study ISIS-1 was divided into 100 "cells" and ISIS-2 into 200 "cells" and the study determined the fraction of each track which was clear. Histograms were made giving the percentage of tracks with a given fraction of the track clear. The results of the two approaches were in qualitative agreement.

The original design of ISIS consisted of a sense wire plane at beam height sandwiched between two high voltage planes at a distance of 50cm. Because the symmetry of the configuration results in the fact that the single sense wire plane may receive signals from both the upper and lower halves of ISIS at the same time, the probability of track interference is approximately doubled. Table III shows the effect of this reflection symmetry. In this table f_{160} is the fraction of tracks with 160 of 187 cells clear as a function of momentum and primary multiplicity. The improvement in resolution by eliminating this reflection symmetry is quite dramatic. Studies were made in an attempt to eliminate or reduce the effect of this reflection symmetry. These studies resulted in a modification to the high voltage - sense wire plane configuration of ISIS.

It was suggested at the Fermilab workshop in May 1976 that a way to improve the acceptance of ISIS without increasing the drift distance would be to position the device with lengthened sense wires perpendicular to the magnetic field and where the largest aperture is necessary. Table IV compares the track overlap characteristics for ISIS-1 and ISIS-2 with wires parallel to and perpendicular to the magnetic field. The loss in track resolution indicates that the orientation of ISIS with the sense wires parallel to the magnetic field is desirable. All succeeding test results will be given only for the case with the wires parallel to the B. C. magnetic field.

In an attempt to improve resolution, tests were made by offsetting the signal wire plane from beam height and also by rotating by angles between $\pm 6^{o}$ about the axis parallel to the sense wires through the center of each ISIS module. All of these tests resulted in a decrease in track resolution.

Since track resolution is seen to be a serious problem and no improvement is obtained by trying different orientations of the original design, tests were run to compare the original design, A) signal wire plane at beam height with high voltage planes at $\pm$ 50cm, with the following alternatives, B) high voltage plane at beam height with two separately analyzed signal planes at $\pm$ 50cm, and C) high voltage plane at beam height with two separately analyzed signal planes at $\pm$ 25cm and two more high voltage planes at $\pm$ 50cm (see figure 7). Design B eliminates the problem of reflection symmetry. Design C eliminates the reflection symmetry problem about the y=0 plane but introduces reflection symmetry about the planes y=$\pm$25cm. However design C is an improvement over the original design since each sense plane receives signals from only half the volume of ISIS and thus the probability of track overlap is reduced. Table V gives the fraction of tracks entering the full ISIS as a function of the amount of the track which is clearly resolved for each of the three designs. Designs B and C are a substantial improvement over the original design A.

Design C has the additional attractive feature that the maximum drift distance is reduced by a factor of 2 and thus the chamber may be operated at half the voltage originally anticipated for ISIS. Since high voltage tests in Argon (20%) CO_2 have shown that breakdown and corona may be a problem in a device with a 50cm drift space, design C, with a 25cm drift space, is especially attractive. Therefore, since the track resolution of design C is at an acceptable level, this design has been proposed for ISIS.

Table VI gives the fraction of tracks of a given momentum and primary multiplicity entering the full ISIS as a function of the amount of track which is clearly resolved for design C. Table VII gives the same data with the event-related background described in section I. Since this slowly diverging background has been found to be rather pessimistic, the actual results should be somewhere between those of Tables VI and VII. Nevertheless, in view of the difference between Tables VI and VII, it clearly would be very desirable to reduce the background by increasing the aperture in the magnet.

Since it may be possible to improve the spacial resolution because of the smaller drift space, a study has been made of the track overlap characteristics for a spacial resolution of 0.5cm. Table VIII gives these results together with those for 1.0cm spacial resolution. The factor of two in track resolution is seen to give an approximately 13% increase in the fraction of

tracks which are at least 90% clear.

Additional studies were made to determine the effect of connecting signal wires from the two signal wire planes in a systematic way to reduce the amount of electronics required for analysis. The following two schemes were tested, 1) wires in the upper plane were successively connected from the front to wires in the lower plane from the back, and 2) wires from the front half of the upper plane were successively connected to wires in the back half of the lower plane and wires from the back half of the upper plane were successively connected to wires in the front half of the lower plane (see figure 8). Both tests gave virtually identical results. Table IX compares these tests with the test of design C. In view of these results it is not desirable to connect signal wires from the two sense wire planes.

III. Particle Identification

The ability of ISIS to identify particles rests on an accurate determination of the ionization loss dE/dx. Figure 9 taken from W. W. M. Allison et al.[4] shows the mean ionization of a π, k, and p in A(20%) CO_2 as a function of particle momentum. However, since a series of measurements of dE/dx will be distributed in a Landau distribution such as that shown in figure 10, a large number of measurements will be needed to get an accurate determination of the mean ionization. If one then plots a distribution of the calculated mean ionization for all particles seen by ISIS for a given momentum one will obtain

peaks corresponding to different particle types. The locations of these peaks will correspond to their relative ionizations and their widths to the expected resolution of ISIS. This resolution depends both on the statistics of the amount of ionization in each sample and on the number of samples. Thus it is proportional to the square root of the number of samples used in calculating the mean. W. W. M. Allison et al. have shown that 6.2% full width at half maximum (FWHM) may be obtained with 330 samples. Since the Fermilab ISIS will provide a maximum of 192 samples the expected width of these peaks with maximum track resolution is 8.1% FWHM. Figures 11, 12, 13 and 14 show results for several momenta assuming that the ratio of $\pi/k/p$ is 10/1/1.

For the purposes of this study, a particle identification was made from figures 11 through 14 by making two partitions in the mean ionization loss corresponding to the point where a particle is as likely to be a kaon as a proton and the point where a particle is as likely to be a kaon as a pion. All particles with a mean ionization loss less than the first partition are identified as protons and all particles with a mean ionization loss greater than the second partition are identified as pions. The remaining particles with mean ionization loss between the two partitions are identified as kaons.

Figure 15 gives the percentage of pions, protons and kaons which are correctly identified with 192 ionization samples for all particles. The efficiency of ISIS for identifying protons is $\gtrsim$ 80% for the entire range from 5 to 80 GeV/c. The percentage of kaons which are correctly identified falls from 75% at 7 GeV/c to 50% at 43 GeV/c.

An important parameter in the analysis of ISIS data will be the probability that a given particle is correctly identified. For this purpose figure 16 gives the percentage of the particles called kaons which are correctly identified. Corresponding curves for protons and pions are also given. Although figure 15 states that only 50% of the kaons will be correctly identified at 43 GeV/c, figure 16 states that of those particles identified as kaons 62% will actually be kaons at 43 GeV/c. The apparent discrepancy between figure 15 and 16 results from the fact that in figure 16 the number of particles called a given type is not independent of momentum. Although more kaons are misidentified at higher momenta which results in the fast fall of the kaon curve in figure 15, the fall is less drastic in figure 16 because fewer particles are called kaons at higher momenta. Figure 16 indicates that the Fermilab ISIS will be a useful kaon identifier up to at least 40 GeV/c.

In conclusion it should be stated that although these last figures are a realistic estimate of the ultimate resolution of the Fermilab ISIS based on the current state of the technique, we are looking into the possibility of improving the particle identification by looking not only at the mean ionization, but also at the width of the Landau distributions of the ionization samples. Others have found that such considerations should lead to a significant improvement in resolution.(5)

IV. Conclusion

The Fermilab ISIS will be a two module device. The first module, ISIS-1, will be 1x1x1m with its entrance plane at x=2.375m. The second module, ISIS-2, will be 1x1x2m with its entrance plane at x=4.125m. 97% of the particles which escape the aperture of the bubble chamber magnet traverse the entire length of ISIS-1 while 80% of the particles traverse the entire length of ISIS-2.

The Fermilab ISIS will consist of a sandwich of two signal wire planes and three high voltage planes. The high voltage plane in the center of the sandwich will be at beam height. For this configuration an average of approximately 80% of the ionization samples for tracks with momentum between 5 and 80 GeV/c will be useful if there is no background. For a pessimistic simulated background this average falls to approximately 70%. Again for the case with no background, the average percentage of useful ionization samples varies from 60% at 5 GeV/c to 85% at 80 GeV/c.

Particle identification studies have shown that for 192 ionization samples between 85 and 80% of the protons are correctly identified in the range from 5 to 80 GeV/c. The percentage of kaons which are correctly identified falls approximately linearly from 75% at 7 GeV/c to 37% at 60 GeV/c. Nevertheless the Fermilab ISIS will be a useful kaon identifier up to at least 40 GeV/c. The particle identification may be improved, as others have found, by looking not only at the mean ionization, but also at the width of the Landau distributions of the ionization samples. This possibility will be studied.

REFERENCES

1. D. Fong et al., Nucl. Phys. B102, 386 (1974)
2. A. Firestone et al., Phys. Rev. D14, 2902 (1976)
3. W. W. M. Allison and R. W. Pleming, ISIS note 25
4. W. W. M. Allison et al., Nucl. Inst. and Meth. 119, 499 (1974)
5. Time Projection Chamber Group Proposal to PEP

Figure 1 Momentum distribution for all particles from simulated 300 GeV/c events and for those which escape through the bubble chamber magnet aperture into the downstream system (unshaded).

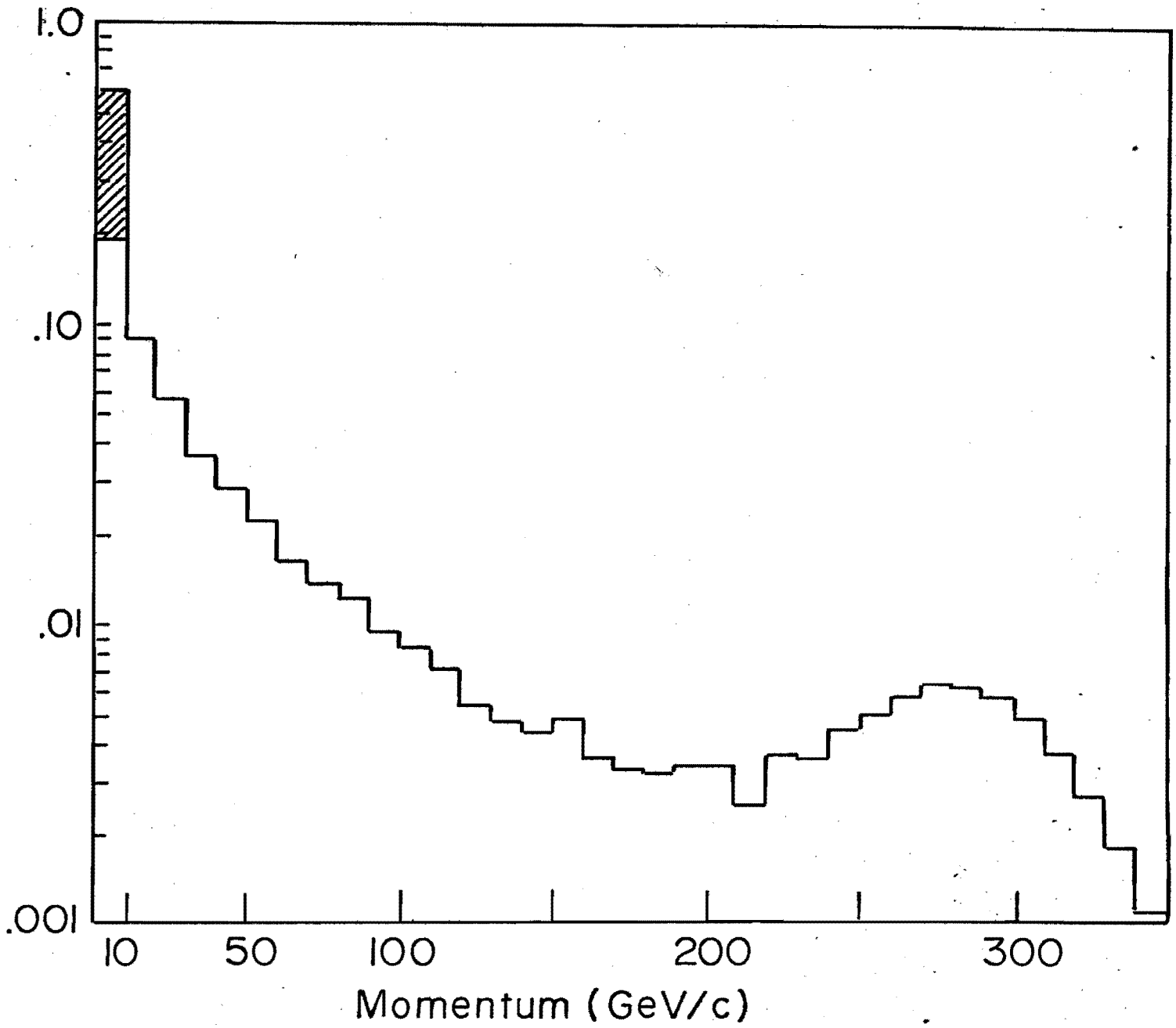
1.0
.10
.01
.001
10
50
100
200
300
Momentum (GeV/c)

Figure 2 Rapidity distribution for A) all particles from the simulated 300 GeV/c events, B) the particles which escape the magnet, C) the particles with $p > 5$ GeV/c which escape the magnet, and D) the particles with $p > 5$ which pass through a 1m x 1m x 3m long ISIS ending of $x = 6.125$m.

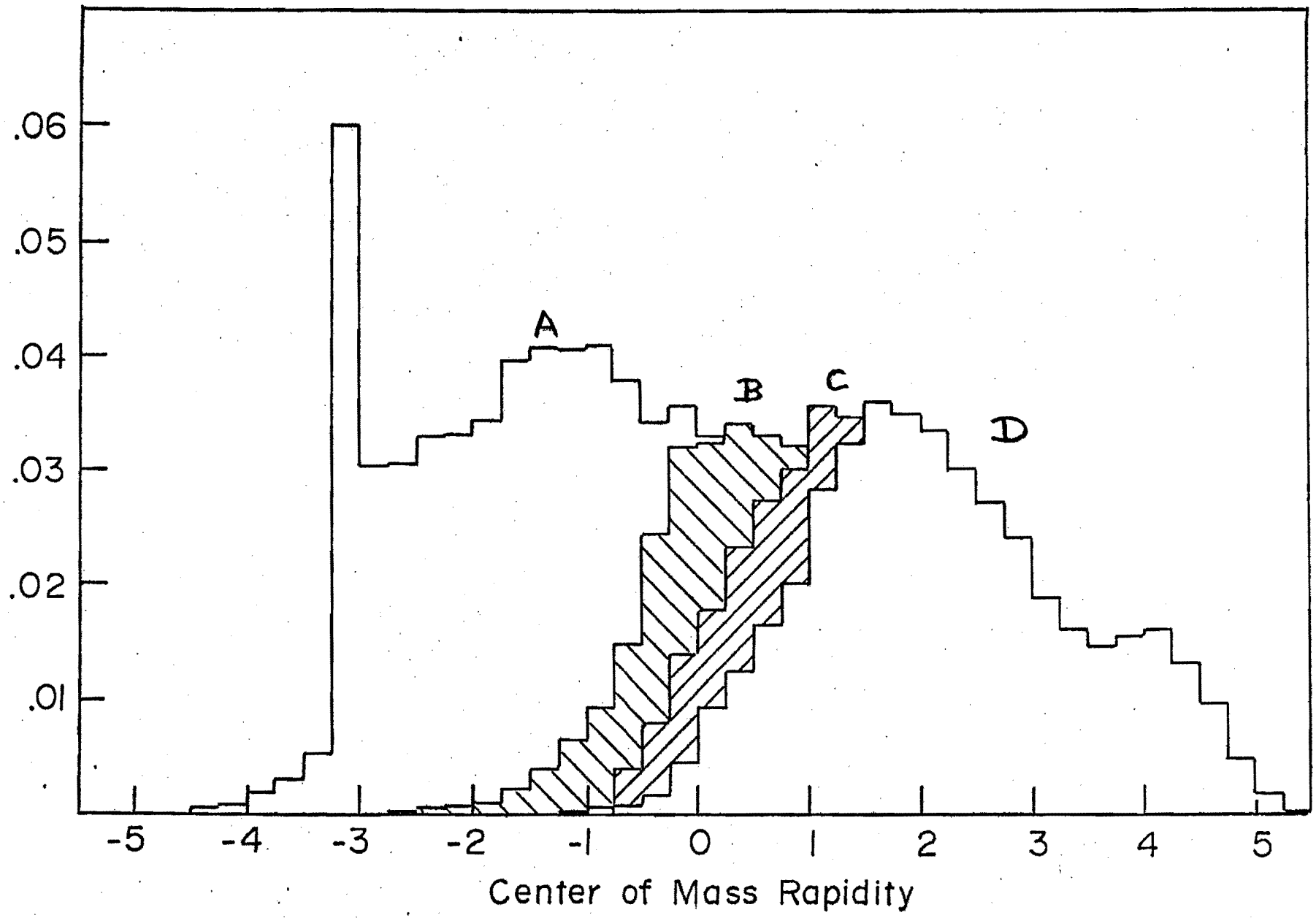
.06
.05
.04
.03
.02
.01
A
B
C
D
-5
-4
-3
-2
-1
0
1
2
3
4
5
Center of Mass Rapidity

Figure 3 Distribution of the number of events which result in a given number of charged particles in ISIS-1.

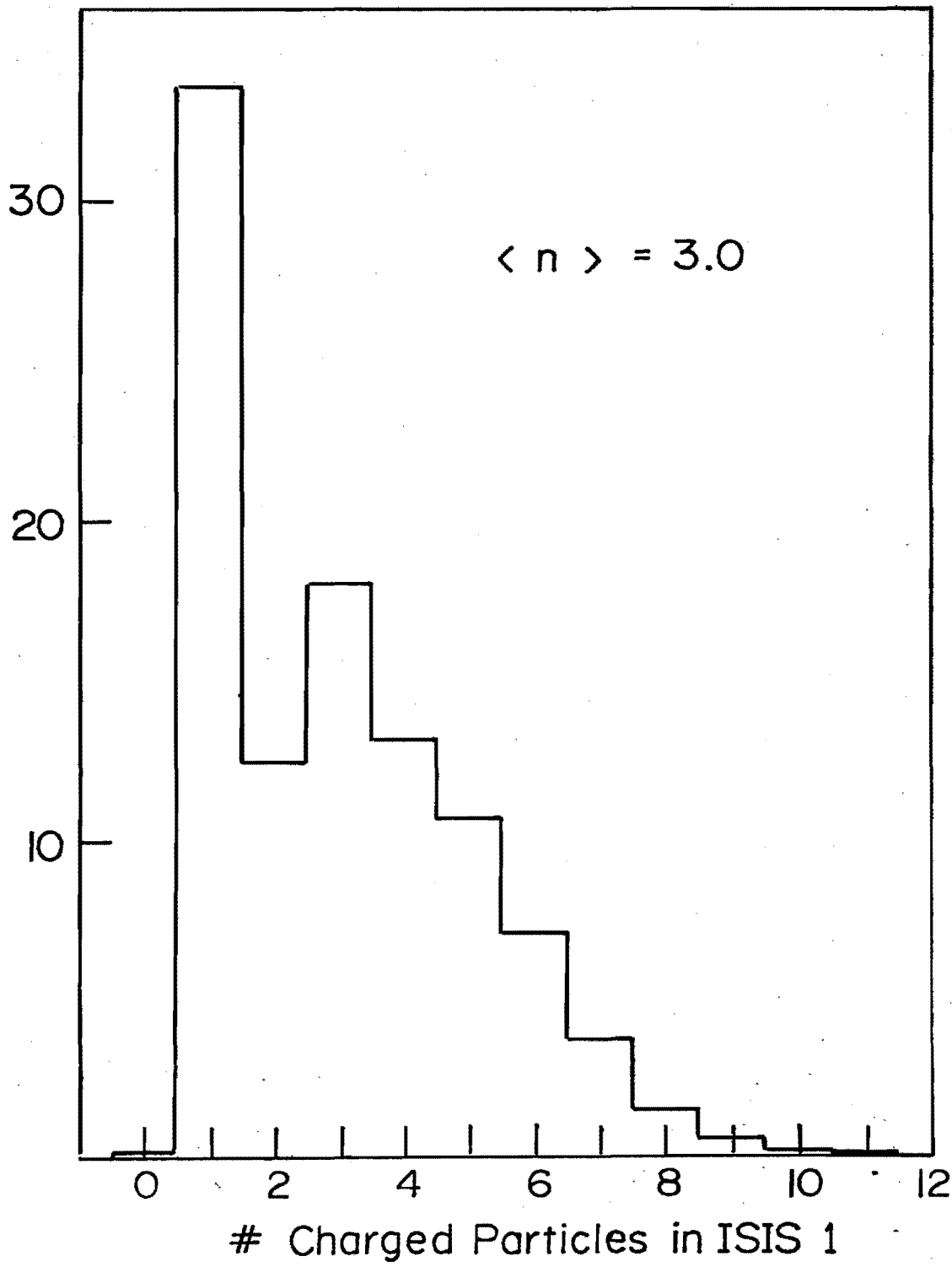
30
20
10
< n > = 3.0
0
2
4
6
8
10
12
Charged Particles in ISIS 1

Figure 4 Distribution of the number of events which result in a given number of charged particles in ISIS-2.

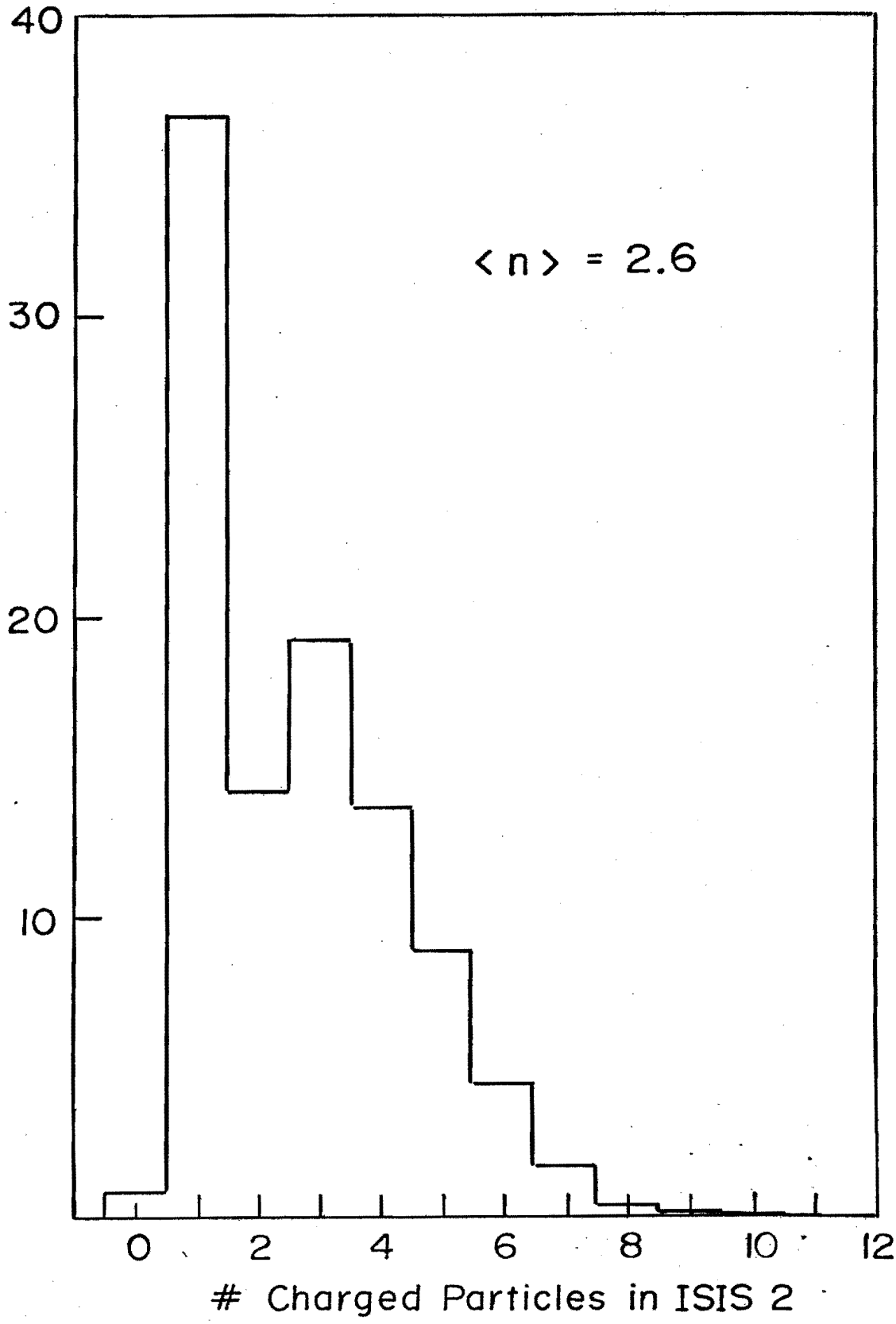
40
30
20
10
⟨n⟩ = 2.6
0
2
4
6
8
10
12
Charged Particles in ISIS 2

Figure 5 Charged prong multiplicity distribution 360 GeV/c $\pi^- p$ [3]

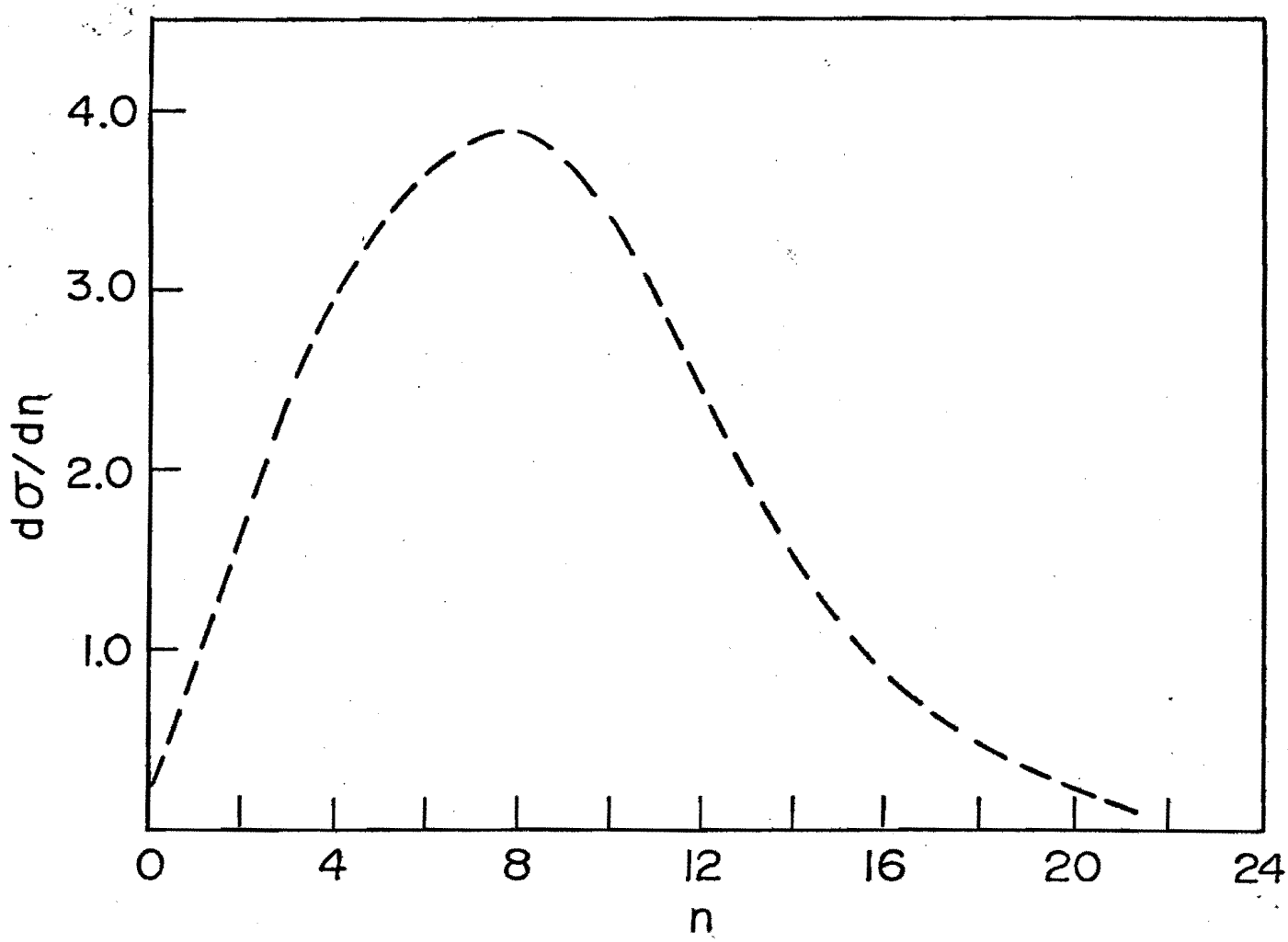
4.0
3.0
2.0
1.0
dσ/dη
0
4
8
12
16
20
24
n

Figure 6 Number of tracks as a function of multiplicity for 300 GeV/c $\pi^- p$. Solid line-entrance to ISIS-1. Dashed line-entrance to ISIS-2.

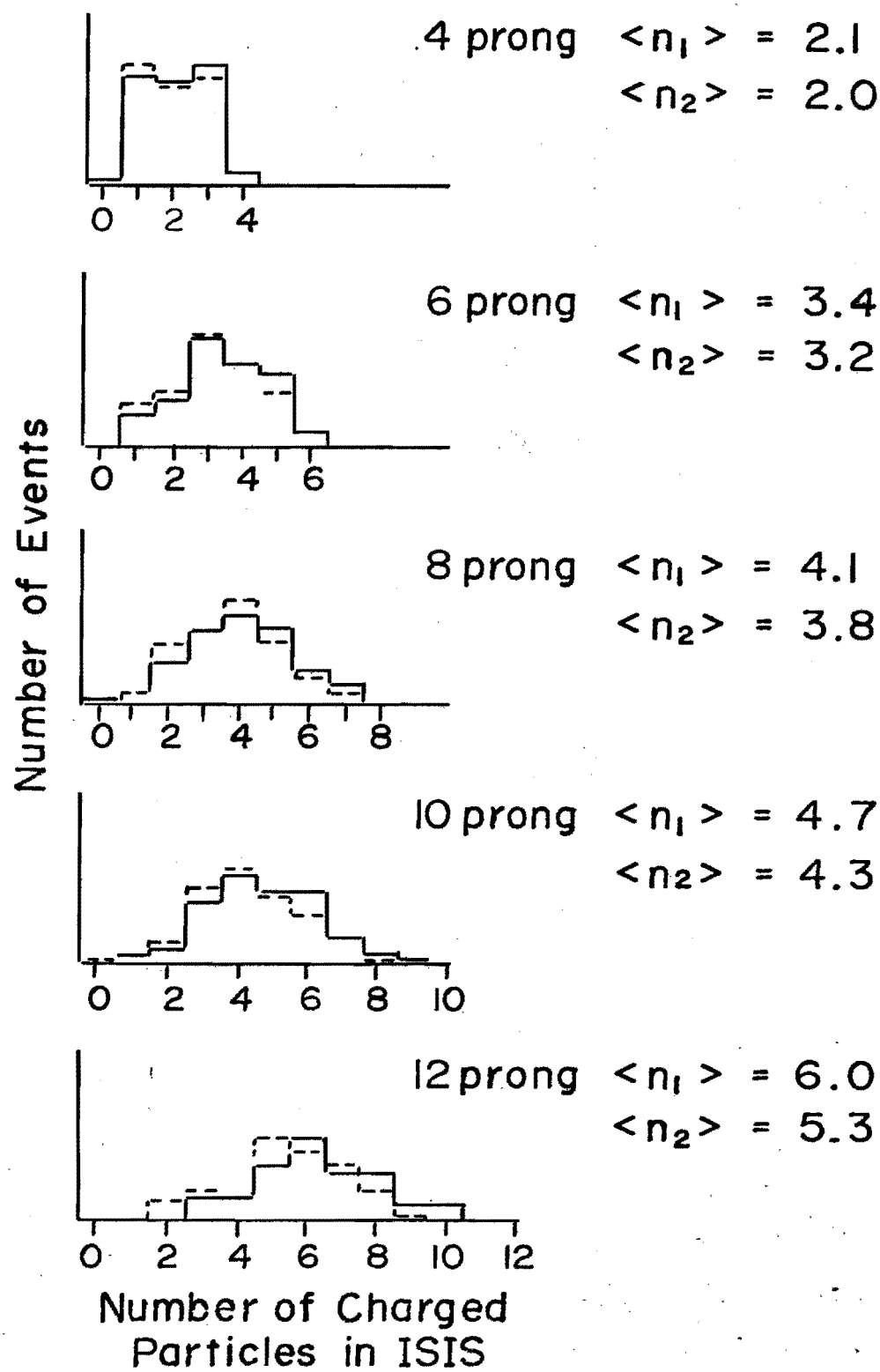
4 prong
<n1> = 2.1
<n2> = 2.0
6 prong
<n1> = 3.4
<n2> = 3.2
8 prong
<n1> = 4.1
<n2> = 3.8
10 prong
<n1> = 4.7
<n2> = 4.3
12 prong
<n1> = 6.0
<n2> = 5.3
Number of Events
Number of Charged Particles in ISIS

Figure 7: Configuration of the high voltage and signal wire planes for the three designs of ISIS which were tested. For a comparison of these designs, see Table V.

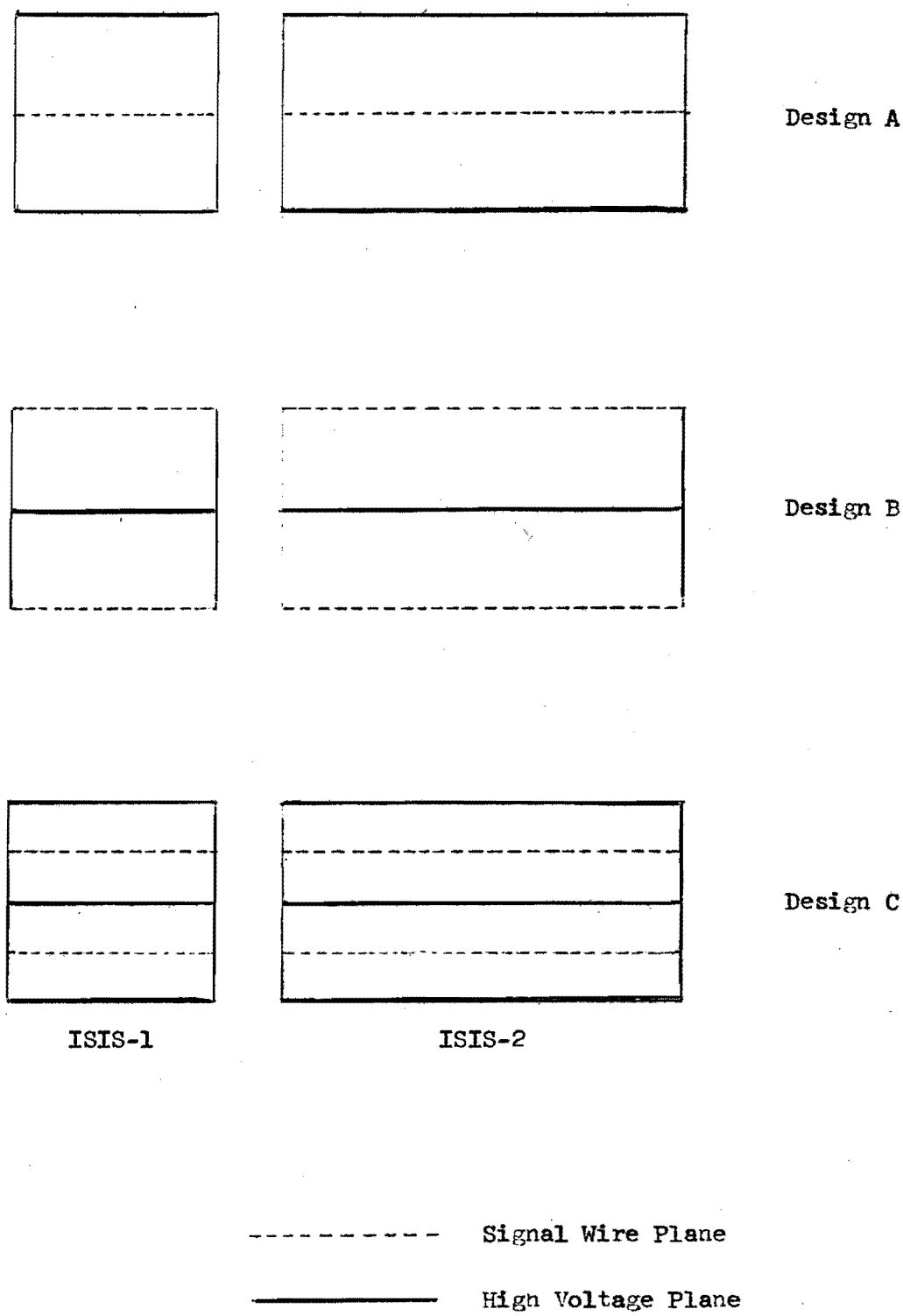
Design A
Design B
Design C
ISIS-1
ISIS-2
Signal Wire Plane
High Voltage Plane

Figure 8: Drawings showing how the signal wires could be connected to reduce the amount of required electronics. For a comparison of these two configurations with design C of Figure 7, see Table IX.

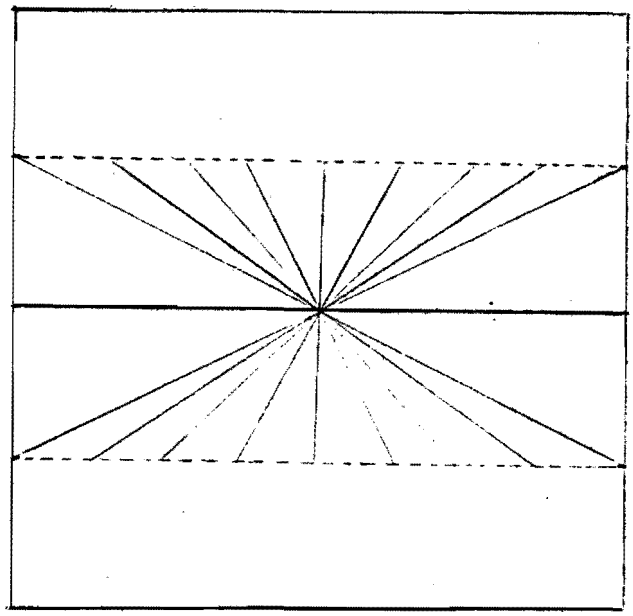

Test 1

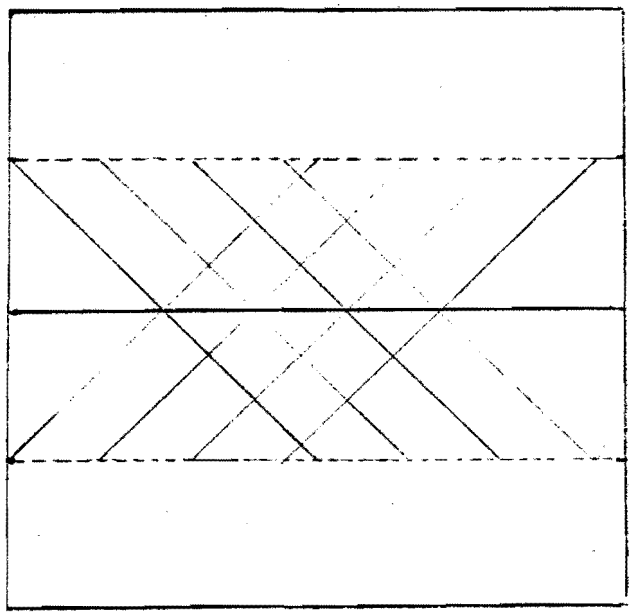

Test 2

Diagonal Lines Denote Wire Conections

Figure 9 Mean ionization loss in 80% A-20% CO_2 as a function of momentum for pions, kaons, and protons (taken from ref. 4).

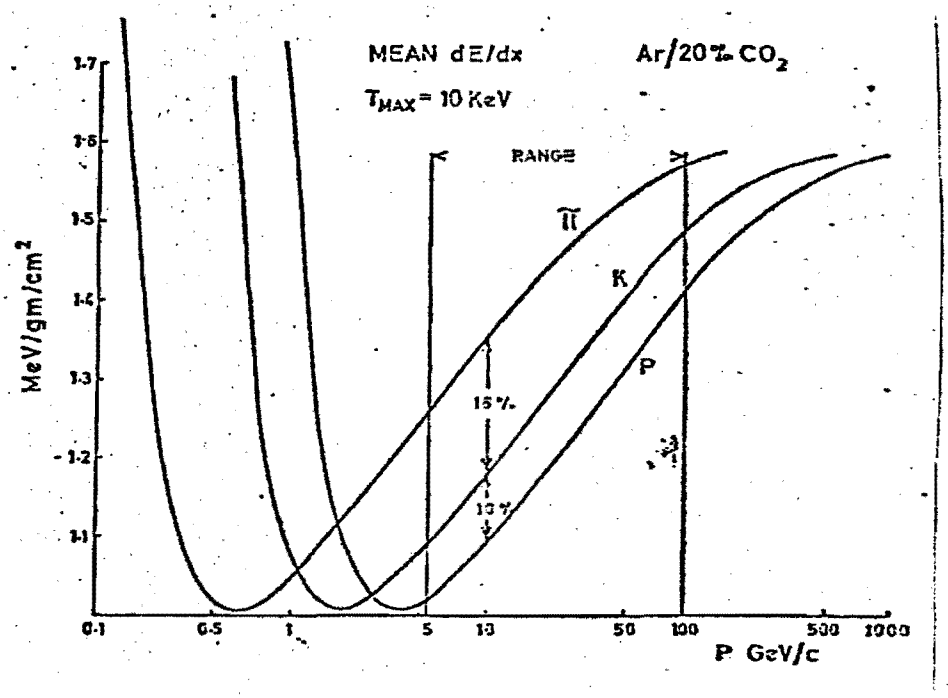
MEAN dE/dx
Ar/20% CO2
TMAX = 10 KeV
RANGE
π
K
P
15%
13%
MeV/gm/cm2
1.7
1.6
1.5
1.4
1.3
1.2
1.1
0.1
0.5
1
5
10
50
100
500
1000
P GeV/c

Figure 10: Ionization loss for 3 GeV/c pions in 1.5cm of 93% A-7% CHy (taken from ref. 4).

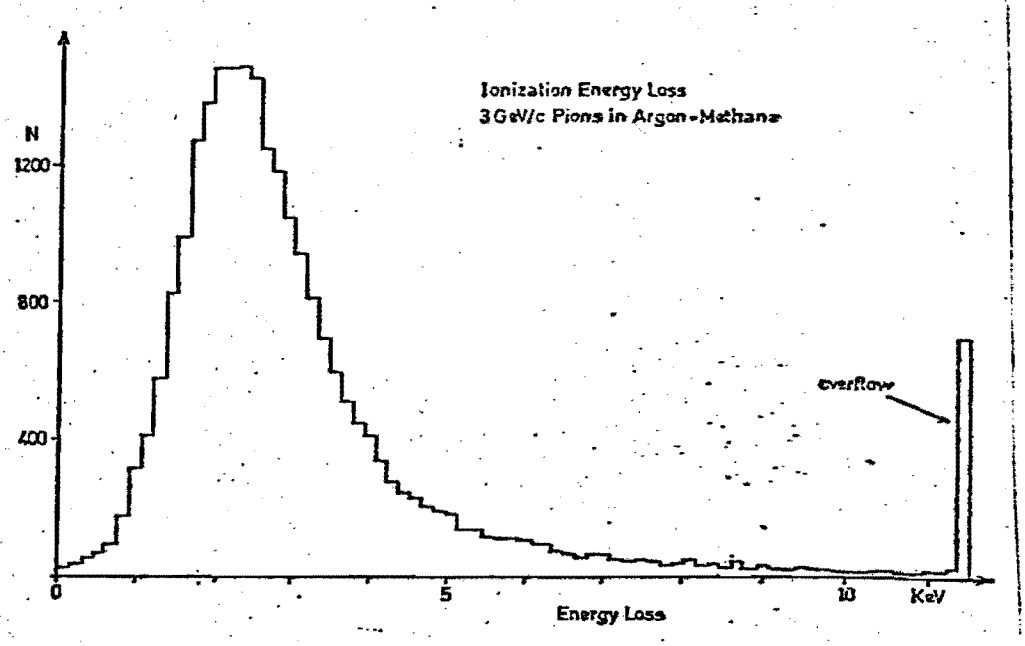
Ionization Energy Loss
3 GeV/c Pions in Argon-Methane
N
1200
800
400
0
5
10
KeV
Energy Loss
overflow

Figure 11: Mean ionization loss in ISIS for 5 Gev/c protons, kaons and pions ($p:k:\pi = 1:1:10$).

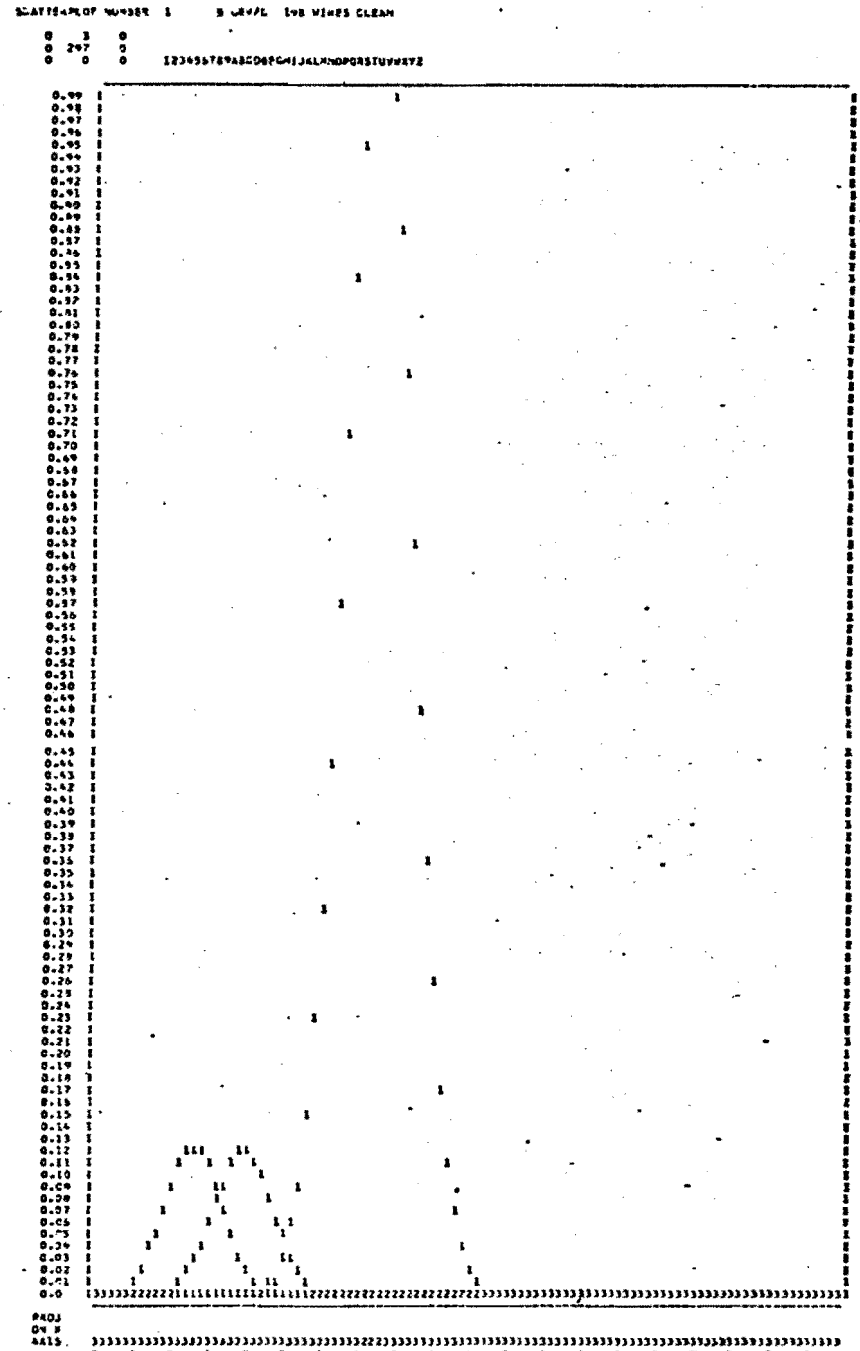
SCATTERPLOT NUMBER 1
PROJ BY X AXIS
PROJ BY Y AXIS
LOW EDGE VALU

Figure 12: Mean ionization loss in ISIS fo 10 Gev/c protons, kaons and pions ($p:k:\pi = 1:1:10$).

SCATTERPLOT NUMBER 5 10 LEV/C 198 NIAES CLEAN

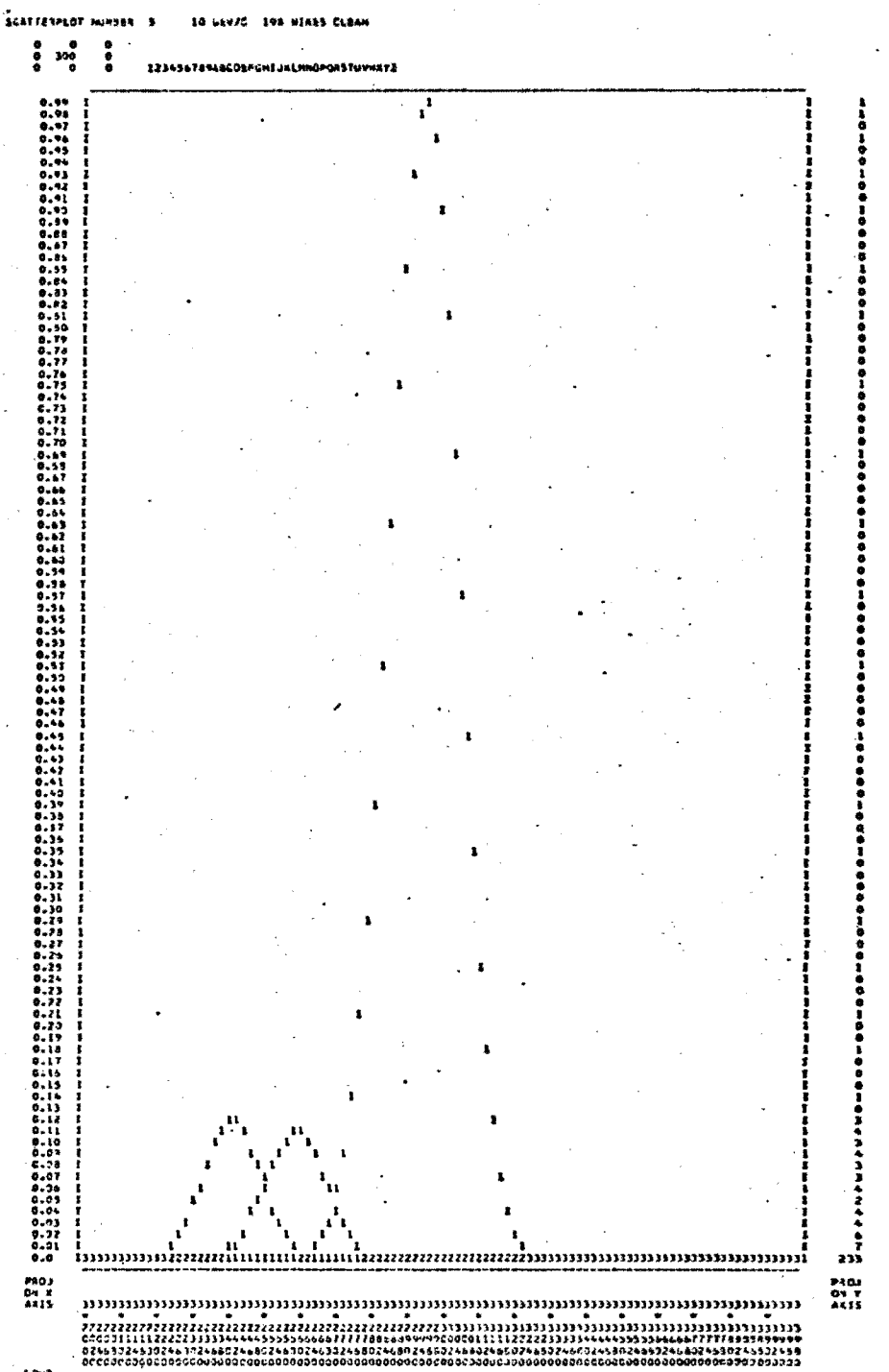

Figure 13: Mean ionization loss in ISIS for 20 Gev/c protons, kaons and pions ($p:k:\pi = 1:1:10$).

SCATTERPLOT NUMBER 5 20 LEVEL 198 WIRES CLEAN

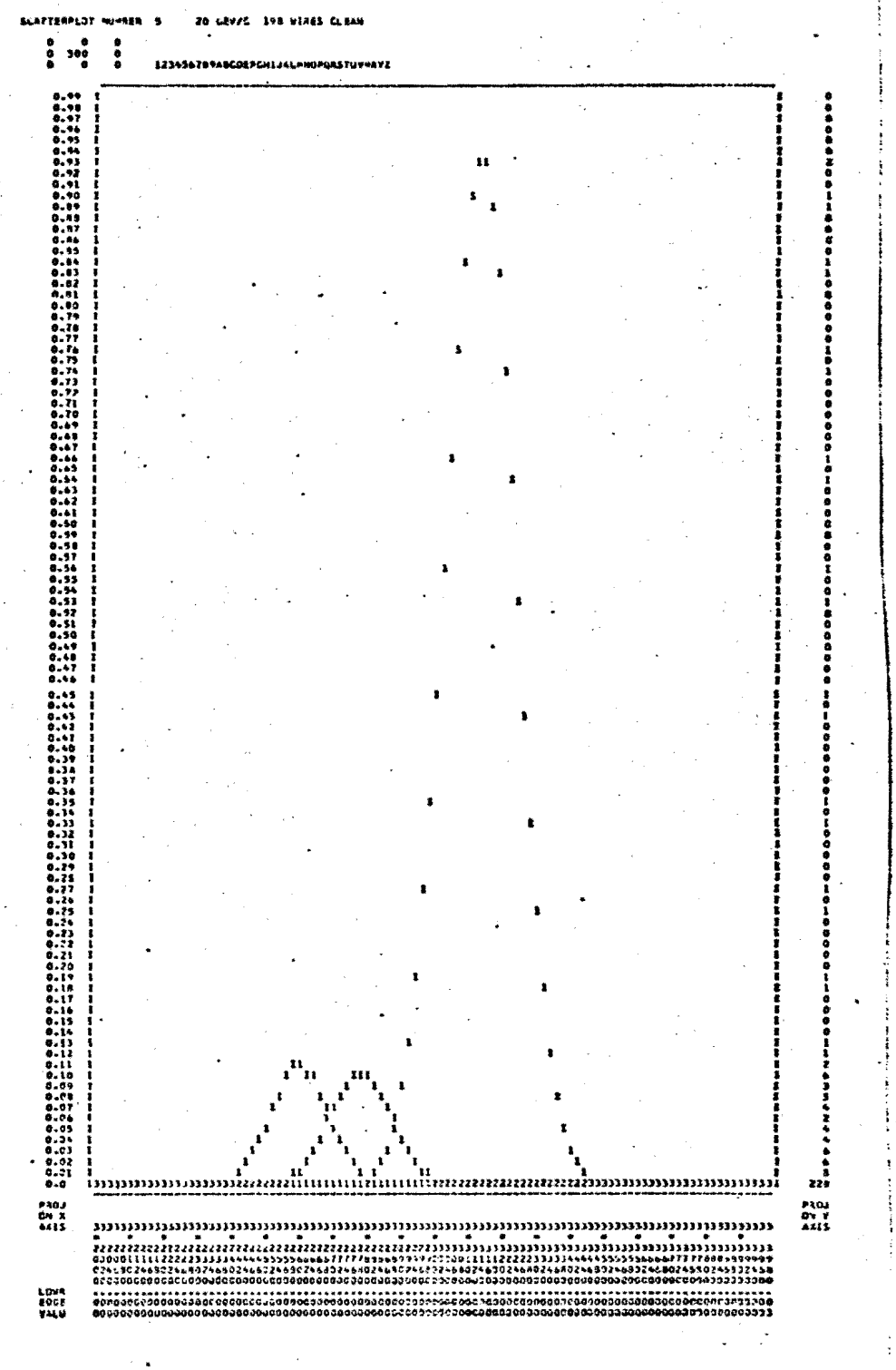

Figure 14: Mean ionization loss in ISIS for 60 Gev/c protons, kaons and pions ($p:k:\pi = 1:1:10$).

SCATTERPLOT NUMBER 9 6D GEV/C 1V6 WIRES CLEAN

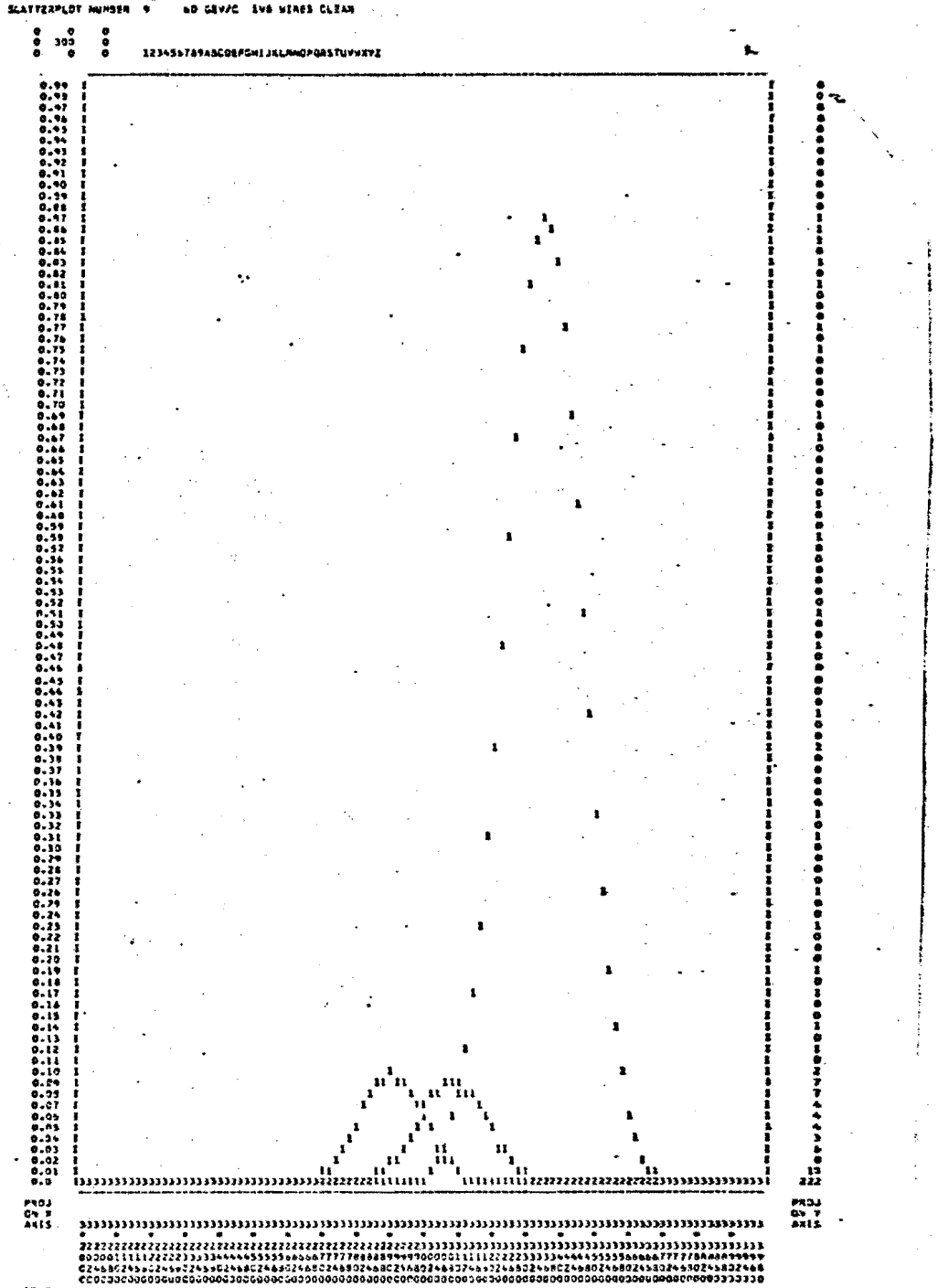

Figure 15: Percentage of particles of a given type which are correctly identified assuming that the ratio of $\pi/k/p$ is 10/1/1 for all momenta.

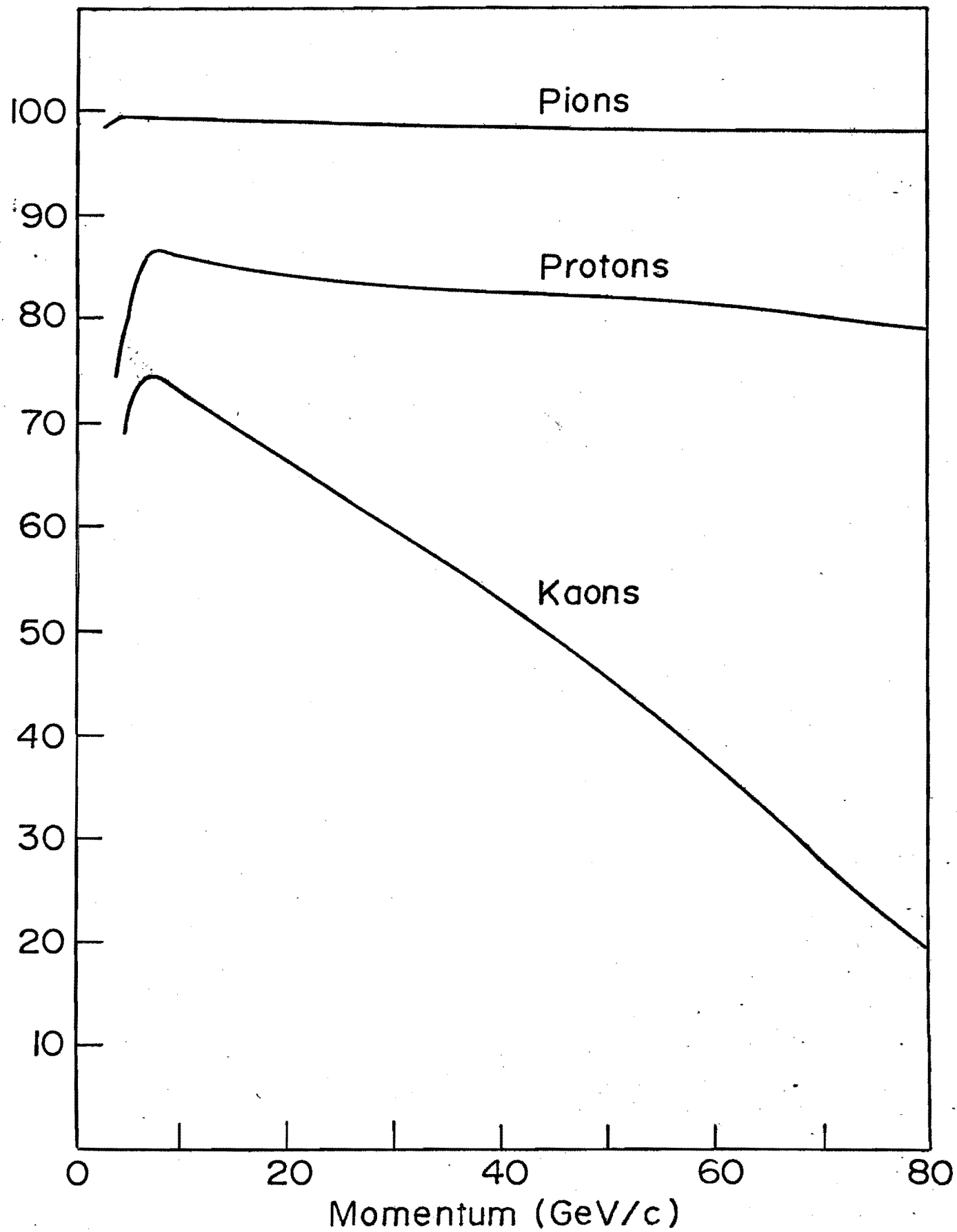
Pions
Protons
Kaons
100
90
80
70
60
50
40
30
20
10
0
20
40
60
80
Momentum (GeV/c)

Figure 16: Percentage of particles called a given type which are correctly identified assuming that the ratio of $\pi/k/p$ is 10/1/1 for all momenta.

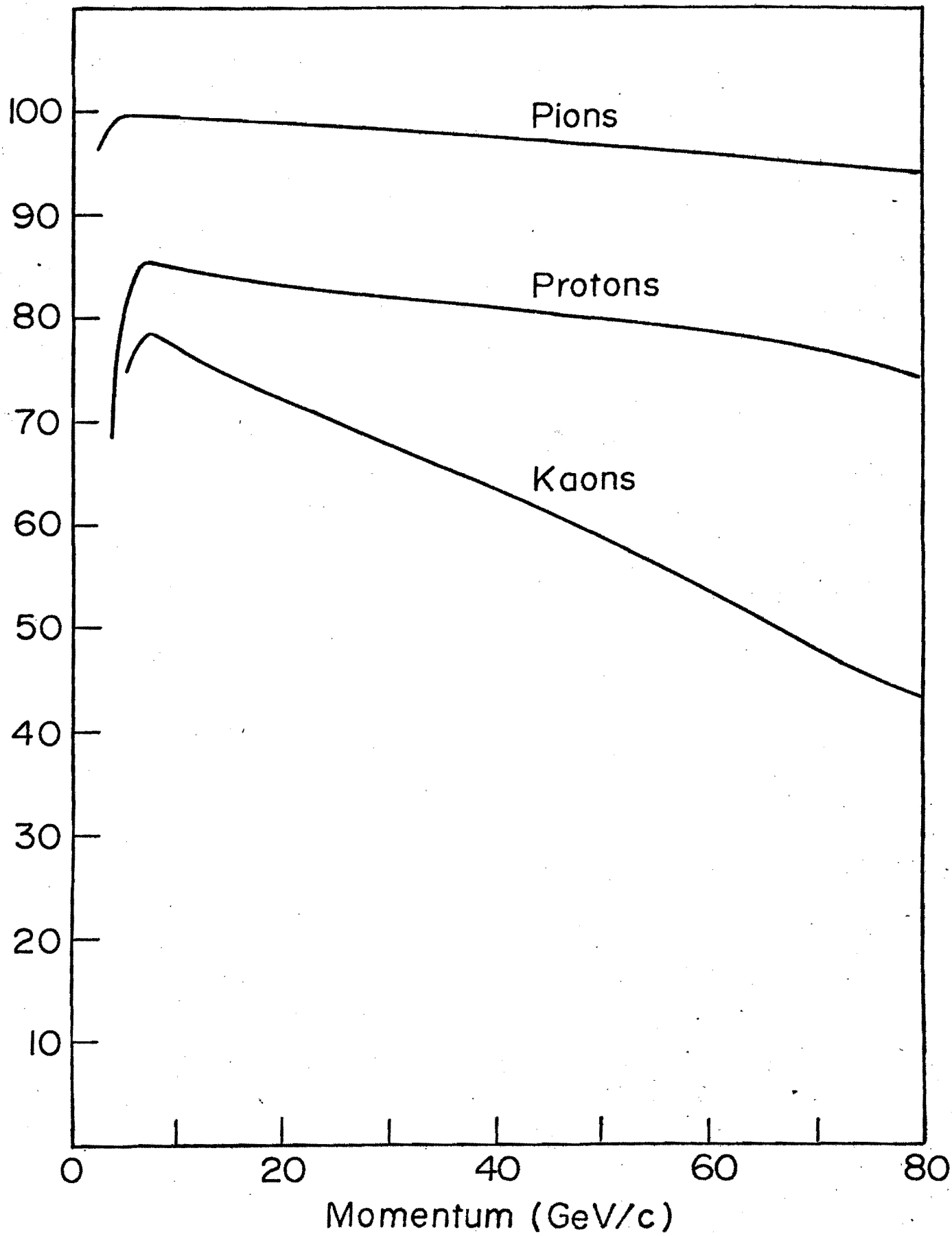
100
90
80
70
60
50
40
30
20
10
Pions
Protons
Kaons
0
20
40
60
80
Momentum (GeV/c)

Table I

PERCENTAGE OF TRACKS WHICH ESCAPE THE MAGNET AND TRAVERSE THE ENTIRE LENGTH OF ISIS-1 FOR VARIOUS DIMENSIONS OF ISIS IN METERS IN THE Y DIRECTION (COLUMNS) AND THE Z DIRECTION (ROWS)

	1.000	1.025	1.050	1.075	1.100	1.125	1.150	1.175	1.200
1.000	96.6	97.0	97.3	97.7	97.9	98.1	98.3	98.4	98.6
1.025	96.7	97.0	97.4	97.7	98.0	98.2	98.3	98.5	98.6
1.050	96.7	97.0	97.4	97.7	98.0	98.2	98.3	98.5	98.6
1.075	96.7	97.0	97.4	97.7	98.0	98.2	98.3	98.5	98.6
1.100	96.7	97.0	97.4	97.7	98.0	98.2	98.3	98.5	98.6
1.125	96.7	97.0	97.4	97.7	98.0	98.2	98.3	98.5	98.6
1.150	96.7	97.0	97.4	97.7	98.0	98.2	98.3	98.5	98.6
1.175	96.7	97.0	97.4	97.7	98.0	98.2	98.3	98.5	98.6
1.200	96.7	97.0	97.4	97.7	98.0	98.2	98.3	98.5	98.6

Table II

PERCENTAGE OF TRACKS WHICH ESCAPE THE MAGNET AND TRAVERSE THE ENTIRE LENGTH OF ISIS-2 FOR VARIOUS DIMENSIONS OF ISIS IN METERS IN THE Y DIRECTION (COLUMNS) AND THE Z DIRECTION (ROWS)

	1.000	1.025	1.050	1.075	1.100	1.125	1.150	1.175	1.200
1.000	79.7	80.5	81.1	81.7	82.5	83.1	83.7	84.3	84.7
1.025	79.9	80.7	81.3	81.9	82.6	83.3	83.9	84.4	84.9
1.050	80.0	80.8	81.4	82.0	82.7	83.4	84.0	84.6	85.0
1.075	80.1	80.9	81.5	82.2	82.9	83.6	84.2	84.7	85.1
1.100	80.2	81.0	81.6	82.2	83.0	83.6	84.2	84.8	85.2
1.125	80.3	81.1	81.7	82.4	83.1	83.8	84.4	85.0	85.4
1.150	80.5	81.3	81.9	82.5	83.2	83.9	84.5	85.1	85.6
1.175	80.5	81.4	82.0	82.6	83.4	84.1	84.7	85.2	85.7
1.200	80.6	81.4	82.1	82.7	83.4	84.1	84.7	85.3	85.7

Table III. Comparison of results both with and without signal wire plane reflection as a function of momentum and primary multiplicity. f_{160} is the fraction of tracks with 160 of 187 cells clear.

Momentum Range	Number of Prongs	f_{160} Reflected	f_{160} Not Reflected
5<p<10	4	.58	.51
	6	.48	.56
	8	.46	.51
	10	.36	.46
	12	.37	.44
10<p<20	4	.75	.91
	6	.72	.87
	8	.66	.83
	10	.64	.80
	12	.50	.74
20<p<70	4	.56	.89
	6	.44	.80
	8	.49	.75
	10	.44	.78
	12	.37	.73

Table IV. Comparison of the track overlap characteristics of the full ISIS with vertical and with horizontal wire orientations. The table gives the percentage of all tracks with $5<p<70$ GeV/c from events with multiplicity greater than or equal to 4 as a function of the percentage of the track which can be resolved from all other tracks in the event.

	% of track which is resolvable				
	90-100%	70-90%	50-70%	30-50%	10-30%
Verticle wire (y)	35%	7%	12%	9%	5%
Horizontal wire (z)	46%	14%	16%	10%	5%

Table V. Comparison of the track overlap characteristics of the full ISIS for the three designs described in the text. The table gives, as a function of momentum, the percentage of all tracks which traverse the entire length of ISIS with at least 90% of the track clear and the percentage of tracks with between 70 and 90% of the track clear. Also given are the average percentage clear for tracks at a given momentum and also the number of tracks in the test sample.

	Momentum	% of track clear		Avg.% Clear	Sample Size
		90-100%	70-90%		
Design A	5-10	27.1	39.7	74.2	1063
	10-20	29.6	35.9	72.5	2431
	20-40	28.0	26.8	65.6	2852
	40-80	26.4	22.4	60.9	2515
Design B	5-10	85.9	5.6	94.2	1063
	10-20	86.0	3.1	92.0	2431
	20-40	80.5	4.0	87.7	2852
	40-80	75.8	5.7	84.6	2515
Design C	5-10	75.8	15.0	90.9	1030
	10-20	80.2	8.9	89.5	2368
	20-40	77.3	7.7	86.5	2647
	40-80	73.5	8.9	83.9	2177

Table VIa-n: The following tables give as a function of momentum and primary multiplicity for ISIS-1, ISIS-2; and the full ISIS (ISIS-3) the fraction of particles with a given percentage of their track clearly resolvable from other tracks in the same event. The table also gives the average percentage of the track which is lost due to overlap or to exiting from the sides of ISIS. The total number of particles used to calculate any particular set of data in the table is also given.

Table VIa: Track resolution characteristics for all particles entering ISIS.

MOMENTUM	PRONGS			0-9	1-30	3-50	5-70	70-	AVE	SAMPLE
5-10 GEV/C	ALL	FLAG1	ISIS1	.596	.234	.053	.027	.090	15.8	2747.
5-10 GEV/C	ALL	FLAG1	ISIS2	.295	.129	.076	.079	.421	50.4	2747.
5-10 GEV/C	ALL	FLAG1	ISIS3	.304	.144	.133	.201	.217	38.7	2747.
10-20 GEV/C	ALL	FLAG1	ISIS1	.713	.164	.014	.016	.093	13.3	2795.
10-20 GEV/C	ALL	FLAG1	ISIS2	.664	.171	.037	.032	.096	15.6	2795.
10-20 GEV/C	ALL	FLAG1	ISIS3	.705	.117	.069	.047	.062	14.7	2795.
20-40 GEV/C	ALL	FLAG1	ISIS1	.691	.123	.018	.015	.153	18.6	2903.
20-40 GEV/C	ALL	FLAG1	ISIS2	.777	.101	.017	.011	.094	12.5	2903.
20-40 GEV/C	ALL	FLAG1	ISIS3	.756	.080	.050	.022	.091	14.4	2903.
40-80 GEV/C	ALL	FLAG1	ISIS1	.676	.095	.022	.026	.181	21.7	2538.
40-80 GEV/C	ALL	FLAG1	ISIS2	.762	.100	.009	.012	.115	14.3	2538.
40-80 GEV/C	ALL	FLAG1	ISIS3	.726	.090	.046	.022	.116	16.7	2538.

Table VIb: Track resolution characteristics for all particles which traverse the entire length of ISIS.

MOMENTUM	PRONGS			0-9	1-30	3-50	5-70	70-	AVE	SAMPLE
5-10 GEV/C	ALL	FLAGO	ISIS1	.665	.240	.025	.011	.059	11.2	2417.
5-10 GEV/C	ALL	FLAGO	ISIS2	.745	.200	.020	.005	.031	8.0	1049.
5-10 GEV/C	ALL	FLAGO	ISIS3	.758	.150	.052	.017	.022	9.1	1030.
10-20 GEV/C	ALL	FLAGO	ISIS1	.717	.164	.013	.015	.091	13.0	2743.
10-20 GEV/C	ALL	FLAGO	ISIS2	.756	.168	.012	.009	.055	9.5	2411.
10-20 GEV/C	ALL	FLAGO	ISIS3	.802	.089	.041	.013	.054	10.5	2368.
20-40 GEV/C	ALL	FLAGO	ISIS1	.691	.125	.018	.013	.153	18.5	2760.
20-40 GEV/C	ALL	FLAGO	ISIS2	.791	.100	.014	.009	.086	11.5	2788.
20-40 GEV/C	ALL	FLAGO	ISIS3	.773	.077	.048	.015	.087	13.5	2647.
40-80 GEV/C	ALL	FLAGO	ISIS1	.676	.093	.023	.023	.185	21.9	2333.
40-80 GEV/C	ALL	FLAGO	ISIS2	.769	.103	.008	.012	.108	13.6	2380.
40-80 GEV/C	ALL	FLAGO	ISIS3	.735	.089	.048	.016	.112	16.1	2177.

Table VIc: Track resolution characteristics for all particles entering ISIS from 4 prong events.

MOMENTUM	PRONGS			0-9	1-30	3-50	5-70	70-	AVE	SAMPLE
5-10 GEV/C	4	FLAG1	ISIS1	.801	.075	.033	.039	.052	9.5	306.
5-10 GEV/C	4	FLAG1	ISIS2	.458	.065	.072	.069	.337	40.5	306.
5-10 GEV/C	4	FLAG1	ISIS3	.458	.101	.108	.212	.121	30.0	306.
10-20 GEV/C	4	FLAG1	ISIS1	.913	.044	.006	.003	.035	4.6	344.
10-20 GEV/C	4	FLAG1	ISIS2	.869	.052	.015	.020	.044	6.9	344.
10-20 GEV/C	4	FLAG1	ISIS3	.887	.029	.035	.029	.020	6.1	344.
20-40 GEV/C	4	FLAG1	ISIS1	.884	.028	.002	.0	.086	9.0	466.
20-40 GEV/C	4	FLAG1	ISIS2	.929	.024	.006	.002	.039	4.5	466.
20-40 GEV/C	4	FLAG1	ISIS3	.897	.015	.045	.006	.036	6.0	466.
40-80 GEV/C	4	FLAG1	ISIS1	.821	.029	.033	.010	.107	13.2	485.
40-80 GEV/C	4	FLAG1	ISIS2	.918	.023	.0	.006	.054	6.1	485.
40-80 GEV/C	4	FLAG1	ISIS3	.845	.058	.037	.0	.060	8.4	485.

Table VId: Track resolution characteristics for all particles from 4 prong events which traverse the entire length of ISIS.

MOMENTUM	PRONGS			0-9	1-30	3-50	5-70	70-	AVE	SAMPLE
5-10 GEV/C	4	FLAGO	ISIS1	.896	.048	.007	.019	.030	4.9	269.
5-10 GEV/C	4	FLAGO	ISIS2	.936	.043	.014	.007	.0	2.1	140.
5-10 GEV/C	4	FLAGO	ISIS3	.921	.043	.036	.0	.0	3.0	139.
10-20 GEV/C	4	FLAGO	ISIS1	.915	.041	.006	.003	.035	4.6	341.
10-20 GEV/C	4	FLAGO	ISIS2	.936	.045	.0	.003	.016	2.5	314.
10-20 GEV/C	4	FLAGO	ISIS3	.955	.006	.019	.003	.016	3.1	312.
20-40 GEV/C	4	FLAGO	ISIS1	.881	.027	.002	.0	.090	9.3	445.
20-40 GEV/C	4	FLAGO	ISIS2	.937	.023	.005	.002	.034	3.9	444.
20-40 GEV/C	4	FLAGO	ISIS3	.905	.012	.045	.005	.033	5.5	423.
40-80 GEV/C	4	FLAGO	ISIS1	.811	.027	.036	.009	.117	14.0	445.
40-80 GEV/C	4	FLAGO	ISIS2	.918	.024	.0	.006	.052	6.0	462.
40-80 GEV/C	4	FLAGO	ISIS3	.841	.057	.038	.0	.064	8.8	422.

Table VIe: Track resolution characteristics for all particles entering ISIS from 6 prong events.

MOMENTUM	PRONGS			0-9	1-30	3-50	5-70	70-	AVE	SAMPLE
5-10 GEV/C	6	FLAG1	ISIS1	.689	.149	.049	.024	.090	13.8	636.
5-10 GEV/C	6	FLAG1	ISIS2	.327	.119	.068	.083	.403	49.0	636.
5-10 GEV/C	6	FLAG1	ISIS3	.347	.121	.132	.204	.195	37.1	636.
10-20 GEV/C	6	FLAG1	ISIS1	.810	.096	.007	.006	.081	9.9	678.
10-20 GEV/C	6	FLAG1	ISIS2	.726	.150	.028	.010	.086	12.4	678.
10-20 GEV/C	6	FLAG1	ISIS3	.786	.086	.043	.040	.046	11.4	678.
20-40 GEV/C	6	FLAG1	ISIS1	.724	.088	.017	.017	.153	18.2	804.
20-40 GEV/C	6	FLAG1	ISIS2	.786	.095	.016	.009	.095	12.1	804.
20-40 GEV/C	6	FLAG1	ISIS3	.784	.058	.044	.026	.088	14.0	804.
40-80 GEV/C	6	FLAG1	ISIS1	.681	.093	.011	.039	.176	21.4	664.
40-80 GEV/C	6	FLAG1	ISIS2	.803	.060	.008	.008	.122	14.1	664.
40-80 GEV/C	6	FLAG1	ISIS3	.748	.071	.038	.024	.119	16.4	664.

Table VIf: Track resolution characteristics for all particles from 6 prong events which traverse the entire length of ISIS.

MOMENTUM	PRONGS			0-9	1-30	3-50	5-70	70-	AVE	SAMPLE
5-10 GEV/C	6	FLAGO	ISIS1	.775	.143	.013	.011	.058	8.9	552.
5-10 GEV/C	6	FLAGO	ISIS2	.804	.160	.012	.0	.024	6.0	250.
5-10 GEV/C	6	FLAGO	ISIS3	.844	.074	.053	.016	.012	7.1	244.
10-20 GEV/C	6	FLAGO	ISIS1	.817	.095	.006	.006	.077	9.5	666.
10-20 GEV/C	6	FLAGO	ISIS2	.808	.128	.010	.002	.052	7.8	600.
10-20 GEV/C	6	FLAGO	ISIS3	.875	.039	.027	.010	.049	8.4	590.
20-40 GEV/C	6	FLAGO	ISIS1	.728	.089	.018	.013	.152	17.9	768.
20-40 GEV/C	6	FLAGO	ISIS2	.795	.093	.015	.008	.089	11.5	776.
20-40 GEV/C	6	FLAGO	ISIS3	.800	.055	.038	.018	.089	13.3	740.
40-80 GEV/C	6	FLAGO	ISIS1	.686	.092	.011	.034	.176	21.2	609.
40-80 GEV/C	6	FLAGO	ISIS2	.814	.061	.008	.006	.111	13.0	622.
40-80 GEV/C	6	FLAGO	ISIS3	.771	.065	.042	.018	.104	14.7	567.

Table VIg: Track resolution characteristics for all particles entering ISIS from 8 prong events.

MOMENTUM	PRONGS			0-9	1-30	3-50	5-70	70-	AVE	SAMPLE
5-10 GEV/C	8	FLAG1	ISIS1	.609	.222	.050	.030	.088	15.6	724.
5-10 GEV/C	8	FLAG1	ISIS2	.291	.141	.068	.086	.414	49.6	724.
5-10 GEV/C	8	FLAG1	ISIS3	.298	.156	.134	.214	.198	38.0	724.
10-20 GEV/C	8	FLAG1	ISIS1	.665	.184	.017	.027	.106	15.6	744.
10-20 GEV/C	8	FLAG1	ISIS2	.617	.192	.056	.042	.093	17.1	744.
10-20 GEV/C	8	FLAG1	ISIS3	.660	.144	.079	.048	.069	16.4	744.
20-40 GEV/C	8	FLAG1	ISIS1	.669	.134	.021	.021	.156	19.5	718.
20-40 GEV/C	8	FLAG1	ISIS2	.773	.103	.014	.011	.099	13.0	718.
20-40 GEV/C	8	FLAG1	ISIS3	.749	.085	.052	.014	.100	15.0	718.
40-80 GEV/C	8	FLAG1	ISIS1	.641	.099	.019	.021	.220	25.0	618.
40-80 GEV/C	8	FLAG1	ISIS2	.702	.131	.015	.015	.138	17.2	618.
40-80 GEV/C	8	FLAG1	ISIS3	.694	.094	.045	.023	.144	19.7	618.

Table V Ih: Track resolution characteristics for all particles from8 prong events which traverse the entire length of ISIS.

MOMENTUM	PRONGS			0-9	1-30	3-50	5-70	70-	AVE	SAMPLE
5-10 GEV/C	8	FLAGO	ISIS1	.667	.234	.025	.012	.062	11.6	645.
5-10 GEV/C	8	FLAGO	ISIS2	.737	.212	.014	.0	.036	8.5	278.
5-10 GEV/C	8	FLAGO	ISIS3	.754	.147	.048	.018	.033	10.0	272.
10-20 GEV/C	8	FLAGO	ISIS1	.669	.186	.017	.023	.105	15.2	726.
10-20 GEV/C	8	FLAGO	ISIS2	.715	.200	.017	.013	.055	10.7	631.
10-20 GEV/C	8	FLAGO	ISIS3	.765	.110	.047	.016	.062	12.2	616.
20-40 GEV/C	8	FLAGO	ISIS1	.672	.136	.021	.018	.154	19.2	676.
20-40 GEV/C	8	FLAGO	ISIS2	.790	.100	.010	.009	.091	12.0	690.
20-40 GEV/C	8	FLAGO	ISIS3	.770	.080	.052	.008	.089	13.7	649.
40-80 GEV/C	8	FLAGO	ISIS1	.643	.096	.017	.019	.224	25.2	572.
40-80 GEV/C	8	FLAGO	ISIS2	.704	.136	.012	.014	.134	16.9	582.
40-80 GEV/C	8	FLAGO	ISIS3	.694	.097	.045	.022	.142	19.5	536.

Table VIi: Track resolution characteristics for all particles entering ISIS from 10 prong events.

MOMENTUM	PRONGS			0-9	1-30	3-50	5-70	70-	AVE	SAMPLE
5-10 GEV/C	10	FLAG1	ISIS1	.520	.311	.053	.029	.086	17.2	546.
5-10 GEV/C	10	FLAG1	ISIS2	.245	.136	.095	.066	.458	53.7	546.
5-10 GEV/C	10	FLAG1	ISIS3	.256	.163	.130	.205	.245	41.3	546.
10-20 GEV/C	10	FLAG1	ISIS1	.640	.215	.022	.018	.105	15.8	503.
10-20 GEV/C	10	FLAG1	ISIS2	.590	.207	.032	.046	.125	19.5	503.
10-20 GEV/C	10	FLAG1	ISIS3	.638	.133	.087	.064	.078	18.1	503.
20-40 GEV/C	10	FLAG1	ISIS1	.567	.213	.029	.011	.179	22.8	441.
20-40 GEV/C	10	FLAG1	ISIS2	.712	.145	.016	.018	.109	15.2	441.
20-40 GEV/C	10	FLAG1	ISIS3	.692	.120	.057	.020	.111	17.6	441.
40-80 GEV/C	10	FLAG1	ISIS1	.611	.114	.024	.041	.211	25.9	370.
40-80 GEV/C	10	FLAG1	ISIS2	.649	.168	.011	.032	.141	19.3	370.
40-80 GEV/C	10	FLAG1	ISIS3	.659	.111	.054	.035	.141	21.4	370.

Table VIj: Track resolution characteristics for all particles from 10 prong events which traverse the entire length of ISIS.

MOMENTUM	PRONGS			0-9	1-30	3-50	5-70	70-	AVE	SAMPLE
5-10 GEV/C	10	FLAGO	ISIS1	.586	.320	.027	.010	.056	12.6	481.
5-10 GEV/C	10	FLAGO	ISIS2	.672	.255	.026	.010	.036	10.0	192.
5-10 GEV/C	10	FLAGO	ISIS3	.686	.218	.048	.021	.027	10.9	188.
10-20 GEV/C	10	FLAGO	ISIS1	.640	.219	.022	.018	.101	15.6	494.
10-20 GEV/C	10	FLAGO	ISIS2	.689	.217	.012	.012	.071	12.0	424.
10-20 GEV/C	10	FLAGO	ISIS3	.740	.130	.050	.022	.058	12.8	416.
20-40 GEV/C	10	FLAGO	ISIS1	.569	.217	.027	.012	.176	22.5	415.
20-40 GEV/C	10	FLAGO	ISIS2	.729	.146	.012	.012	.101	14.0	425.
20-40 GEV/C	10	FLAGO	ISIS3	.715	.120	.050	.015	.100	16.1	400.
40-80 GEV/C	10	FLAGO	ISIS1	.616	.116	.023	.035	.209	25.5	344.
40-80 GEV/C	10	FLAGO	ISIS2	.662	.172	.006	.032	.128	18.1	343.
40-80 GEV/C	10	FLAGO	ISIS3	.682	.104	.053	.025	.135	20.2	318.

Table VIk: Track resolution characteristics for all particles entering ISIS from 12 prong events.

MOMENTUM	PRONGS			0-9	1-30	3-50	5-70	70-	AVE	SAMPLE
5-10 GEV/C	12	FLAG1	ISIS1	.363	.398	.066	.019	.154	24.3	259.
5-10 GEV/C	12	FLAG1	ISIS2	.208	.100	.077	.085	.529	61.0	259.
5-10 GEV/C	12	FLAG1	ISIS3	.189	.131	.151	.174	.355	48.5	259.
10-20 GEV/C	12	FLAG1	ISIS1	.498	.322	.021	.026	.133	20.9	233.
10-20 GEV/C	12	FLAG1	ISIS2	.545	.240	.043	.030	.142	21.4	233.
10-20 GEV/C	12	FLAG1	ISIS3	.541	.215	.086	.069	.090	21.1	233.
20-40 GEV/C	12	FLAG1	ISIS1	.503	.219	.022	.016	.240	29.8	183.
20-40 GEV/C	12	FLAG1	ISIS2	.639	.148	.044	.011	.158	21.2	183.
20-40 GEV/C	12	FLAG1	ISIS3	.596	.131	.077	.044	.153	23.9	183.
40-80 GEV/C	12	FLAG1	ISIS1	.535	.232	.035	.007	.190	24.6	142.
40-80 GEV/C	12	FLAG1	ISIS2	.676	.204	.028	.007	.085	13.9	142.
40-80 GEV/C	12	FLAG1	ISIS3	.627	.162	.085	.049	.077	17.3	142.

Table VII: Track resolution chacteristics for all particles from 12 prong events which traverse the entire length of ISIS.

MOMENTUM	PRONGS			0-9	1-30	3-50	5-70	70-	AVE	SAMPLE
5-10 GEV/C	12	FLAGO	ISIS1	.423	.445	.032	.005	.095	17.8	220.
5-10 GEV/C	12	FLAGO	ISIS2	.712	.219	.014	.0	.055	10.3	73.
5-10 GEV/C	12	FLAGO	ISIS3	.644	.247	.055	.0	.055	12.8	73.
10-20 GEV/C	12	FLAGO	ISIS1	.500	.327	.018	.022	.133	20.7	226.
10-20 GEV/C	12	FLAGO	ISIS2	.628	.250	.026	.010	.087	14.9	196.
10-20 GEV/C	12	FLAGO	ISIS3	.621	.205	.068	.016	.089	17.2	190.
20-40 GEV/C	12	FLAGO	ISIS1	.489	.227	.023	.017	.244	30.4	176.
20-40 GEV/C	12	FLAGO	ISIS2	.638	.147	.045	.011	.158	21.3	177.
20-40 GEV/C	12	FLAGO	ISIS3	.582	.135	.082	.035	.165	24.8	170.
40-80 GEV/C	12	FLAGO	ISIS1	.531	.231	.038	.008	.192	25.1	130.
40-80 GEV/C	12	FLAGO	ISIS2	.684	.203	.023	.008	.083	13.4	133.
40-80 GEV/C	12	FLAGO	ISIS3	.620	.174	.099	.025	.083	17.2	121.

Table VIm: Track resolution characteristics for all particles entering ISIS with momentum between 5 and 80 Gev/c.

MOMENTUM	PRONGS			0-9	1-30	3-50	5-70	70-	AVE	SAMPLE
5-80 GEV/C	ALL	FLAG1	ISIS1	.669	.155	.027	.021	.128	17.3	10983.
5-80 GEV/C	ALL	FLAG1	ISIS2	.624	.126	.035	.034	.181	23.2	10983.
5-80 GEV/C	ALL	FLAG1	ISIS3	.623	.108	.075	.073	.121	21.1	10983.
5-80 GEV/C	4	FLAG1	ISIS1	.855	.041	.018	.011	.075	9.4	1601.
5-80 GEV/C	4	FLAG1	ISIS2	.823	.037	.019	.020	.101	12.4	1601.
5-80 GEV/C	4	FLAG1	ISIS3	.795	.047	.052	.049	.056	11.3	1601.
5-80 GEV/C	6	FLAG1	ISIS1	.726	.105	.020	.021	.127	15.9	2782.
5-80 GEV/C	6	FLAG1	ISIS2	.670	.106	.029	.026	.169	21.1	2782.
5-80 GEV/C	6	FLAG1	ISIS3	.676	.082	.062	.070	.110	19.2	2782.
5-80 GEV/C	8	FLAG1	ISIS1	.646	.162	.027	.025	.139	18.6	2804.
5-80 GEV/C	8	FLAG1	ISIS2	.592	.143	.039	.039	.187	24.5	2804.
5-80 GEV/C	8	FLAG1	ISIS3	.597	.121	.079	.077	.127	22.4	2804.
5-80 GEV/C	10	FLAG1	ISIS1	.582	.223	.033	.024	.138	19.9	1860.
5-80 GEV/C	10	FLAG1	ISIS2	.530	.163	.042	.042	.222	28.5	1860.
5-80 GEV/C	10	FLAG1	ISIS3	.543	.134	.086	.089	.147	25.5	1860.
5-80 GEV/C	12	FLAG1	ISIS1	.463	.307	.038	.018	.174	24.6	817.
5-80 GEV/C	12	FLAG1	ISIS2	.482	.169	.051	.039	.258	32.6	817.
5-80 GEV/C	12	FLAG1	ISIS3	.457	.160	.104	.093	.186	29.8	817.

Table VIn: Track resolution characteristics for all particles with momentum between 5 and 80 Gev/c which traverse the entire length of ISIS.

MOMENTUM	PRONGS			0-9	1-30	3-50	5-70	70-	AVE	SAMPLE
5-80 GEV/C	ALL	FLAGO	ISIS1	.689	.156	.019	.015	.121	16.1	10253.
5-80 GEV/C	ALL	FLAGO	ISIS2	.769	.132	.012	.009	.077	11.1	8628.
5-80 GEV/C	ALL	FLAGO	ISIS3	.769	.093	.047	.015	.076	12.8	8222.
5-80 GEV/C	4	FLAGO	ISIS1	.871	.034	.014	.007	.075	8.8	1500.
5-80 GEV/C	4	FLAGO	ISIS2	.930	.030	.003	.004	.032	4.1	1360.
5-80 GEV/C	4	FLAGO	ISIS3	.898	.029	.035	.002	.035	5.7	1296.
5-80 GEV/C	6	FLAGO	ISIS1	.751	.103	.012	.016	.118	14.6	2595.
5-80 GEV/C	6	FLAGO	ISIS2	.805	.101	.012	.005	.078	10.3	2248.
5-80 GEV/C	6	FLAGO	ISIS3	.818	.056	.038	.015	.073	11.6	2141.
5-80 GEV/C	8	FLAGO	ISIS1	.664	.165	.020	.018	.133	17.5	2619.
5-80 GEV/C	8	FLAGO	ISIS2	.739	.153	.013	.010	.085	12.5	2181.
5-80 GEV/C	8	FLAGO	ISIS3	.747	.102	.048	.015	.087	14.3	2073.
5-80 GEV/C	10	FLAGO	ISIS1	.603	.226	.025	.018	.128	18.4	1734.
5-80 GEV/C	10	FLAGO	ISIS2	.692	.189	.012	.017	.090	13.8	1384.
5-80 GEV/C	10	FLAGO	ISIS3	.711	.133	.051	.020	.085	15.3	1322.
5-80 GEV/C	12	FLAGO	ISIS1	.480	.322	.027	.013	.158	22.9	752.
5-80 GEV/C	12	FLAGO	ISIS2	.655	.204	.029	.009	.104	15.9	579.
5-80 GEV/C	12	FLAGO	ISIS3	.612	.182	.078	.022	.106	19.0	554.

Table VIIa-n: The following tables give as a function of momentum and primary multiplicity for ISIS-1, ISIS-2, and the full ISIS (ISIS-3) the fraction of particles with a given percentage of their track clearly resolvable from other tracks in the event and the simulated background. The table also gives the average percentage of the track which is lost due to overlap or to exiting from the sides of ISIS. The total number of particles used to calculate any particular set of data in the table is also given.

Table VIIa: Track resolution characteristics for all particles entering ISIS.

MOMENTUM	PRONGS			0-9	1-30	3-50	5-70	70-	AVE	SAMPLE
5-10 GEV/C	ALL	FLAG1	ISIS1	.333	.277	.149	.094	.148	29.8	2747.
5-10 GEV/C	ALL	FLAG1	ISIS2	.169	.153	.119	.106	.454	57.1	2747.
5-10 GEV/C	ALL	FLAG1	ISIS3	.146	.180	.175	.194	.305	47.7	2747.
10-20 GEV/C	ALL	FLAG1	ISIS1	.433	.252	.097	.069	.150	26.5	2795.
10-20 GEV/C	ALL	FLAG1	ISIS2	.391	.262	.145	.077	.126	27.0	2795.
10-20 GEV/C	ALL	FLAG1	ISIS3	.359	.278	.180	.096	.087	26.7	2795.
20-40 GEV/C	ALL	FLAG1	ISIS1	.449	.201	.094	.055	.201	30.1	2903.
20-40 GEV/C	ALL	FLAG1	ISIS2	.493	.223	.105	.055	.124	23.5	2903.
20-40 GEV/C	ALL	FLAG1	ISIS3	.421	.257	.152	.058	.112	25.6	2903.
40-80 GEV/C	ALL	FLAG1	ISIS1	.437	.204	.077	.054	.229	32.1	2538.
40-80 GEV/C	ALL	FLAG1	ISIS2	.507	.214	.080	.043	.155	24.9	2538.
40-80 GEV/C	ALL	FLAG1	ISIS3	.411	.267	.127	.050	.145	27.1	2538.

Table VIIb: Track resolution characteristics for all particles which traverse the entire length of ISIS.

MOMENTUM	PRONGS			0-9	1-30	3-50	5-70	70-	AVE	SAMPLE
5-10 GEV/C	ALL	FLAGO	ISIS1	.373	.295	.135	.081	.115	26.0	2417.
5-10 GEV/C	ALL	FLAGO	ISIS2	.425	.320	.147	.058	.050	20.3	1049.
5-10 GEV/C	ALL	FLAGO	ISIS3	.370	.321	.199	.072	.038	22.1	1030.
10-20 GEV/C	ALL	FLAGO	ISIS1	.434	.252	.097	.069	.148	26.4	2743.
10-20 GEV/C	ALL	FLAGO	ISIS2	.446	.280	.139	.053	.082	21.8	2411.
10-20 GEV/C	ALL	FLAGO	ISIS3	.409	.292	.168	.063	.068	23.1	2368.
20-40 GEV/C	ALL	FLAGO	ISIS1	.447	.199	.096	.055	.203	30.3	2760.
20-40 GEV/C	ALL	FLAGO	ISIS2	.502	.222	.106	.053	.116	22.7	2788.
20-40 GEV/C	ALL	FLAGO	ISIS3	.427	.259	.154	.054	.105	24.9	2647.
40-80 GEV/C	ALL	FLAGO	ISIS1	.433	.201	.079	.051	.235	32.7	2333.
40-80 GEV/C	ALL	FLAGO	ISIS2	.510	.218	.081	.044	.146	24.3	2380.
40-80 GEV/C	ALL	FLAGO	ISIS3	.413	.267	.131	.049	.139	26.9	2177.

Table VIIc: Track resolution characteristics for all particles entering ISIS from 4 prong events.

MOMENTUM	PRONGS			0-9	1-30	3-50	5-70	70-	AVE	SAMPLE
5-10 GEV/C	4	FLAG1	ISIS1	.461	.216	.131	.088	.105	24.1	306.
5-10 GEV/C	4	FLAG1	ISIS2	.268	.170	.111	.088	.363	47.5	306.
5-10 GEV/C	4	FLAG1	ISIS3	.222	.212	.160	.186	.219	39.5	306.
10-20 GEV/C	4	FLAG1	ISIS1	.538	.224	.070	.058	.110	20.2	344.
10-20 GEV/C	4	FLAG1	ISIS2	.544	.198	.142	.061	.055	18.6	344.
10-20 GEV/C	4	FLAG1	ISIS3	.480	.244	.183	.052	.041	19.0	344.
20-40 GEV/C	4	FLAG1	ISIS1	.592	.159	.062	.045	.142	21.8	466.
20-40 GEV/C	4	FLAG1	ISIS2	.607	.185	.107	.041	.060	16.0	466.
20-40 GEV/C	4	FLAG1	ISIS3	.545	.236	.116	.047	.056	17.8	466.
40-80 GEV/C	4	FLAG1	ISIS1	.563	.161	.087	.039	.151	23.6	485.
40-80 GEV/C	4	FLAG1	ISIS2	.612	.177	.085	.033	.093	17.7	485.
40-80 GEV/C	4	FLAG1	ISIS3	.507	.262	.115	.033	.082	19.5	485.

Table VIId: Track resolution characteristics for all particles from 4 prong events which traverse the entire length of ISIS.

MOMENTUM	PRONGS			0-9	1-30	3-50	5-70	70-	AVE	SAMPLE
5-10 GEV/C	4	FLAGO	ISIS1	.520	.212	.112	.074	.082	20.5	269.
5-10 GEV/C	4	FLAGO	ISIS2	.557	.293	.093	.036	.021	13.5	140.
5-10 GEV/C	4	FLAGO	ISIS3	.460	.309	.180	.043	.007	15.5	139.
10-20 GEV/C	4	FLAGO	ISIS1	.537	.223	.070	.059	.111	20.3	341.
10-20 GEV/C	4	FLAGO	ISIS2	.583	.210	.137	.045	.025	14.8	314.
10-20 GEV/C	4	FLAGO	ISIS3	.513	.250	.186	.029	.022	16.4	312.
20-40 GEV/C	4	FLAGO	ISIS1	.587	.155	.065	.045	.148	22.4	445.
20-40 GEV/C	4	FLAGO	ISIS2	.613	.180	.110	.041	.056	15.5	444.
20-40 GEV/C	4	FLAGO	ISIS3	.544	.236	.121	.047	.052	17.6	423.
40-80 GEV/C	4	FLAGO	ISIS1	.551	.157	.090	.038	.164	25.0	445.
40-80 GEV/C	4	FLAGO	ISIS2	.617	.180	.082	.032	.089	17.2	462.
40-80 GEV/C	4	FLAGO	ISIS3	.495	.263	.126	.033	.083	20.0	422.

Table VIIe: Track resolution characteristics for all particles entering ISIS from 6 prong events.

MOMENTUM	PRONGS			0-9	1-30	3-50	5-70	70-	AVE	SAMPLE
5-10 GEV/C	6	FLAG1	ISIS1	.388	.244	.145	.086	.137	27.7	636.
5-10 GEV/C	6	FLAG1	ISIS2	.200	.154	.105	.105	.436	55.5	636.
5-10 GEV/C	6	FLAG1	ISIS3	.176	.178	.170	.187	.289	46.0	636.
10-20 GEV/C	6	FLAG1	ISIS1	.468	.237	.114	.063	.118	23.3	678.
10-20 GEV/C	6	FLAG1	ISIS2	.435	.251	.137	.066	.111	24.6	678.
10-20 GEV/C	6	FLAG1	ISIS3	.403	.291	.149	.090	.068	24.0	678.
20-40 GEV/C	6	FLAG1	ISIS1	.476	.195	.091	.055	.183	28.4	804.
20-40 GEV/C	6	FLAG1	ISIS2	.527	.215	.095	.047	.116	21.8	804.
20-40 GEV/C	6	FLAG1	ISIS3	.461	.251	.141	.037	.109	23.8	804.
40-80 GEV/C	6	FLAG1	ISIS1	.423	.211	.066	.075	.224	32.7	664.
40-80 GEV/C	6	FLAG1	ISIS2	.532	.202	.071	.032	.164	24.6	664.
40-80 GEV/C	6	FLAG1	ISIS3	.434	.244	.114	.056	.152	27.1	664.

Table VIIf: Track resolution characteristics for all particles from 6 prong events which traverse the entire length of ISIS.

MOMENTUM	PRONGS			0-9	1-30	3-50	5-70	70-	AVE	SAMPLE
5-10 GEV/C	6	FLAGO	ISIS1	.440	.257	.121	.076	.105	23.6	552.
5-10 GEV/C	6	FLAGO	ISIS2	.496	.284	.128	.052	.040	18.1	250.
5-10 GEV/C	6	FLAGO	ISIS3	.430	.303	.172	.066	.029	20.1	244.
10-20 GEV/C	6	FLAGO	ISIS1	.471	.237	.114	.063	.114	23.0	666.
10-20 GEV/C	6	FLAGO	ISIS2	.483	.255	.130	.057	.075	20.6	600.
10-20 GEV/C	6	FLAGO	ISIS3	.449	.288	.144	.056	.063	21.4	590.
20-40 GEV/C	6	FLAGO	ISIS1	.477	.193	.095	.052	.184	28.4	768.
20-40 GEV/C	6	FLAGO	ISIS2	.536	.211	.097	.045	.111	21.2	776.
20-40 GEV/C	6	FLAGO	ISIS3	.470	.251	.139	.035	.104	23.2	740.
40-80 GEV/C	6	FLAGO	ISIS1	.422	.209	.067	.074	.228	33.1	609.
40-80 GEV/C	6	FLAGO	ISIS2	.527	.212	.074	.032	.154	24.0	622.
40-80 GEV/C	6	FLAGO	ISIS3	.437	.247	.123	.056	.136	26.3	567.

Table VIIg: Track resolution characteristics for all particles entering ISIS from 8 prong events.

MOMENTUM	PRONGS			0-9	1-30	3-50	5-70	70-	AVE	SAMPLE
5-10 GEV/C	8	FLAG1	ISIS1	.359	.265	.145	.087	.144	28.7	724.
5-10 GEV/C	8	FLAG1	ISIS2	.162	.166	.104	.122	.448	56.7	724.
5-10 GEV/C	8	FLAG1	ISIS3	.144	.191	.180	.200	.286	47.2	724.
10-20 GEV/C	8	FLAG1	ISIS1	.415	.259	.090	.065	.171	28.2	744.
10-20 GEV/C	8	FLAG1	ISIS2	.355	.277	.160	.085	.124	28.2	744.
10-20 GEV/C	8	FLAG1	ISIS3	.320	.304	.187	.094	.095	28.0	744.
20-40 GEV/C	8	FLAG1	ISIS1	.425	.194	.102	.064	.216	32.0	718.
20-40 GEV/C	8	FLAG1	ISIS2	.471	.230	.096	.063	.141	25.6	718.
20-40 GEV/C	8	FLAG1	ISIS3	.387	.259	.164	.067	.123	27.6	718.
40-80 GEV/C	8	FLAG1	ISIS1	.427	.207	.066	.036	.264	33.9	618.
40-80 GEV/C	8	FLAG1	ISIS2	.463	.220	.092	.049	.176	27.6	618.
40-80 GEV/C	8	FLAG1	ISIS3	.401	.252	.129	.049	.168	29.5	618.

Table VIIh: Track resolution characteristics for all particles from 8 prong events which traverse the entire length of ISIS.

MOMENTUM	PRONGS			0-9	1-30	3-50	5-70	70-	AVE	SAMPLE
5-10 GEV/C	8	FLAGO	ISIS1	.397	.285	.132	.076	.110	25.1	645.
5-10 GEV/C	8	FLAGO	ISIS2	.406	.338	.129	.065	.061	21.6	278.
5-10 GEV/C	8	FLAGO	ISIS3	.371	.342	.162	.066	.059	22.7	272.
10-20 GEV/C	8	FLAGO	ISIS1	.416	.260	.091	.063	.169	28.1	726.
10-20 GEV/C	8	FLAGO	ISIS2	.410	.304	.147	.055	.082	22.8	631.
10-20 GEV/C	8	FLAGO	ISIS3	.373	.318	.164	.068	.076	24.5	616.
20-40 GEV/C	8	FLAGO	ISIS1	.422	.195	.102	.065	.216	32.2	676.
20-40 GEV/C	8	FLAGO	ISIS2	.480	.230	.096	.061	.133	24.7	690.
20-40 GEV/C	8	FLAGO	ISIS3	.393	.265	.169	.060	.112	26.6	649.
40-80 GEV/C	8	FLAGO	ISIS1	.427	.203	.068	.033	.269	34.4	572.
40-80 GEV/C	8	FLAGO	ISIS2	.462	.223	.091	.050	.174	27.4	582.
40-80 GEV/C	8	FLAGO	ISIS3	.399	.252	.131	.050	.168	29.7	536.

Table VIIi: Track resolution characteristics for all particles entering ISIS from 10 prong events.

MOMENTUM	PRONGS			0-9	1-30	3-50	5-70	70-	AVE	SAMPLE
5-10 GEV/C	10	FLAG1	ISIS1	.269	.333	.150	.099	.148	31.0	546.
5-10 GEV/C	10	FLAG1	ISIS2	.137	.141	.136	.097	.489	60.0	546.
5-10 GEV/C	10	FLAG1	ISIS3	.119	.170	.168	.214	.328	50.1	546.
10-20 GEV/C	10	FLAG1	ISIS1	.392	.270	.097	.078	.163	28.8	503.
10-20 GEV/C	10	FLAG1	ISIS2	.342	.286	.131	.072	.169	30.5	503.
10-20 GEV/C	10	FLAG1	ISIS3	.324	.260	.197	.109	.109	29.8	503.
20-40 GEV/C	10	FLAG1	ISIS1	.340	.256	.122	.050	.231	34.5	441.
20-40 GEV/C	10	FLAG1	ISIS2	.408	.245	.141	.059	.147	27.4	441.
20-40 GEV/C	10	FLAG1	ISIS3	.336	.286	.175	.075	.129	29.6	441.
40-80 GEV/C	10	FLAG1	ISIS1	.346	.232	.081	.070	.270	37.7	370.
40-80 GEV/C	10	FLAG1	ISIS2	.435	.249	.065	.068	.184	29.5	370.
40-80 GEV/C	10	FLAG1	ISIS3	.316	.303	.141	.062	.178	32.1	370.

Table VIIj: Track resolution characteristics for all particle s from 10 prong events which traverse the entire length of ISIS.

MOMENTUM	PRONGS			0-9	1-30	3-50	5-70	70-	AVE	SAMPLE
5-10 GEV/C	10	FLAGO	ISIS1	.301	.360	.137	.079	.123	27.4	481.
5-10 GEV/C	10	FLAGO	ISIS2	.365	.344	.182	.057	.052	22.1	192.
5-10 GEV/C	10	FLAGO	ISIS3	.319	.330	.213	.101	.037	24.6	188.
10-20 GEV/C	10	FLAGO	ISIS1	.391	.273	.097	.079	.160	28.6	494.
10-20 GEV/C	10	FLAGO	ISIS2	.399	.316	.130	.040	.116	24.3	424.
10-20 GEV/C	10	FLAGO	ISIS3	.377	.291	.188	.065	.079	25.2	416.
20-40 GEV/C	10	FLAGO	ISIS1	.347	.248	.123	.051	.231	34.6	415.
20-40 GEV/C	10	FLAGO	ISIS2	.416	.247	.141	.056	.139	26.6	425.
20-40 GEV/C	10	FLAGO	ISIS3	.350	.280	.175	.075	.120	28.7	400.
40-80 GEV/C	10	FLAGO	ISIS1	.346	.238	.081	.064	.270	37.4	344.
40-80 GEV/C	10	FLAGO	ISIS2	.449	.245	.067	.073	.166	28.4	343.
40-80 GEV/C	10	FLAGO	ISIS3	.324	.308	.142	.060	.167	31.0	318.

Table VIIk Track resolution characteristics for all particles entering ISIS from 12 prong events.

MOMENTUM	PRONGS			0-9	1-30	3-50	5-70	70-	AVE	SAMPLE
5-10 GEV/C	12	FLAG1	ISIS1	.189	.305	.178	.093	.236	38.9	259.
5-10 GEV/C	12	FLAG1	ISIS2	.131	.085	.131	.085	.568	66.5	259.
5-10 GEV/C	12	FLAG1	ISIS3	.081	.147	.162	.162	.448	57.1	259.
10-20 GEV/C	12	FLAG1	ISIS1	.305	.330	.086	.099	.180	32.9	233.
10-20 GEV/C	12	FLAG1	ISIS2	.313	.253	.163	.086	.185	33.1	233.
10-20 GEV/C	12	FLAG1	ISIS3	.283	.266	.176	.150	.124	32.9	233.
20-40 GEV/C	12	FLAG1	ISIS1	.333	.240	.060	.055	.311	40.6	183.
20-40 GEV/C	12	FLAG1	ISIS2	.388	.257	.109	.071	.175	30.7	183.
20-40 GEV/C	12	FLAG1	ISIS3	.317	.251	.164	.082	.186	33.9	183.
40-80 GEV/C	12	FLAG1	ISIS1	.366	.275	.113	.028	.218	32.2	142.
40-80 GEV/C	12	FLAG1	ISIS2	.458	.282	.099	.056	.106	22.6	142.
40-80 GEV/C	12	FLAG1	ISIS3	.352	.324	.169	.063	.092	25.6	142.

Table VIII: Track resolution characteristics for all particles from 12 prong events which traverse the entire length of ISIS.

MOMENTUM	PRONGS			0-9	1-30	3-50	5-70	70-	AVE	SAMPLE
5-10 GEV/C	12	FLAGO	ISIS1	.218	.350	.182	.082	.168	33.6	220.
5-10 GEV/C	12	FLAGO	ISIS2	.466	.260	.151	.055	.068	22.1	73.
5-10 GEV/C	12	FLAGO	ISIS3	.288	.370	.233	.055	.055	25.1	73.
10-20 GEV/C	12	FLAGO	ISIS1	.310	.327	.088	.097	.177	32.6	226.
10-20 GEV/C	12	FLAGO	ISIS2	.362	.265	.179	.061	.133	28.0	196.
10-20 GEV/C	12	FLAGO	ISIS3	.316	.295	.163	.121	.105	29.7	190.
20-40 GEV/C	12	FLAGO	ISIS1	.324	.239	.063	.057	.318	41.4	176.
20-40 GEV/C	12	FLAGO	ISIS2	.390	.260	.107	.068	.175	30.6	177.
20-40 GEV/C	12	FLAGO	ISIS3	.318	.241	.176	.076	.188	34.3	170.
40-80 GEV/C	12	FLAGO	ISIS1	.354	.277	.115	.031	.223	33.0	130.
40-80 GEV/C	12	FLAGO	ISIS2	.459	.293	.098	.053	.098	21.8	133.
40-80 GEV/C	12	FLAGO	ISIS3	.355	.322	.182	.050	.091	25.4	121.

Table VIIm: Track resolution characteristics for all particles entering ISIS with momentum between 5 and 80 Gev/c.

MOMENTUM	PRONGS			0-9	1-30	3-50	5-70	70-	AVE	SAMPLE
5-80 GEV/C	ALL	FLAG1	ISIS1	.413	.234	.104	.068	.181	29.6	10983.
5-80 GEV/C	ALL	FLAG1	ISIS2	.389	.213	.113	.071	.214	33.1	10983.
5-80 GEV/C	ALL	FLAG1	ISIS3	.334	.245	.159	.100	.161	31.8	10983.
5-80 GEV/C	4	FLAG1	ISIS1	.547	.184	.084	.054	.131	22.4	1601.
5-80 GEV/C	4	FLAG1	ISIS2	.530	.182	.109	.052	.127	23.1	1601.
5-80 GEV/C	4	FLAG1	ISIS3	.458	.241	.139	.071	.092	22.7	1601.
5-80 GEV/C	6	FLAG1	ISIS1	.441	.220	.103	.069	.166	28.0	2782.
5-80 GEV/C	6	FLAG1	ISIS2	.431	.207	.102	.061	.199	30.8	2782.
5-80 GEV/C	6	FLAG1	ISIS3	.375	.242	.143	.089	.151	29.7	2782.
5-80 GEV/C	8	FLAG1	ISIS1	.406	.233	.102	.064	.196	30.6	2804.
5-80 GEV/C	8	FLAG1	ISIS2	.358	.224	.114	.081	.223	34.7	2804.
5-80 GEV/C	8	FLAG1	ISIS3	.310	.252	.167	.104	.168	33.2	2804.
5-80 GEV/C	10	FLAG1	ISIS1	.334	.278	.116	.076	.196	32.6	1860.
5-80 GEV/C	10	FLAG1	ISIS2	.316	.226	.122	.075	.261	38.2	1860.
5-80 GEV/C	10	FLAG1	ISIS3	.265	.248	.172	.123	.192	36.1	1860.
5-80 GEV/C	12	FLAG1	ISIS1	.285	.293	.114	.075	.234	36.4	817.
5-80 GEV/C	12	FLAG1	ISIS2	.297	.206	.130	.077	.290	41.3	817.
5-80 GEV/C	12	FLAG1	ISIS3	.239	.235	.168	.124	.235	39.5	817.

Table VIIn: Track resolution characteristics for all particles with momentum between 5 and 80 Gev/c which traverse the entire length of ISIS.

MOMENTUM	PRONGS			0-9	1-30	3-50	5-70	70-	AVE	SAMPLE
5-80 GEV/C	ALL	FLAGO	ISIS1	.423	.237	.102	.064	.175	28.8	10253.
5-80 GEV/C	ALL	FLAGO	ISIS2	.479	.249	.113	.051	.107	22.6	8628.
5-80 GEV/C	ALL	FLAGO	ISIS3	.411	.279	.158	.058	.095	24.6	8222.
5-80 GEV/C	4	FLAGO	ISIS1	.553	.181	.082	.051	.133	22.3	1500.
5-80 GEV/C	4	FLAGO	ISIS2	.601	.199	.105	.038	.057	15.7	1360.
5-80 GEV/C	4	FLAGO	ISIS3	.512	.256	.144	.038	.050	17.8	1296.
5-80 GEV/C	6	FLAGO	ISIS1	.455	.222	.099	.065	.160	27.1	2595.
5-80 GEV/C	6	FLAGO	ISIS2	.515	.231	.103	.045	.105	21.5	2248.
5-80 GEV/C	6	FLAGO	ISIS3	.451	.266	.140	.050	.092	23.2	2141.
5-80 GEV/C	8	FLAGO	ISIS1	.415	.237	.099	.060	.189	29.8	2619.
5-80 GEV/C	8	FLAGO	ISIS2	.446	.264	.114	.057	.120	24.5	2181.
5-80 GEV/C	8	FLAGO	ISIS3	.386	.288	.157	.061	.109	26.3	2073.
5-80 GEV/C	10	FLAGO	ISIS1	.347	.284	.111	.069	.189	31.4	1734.
5-80 GEV/C	10	FLAGO	ISIS2	.412	.281	.125	.056	.126	25.7	1384.
5-80 GEV/C	10	FLAGO	ISIS3	.348	.297	.176	.072	.107	27.5	1322.
5-80 GEV/C	12	FLAGO	ISIS1	.294	.305	.114	.072	.215	35.0	752.
5-80 GEV/C	12	FLAGO	ISIS2	.406	.269	.135	.060	.130	26.6	579.
5-80 GEV/C	12	FLAGO	ISIS3	.321	.294	.181	.083	.121	29.6	554.

Table VIII. Comparison of the track overlap characteristics of the full ISIS for 0.5cm and for 1.0cm spacial resolution. The table gives, as a function of momentum, the percentage of all tracks which traverse the entire length of ISIS with at least 90% of the track clear and the percentage of tracks with between 70 and 90% of the track clear. Also given are the average percentage clear for tracks at a given momentum and also the number of tracks in the test sample.

Minimum Track Resolution Distance	Momentum	% of Track Clear		Avg.% Clear	Sample Size
		90-100%	70-90%		
1.0cm	5<p<10	75.8	15.0	90.9	1030
	10<p<20	80.2	8.9	89.5	2368
	20<p<40	77.3	7.7	86.5	2647
	40<p<80	73.5	8.9	83.9	2177
0.5cm	5<p<10	88.8	7.7	95.2	1030
	10<p<20	90.4	4.1	94.5	2368
	20<p<40	87.5	4.2	92.8	2647
	40<p<80	86.4	3.1	90.8	2177

Table IX. Comparison of the track overlap characteristics of the full ISIS for the signal wires from the two signal wire planes connected as described in the text. The table gives, as a function of momemtum, the percentage of all tracks which traverse the entire length of ISIS with at least 90% of the track clear and the percentage of tracks with between 70 and 90% of the track clear. Also given are the average percentage clear for tracks at a given momentum and also the number of tracks in the test sample.

Description of Wire Connections	Momentum	% of track clear		Avg.% Clear	Sample Size
		90-100%	70-90%		
all signal wires separate	5-10	75.8	15.0	90.9	1030
	10-20	80.2	8.9	89.5	2368
	20-40	77.3	7.7	86.5	2647
	40-80	73.5	8.9	83.9	2177
signal wires connected as described in the text for test 1	5-10	37.2	39.9	80.4	1032
	10-20	43.5	31.7	79.1	2368
	20-40	39.5	26.4	73.9	2650
	40-80	33.5	24.9	68.8	2181
signal wires connected as described in the text for test 2	5-10	35.9	41.9	80.3	1030
	10-20	39.4	37.1	79.1	2368
	20-40	37.1	30.6	74.0	2647
	40-80	35.3	24.6	69.6	2177

APPENDIX III

FNAL Experimental
Proposal 393 (revised)
Spokesman: Irwin A. Pless

HIGH STATISTICS STUDY OF π^0 PRODUCTION IN 150 GeV/c π^- - p INTERACTIONS

Brown University: M. Heller, A. M. Shapiro, M. Widgoff
Illinois Institute of Technology: R. A. Burnstein, C. Fu, M. Nazaretz, H. A. Rubin
University of Illinois: J. W. Cooper, R. Plumer, R. D. Sard, J. Tortora
Indiana University: E. D. Alyea, Jr.
Johns Hopkins University: L. Bachman, C.-Y. Chien, P. Lucas, L. Madansky, A. Pevsner, R. A. Zdanis
Massachusetts Institute of Technology: J. Bober, J. E. Brau, T. Frank, J. Grunhaus, E. S. Hafen, R. I. Hulsizer, U. Karshon, V. Kistiakowsky, P. A. Miller, A. Napier, I. A. Pless, J. P. Silverman, J. Wolfson, R. K. Yamamoto
University of Padova/University of Rome*: S. Centro, G. Ciapetti*, M. DeGiorgi, D. Pascoli, L. Ventura, D. Zanello*, L. Zanello*
Rutgers University/Stevens Institute*/SUNY**, Albany: E. B. Brucker*, P. F. Jacques, M. D. Jones*, E. L. Koller*, T. C. Ou, R. J. Plano, P. Stamer*, C. Sun**, S. Taylor*, T. L. Watts
University of Tennessee/Oak Ridge National Laboratory*: J. Barwick, W. M. Bugg, H. O. Cohn*, G. Condo, T. Handler, E. Hart, R. D. McCulloch*
Yale University/Fermilab*: D. Bogert*, M. Johnson*, G. Koizumi*, H. Kraybill, D. Ljung, T. Ludlam, J. Mayersohn, H. Taft

20 January 1976 (revised)

SUMMARY

We propose a high statistics study of two, four, six, and eight charged particle final state channels in which a single forward going π^0 is also produced in 150 GeV/c $\pi^- p$ interactions. We will also perform high statistics studies of the four, six, and eight charged particle channels without neutrals and inclusive studies of π^0 production as a function of rapidity. We will also study the forward going electromagnetic energy associated with the two-charged prong topology in 150 GeV/c $\pi^- p$ interactions. We believe that there is evidence of a new phenomenon associated with these photons based on previous data (E-154) which cannot be explained on the basis of known reactions with known particles. We propose adding a gamma ray detector behind the last PWC plane in the Fermilab 30" hybrid system. This gamma ray detector should have an energy resolution $\frac{\Delta E}{E} < 1\%$ and a spatial resolution of less than $\pm$ 3mm. We request 10^6 frames taken in the 30" hybrid system with an incident π^- beam of 150 GeV/c. In this exposure there will be $\sim$ 9000 two prong events with electromagnetic energy greater than 20 GeV of which 3000 will be the events associated with the new phenomenon. The precise information on the photons should allow us to determine what is the character of the beam diffraction reaction and whether or not it represents a new phenomenon. This part of the experiment will be performed first and a quick answer should be possible.

Introduction

The purposes of this experiment are twofold: 1) a high statistics study of π^0 production and 2) a study of the forward going neutral energy associated with the two charged particle topology, both in $\pi^- p$ interactions at 150 GeV/c. We propose a change in the experiment discussed in the original version of this proposal (submitted 14 May 1975), replacing operation with a triggered bubble chamber light flash to untriggered operation in which the events of interest are selected in off-line analysis of the forward going neutrals. We still request 10^6 expansions of the 30-inch hybrid system but now replace our original estimate of $\sim 10^5$ pictures with a request for 10^6 pictures. A scan for tagged two charged-particle events would be done first and permit an expeditious elucidation of the second topic listed above.

High Statistics Study

Based on our previous experience in experiment 154 ($\pi^- p$ at 147 GeV/c), we believe that it is possible to use a slightly higher incident flux and therefore request 10^6 pictures with ten tracks per picture of $\pi^- p$ interactions at 150 GeV/c. Table I gives an estimate of the number of events we expect for the various topologies based on our E-154 results. It is seen that this experiment also would permit high statistics studies of the channels in which no neutral particles were produced for the four, six, and eight charged prong topologies.

The primary purpose of this proposed experiment is a study of channels in which one or more π^0's is produced. In order to accomplish this we propose to add to the proportional wire hybrid bubble chamber system a lead glass hodoscope downstream of the last proportional wire chamber that will have a resolution $\frac{\Delta E}{E} \sim 1\%$ and a spatial resolution less than $\pm$ 3mm. It is expected that the prototype device associated with E-299 (see E-299 agreement and other plans - attached)

will suffice and, hence, that we will have suitable equipment for this experiment as soon as the test run with E-299 is completed (spring 1976). We should be able to reconstruct π^0 and η^0 mesons and should be able to distinguish up to six gamma rays ($3\pi^0$). Thus, we would be able to perform a study of the two, four, six, and eight charged prong topologies where one π^0 is observed allowing four constraint (4C) fits. These are channels of which there have not been previous studies. This experiment together with E-154 also would permit high statistics studies of the four, six, and eight charged prong topologies with no neutral particles and comparison with the corresponding channels with π^0 mesons should prove extremely fruitful. For example, our E-154 study of the four charged-particle 4C sample has shown that more than 92% of the cross section is due to beam and target diffraction dissociation. $\rho^0\pi^-$ events make an important contribution to the beam dissociation cross section in the A_1 and A_2 mass region and there is some evidence for a contribution from $f^0\pi^-$. Higher statistics should permit a resolution of the latter question as well as yielding a better understanding of the three-pion system in all invariant mass regions. It would obviously be of great interest to obtain results for the four charged prong, one π^0 channel at a similar level of statistics.

This experiment will also permit an inclusive study of π^0 production as a function of rapidity. Such a study is extremely important in order to verify the previous evidence for the existence of clusters and to determine whether they consist mainly of two pions ("ρ" like) or three pions ("ω" like). Light would also be shed on the question of transverse momentum conservation along the rapidity axis. In particular, the question of local transverse momentum conservation could be answered, whereas with charged-particle rapidity studies only, this is virtually impossible.

Two Charged Prong Events with Forward π^0 Mesons

Another facet of this experiment is the examination of the forward going

neutral energy associated with the production of two charged particles. From experiment 154 we have 376 two-prong inelastic events with an identified proton which we find can be classified into three distinct groups. One group is beam fragmentation, and a second, target fragmentation. The third group is not easily categorized and consists of events shown in figure 1. We had in our PWC system for E-154 a crude gamma ray detector consisting of a two-radiation thick piece of lead followed by three PWC planes. By counting the number of wires that fired in these chambers, we can get a crude idea of the intensity of the electromagnetic energy incident on the lead converter. We have arbitrarily defined a scale ranging from 0-6 where 0 indicates no fired wires and 6 indicates more than 100 fired wires. In the beam fragmentation region, there is essentially always some electromagnetic energy incident on the lead converter with the vast majority of the events having intensity six. In the target fragmentation region, there is almost no electromagnetic energy incident on the lead converter with the vast majority of the events having intensity zero. In the third region, half the events have an electromagnetic intensity zero and the other half have electromagnetic intensity six. This is shown in figure 2.

This in itself is interesting but not unexpected. However, when we look at the beam fragmentation events in detail, within our limited statistics (212 events), we find rather unexpected distributions. The first is that for the P_{lab} of the π^-. Although the statistics are poor, there is an accumulation of events with P_{lab} of the π^- at 110 GeV/c. There is another accumulation at 40 GeV/c and another at 10 GeV/c. This is shown in figure 3. For comparison, figure 4 shows the π^- laboratory distribution for all events. In this distribution, a high momentum peak which includes the leading particle signal (target fragmentation) is clearly visible.

A second unexpected feature is the energy distribution of the missing neutrals (beam fragments) which pass through our gamma detector. This distribution has accumulations at 140 GeV/c and 100 GeV/c. This, of course, is the reflection of the π^- distribution and conservation of energy. This distribution is shown in figure 5.

The physics questions we would like to answer are: What is the composition of the neutral energy shown in figure 5? Does the accumulation at 140 GeV/c consist of a single π^0 or several π^0's? What are the invariant mass distributions between the neutral π^0 or π^0's and the π^-?

We have investigated the possibility that the phenomena we see result from a known reaction, such as A^- production. If this were the case, given that the A^- is an I spin 1 particle and that it decays into two I spin 1 particles, we would expect to have similar behavior in the four-prong sample containing an identified proton. In particular, the events in the beam fragmentation region of the four prongs, the π^+ plays the same role as the π^- in the two-prong sample. Figure 6 shows the distribution of this π^+. As can be seen, this distribution (within the statistics) is quite different from the π^- distribution (fig. 3), particularly in the high energy region.

We believe that the above comments indicate a new phenomenon is occurring in the two-prong events and that a detailed study of this phenomenon is called for. We have tried many Monte Carlo calculations to simulate a final state that might explain our data. These include:

1) $\pi^- + p \rightarrow$ "A^-" $+ P$

$\quad\quad\quad\quad\hookrightarrow$ "ρ^-" $+ \pi^0$

$\quad\quad\quad\quad\quad\quad\hookrightarrow \pi^- + \pi^0$

2) $\pi^- + p \rightarrow$ "A^-" + p

"f^0" + π^-

$\pi^0 \pi^0$

To match the data with reaction 1), one requires "A^-" with widths less than 100 MeV, "ρ^-" with widths less than 10 MeV and angular distributions like $\cos^6\theta$. We have not found parameters that allow us to match the data with reaction 2). Hence, we believe one has to study in detail the electromagnetic energy associated with the two-prong events.

We would use the information from the photon detector to identify those frames in which there was an event with at least 20 GeV of photon energy. These frames would be scanned for two prongs, and we estimate that we will find 9000 two prongs for an exposure of 10^6 frames at ten tracks per frame. Approximately one third of these will be beam fragmentation events. Hence, the data reduction part of this experiment is quite modest and since the scan of preselected frames for two prongs would have the first priority, we should be able to perform this part of the experiment in a short time.

The gamma ray data will allow us to determine π^0 four vectors and form relevant invariant mass distributions. If there is narrow structure in this final state, we will be able to detect it. In any event, we will be able to determine the character of this final state in an exclusive manner and determine if there are any new physical phenomena involved.

Scope of the Experiment

This experiment will be accomplished by use of the Fermilab 30-inch bubble chamber hybrid system with the addition of a gamma ray detector behind the last PWC plane. A total of 10^6 pictures of $\pi^- p$ interactions at 150 GeV/c is requested. The film will first be scanned for two-prong events associated with at least 20 GeV of forward going electromagnetic energy and the measurement and

analysis of the ~9000 events expected could be completed quickly. Then the film will be scanned for all events associated with forward going electromagnetic energy and for all four, six, and eight-prong events. This scanning and the measurement of the events will be carried out by the groups forming the Proportional Hybrid System Consortium (PHSC). If necessary, the number of groups involved in the experiment could be expanded to permit a more rapid reduction of the data.

Table I

Number of Events for 10^6 Pictures with Ten Incident π^- Mesons Per Picture for π p Interactions at 150 GeV/c

Number of Charged Particles		Number of Events
2		55,000
	elastic	35,000
	inelastic	20,000
4		46,000
	4C	6,300
6		52,000
	4C	1,600
8		49,000
≥ 10		75,000
All events		280,000 (11.6 events/μb)

FIGURE CAPTIONS

Figure 1: Scatter plot of the laboratory momentum of the π^- versus the center of mass value of the Feynman x parameter for the proton. The sample is all the inelastic two-prong (π^-, p) events. Shown are our definition of beam fragmentation and target fragmentation regions. Also indicated is the definition of Region III.

Figure 2: For each of the three regions shown in figure 1, we have estimated the electromagnetic intensity seen in the forward direction. The detecting device was two radiation lengths of lead followed by proportional wire planes. The intensity was estimated by the number of struck wires. Bin 0 implies no struck wires and bin 6 implies more than 100 fired wires. As might be expected, in the beam fragmentation region there is relatively more electromagnetic energy seen downstream than for the target fragmentation region.

Figure 3: π^- laboratory momentum for the beam fragmentation region.

Figure 4: π^- laboratory momentum for the whole two-prong inelastic (π^-, p) sample.

Figure 5: For the beam fragmentation region we calculated the missing mass four vector. If this four vector was aimed towards our gamma ray detector, we computed the energy of the missing mass and entered it into this histogram.

Figure 6: The data for this histogram comes from the four-charged prong sample with an identified proton. We made the same cut on the proton as for the two-charged prong sample and then plotted the laboratory momentum of the π^+. Note the events in this sample may or may not have associated missing neutrals.

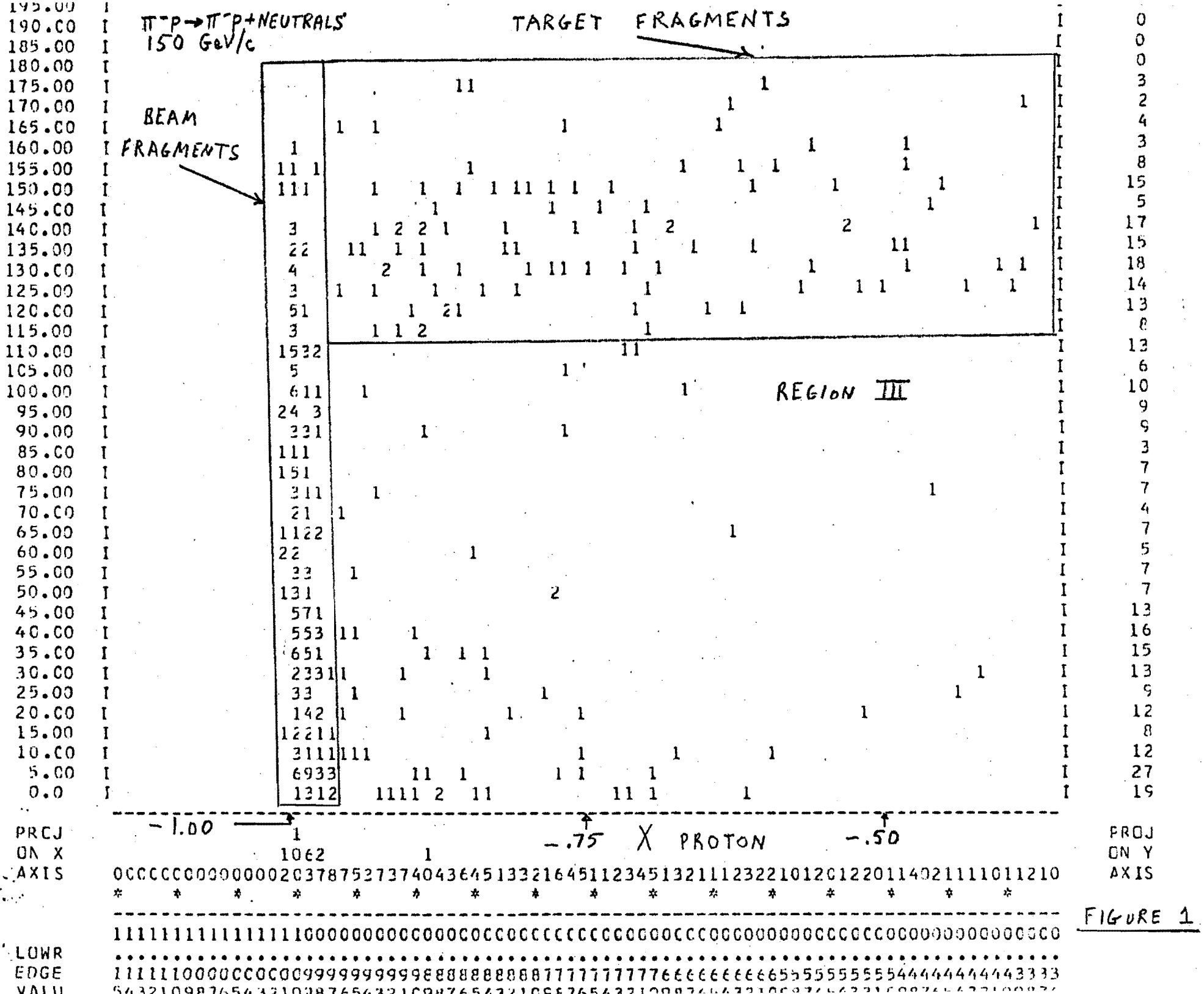
π⁻p→π⁻p+NEUTRALS
150 GeV/c
TARGET FRAGMENTS
BEAM FRAGMENTS
REGION III
X PROTON
-1.00
-.75
-.50
PROJ ON X AXIS
PROJ ON Y AXIS
LOWR EDGE VALU
P_LAB π⁻
-9-

FIGURE 1

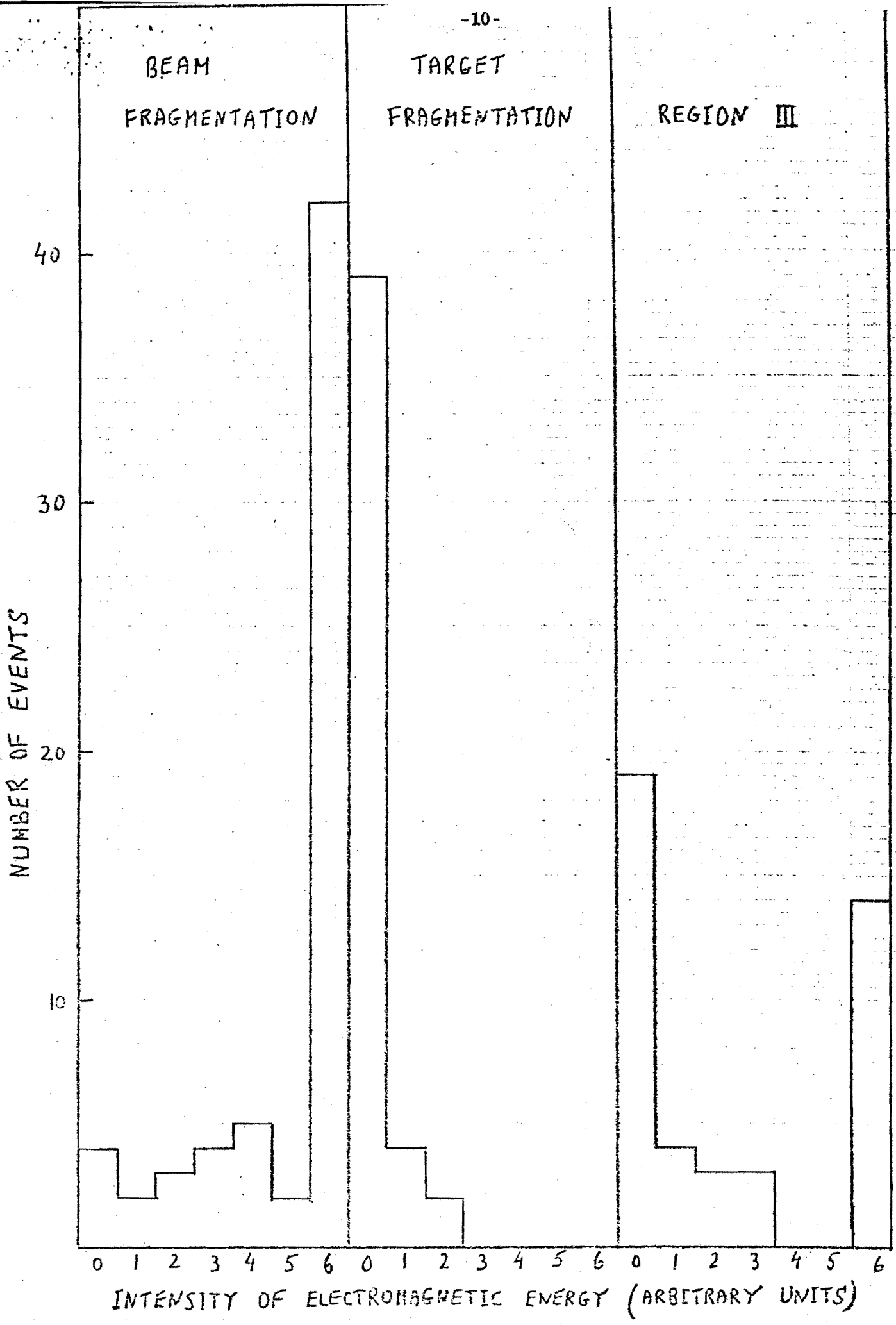
BEAM FRAGMENTATION
TARGET FRAGMENTATION
REGION III
NUMBER OF EVENTS
40
30
20
10
0 1 2 3 4 5 6 0 1 2 3 4 5 6 0 1 2 3 4 5 6
INTENSITY OF ELECTROMAGNETIC ENERGY (ARBITRARY UNITS)

FIGURE

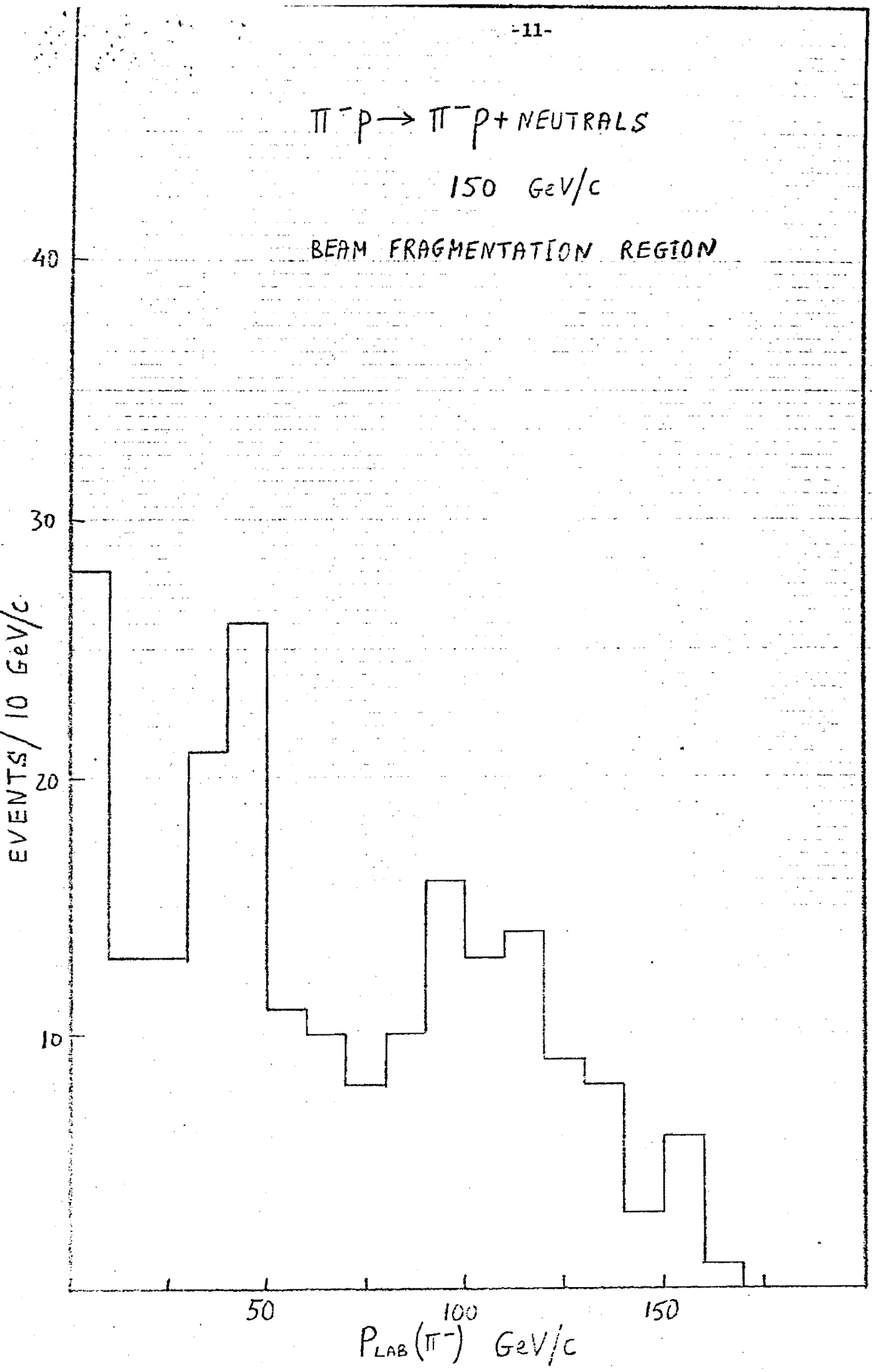
$\pi^- p \rightarrow \pi^- p$ + NEUTRALS
150 GeV/c
BEAM FRAGMENTATION REGION
40
30
20
10
EVENTS/10 GeV/c
50
100
150
$P_{LAB}(\pi^-)$ GeV/c

FIGURE 3

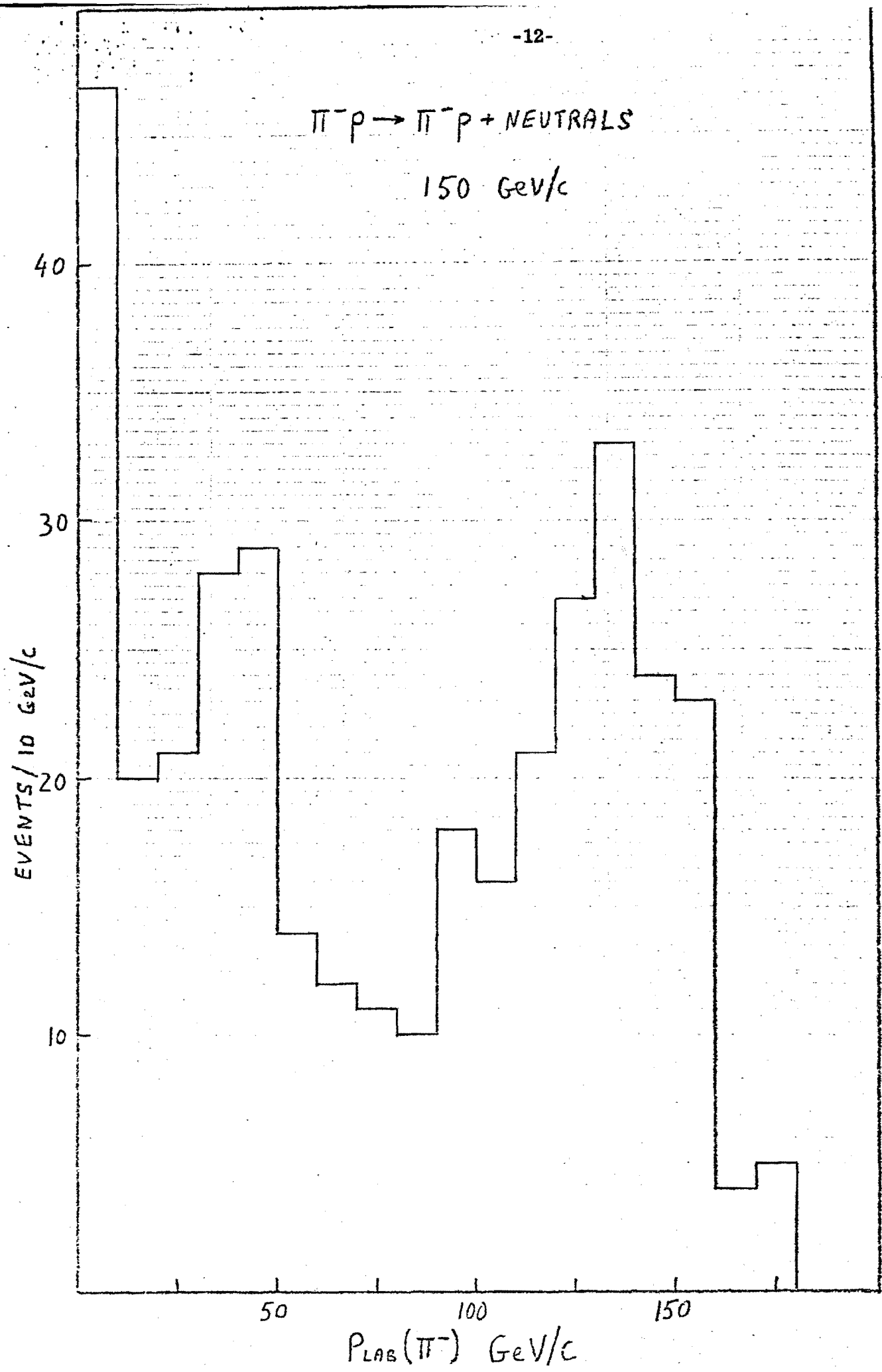
π⁻p → π⁻p + NEUTRALS
150 GeV/c
40
30
20
10
EVENTS/10 GeV/c
50
100
150
P_LAB(π⁻) GeV/c

FIGURE 4

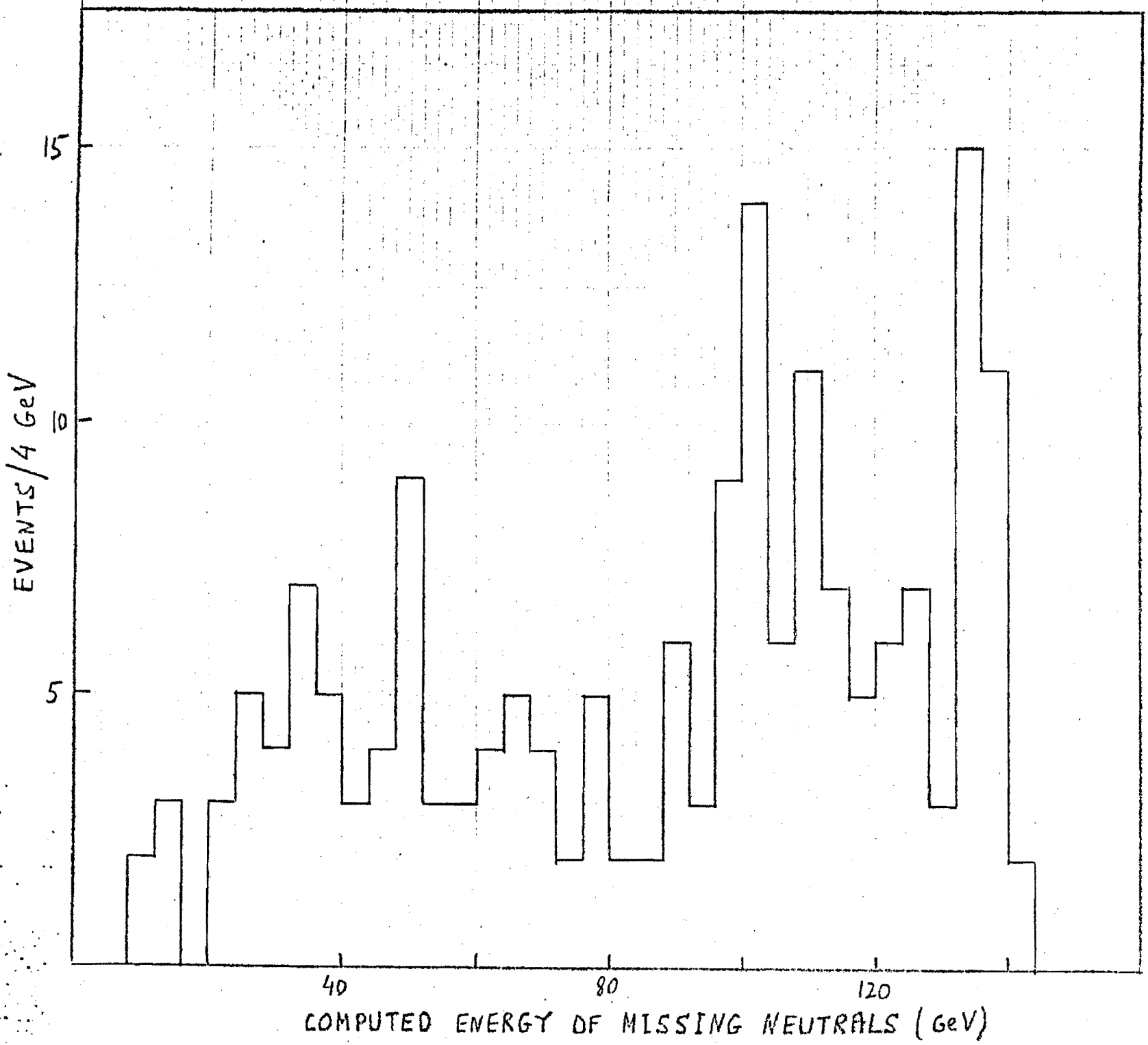
15
10
5
EVENTS/4 GeV
40
80
120
COMPUTED ENERGY OF MISSING NEUTRALS (GeV)

FIGURE 5

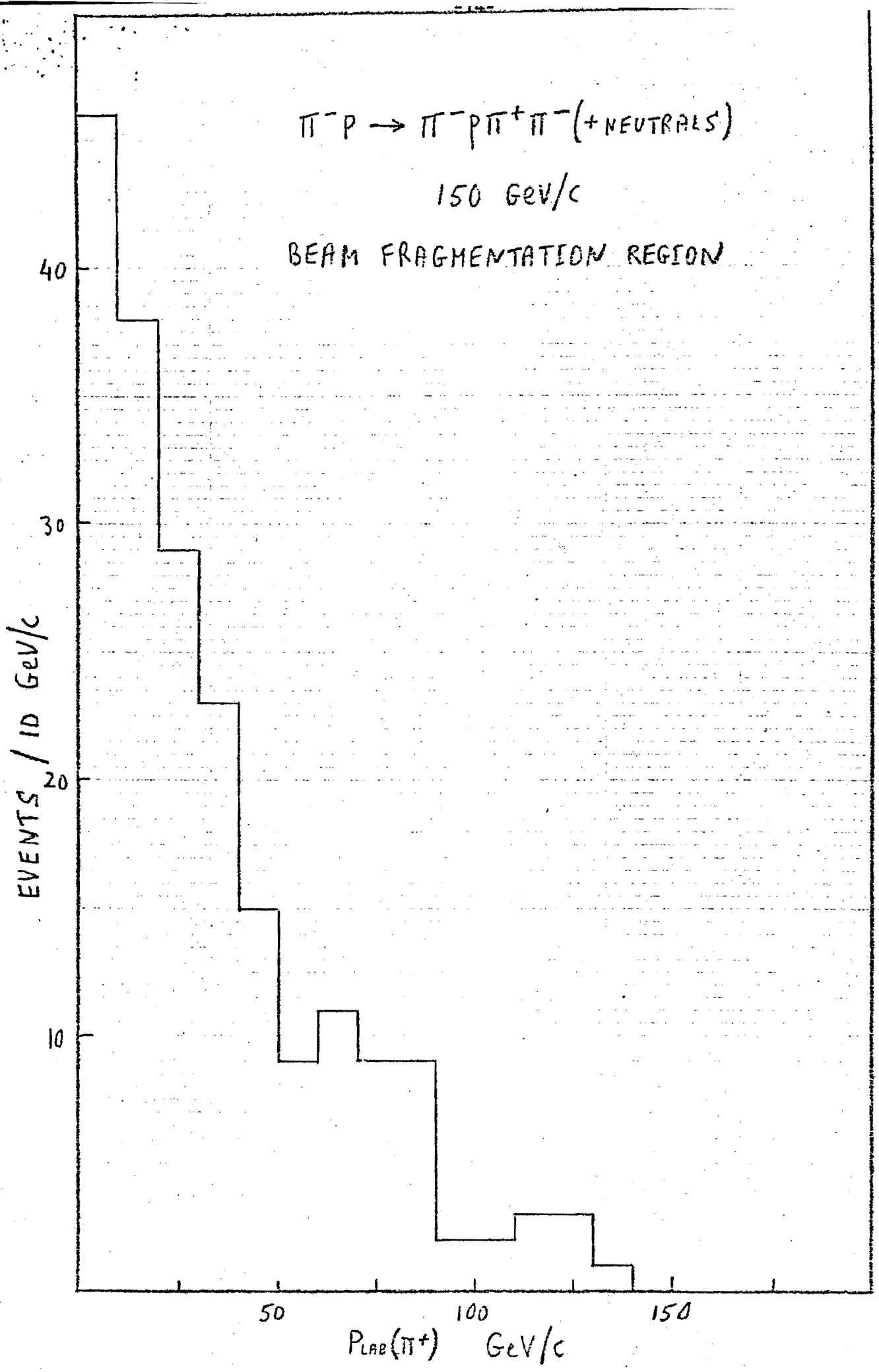
$\pi^- p \rightarrow \pi^- p \pi^+ \pi^-$ (+ NEUTRALS)
150 GeV/c
BEAM FRAGMENTATION REGION
EVENTS / 1D GeV/c
40
30
20
10
50
100
150
$P_{LAB}(\pi^+)$ GeV/c

FIGURE

Agreement

This is an Agreement between Fermi National Accelerator Laboratory and the experimenters of Proposal No. 299. This document contains an enumeration of the major items needed for the proper execution of Experiment No. 299 as expressed in the proposal for the experiment and subsequent correspondence. A one page summary describing the current research objectives of this experiment as expressed by the experimenters is given in Appendix I.

A. Personnel

1. The experimenters committed to this experiment are:

D.G. Fong, M. Heller, A. Janos, A.M. Shapiro, M. Widgoff, Brown University; J.W. Cooper, R. Plumer, R.D. Sard, A.E. Snyder, J. Tortora, University of Illinois; R.A. Burnstein, C. Fu, H.A. Rubin, Illinois Institute of Technology; E.D. Alyea, Indiana University; L. Bachman, C.-Y. Chien, P. Lucas, L. Madansky, A. Pevsner, R.A. Zdanis, Johns Hopkins University; J.E. Brau, J. Grunhaus, E.S. Hafen, R.I. Hulsizer, U. Karshon, V. Kistiakowsky, P.A. Miller, A. Napier, I.A. Pless, P.C. Trepagnier, J. Wolfson, R.K. Yamamoto, Massachusetts Institute of Technology; S. Centro, G. Ciapetti, M. De Giorgi, D. Pascoli, L. Ventura, D. Zanello, Padova/Rome; E.B. Brucker, P.F. Jacques, M.D. Jones, E.L. Koller, T.C. Ou, R.J. Plano, C. Sun, S. Taylor, T.L. Watts, Rutgers University/Stevens Institute/SUNY, Albany; J. Barwick, W. Bugg, H. Cohn, G. Condo, T. Handler, E. Hart, R.D. McCulloch, University of Tennessee/ Oak Ridge; D. Bogert, M. Johnson, H. Kraybill, D. Ljung, T. Ludlam, H. Taft, Yale University/Fermilab.

2. In addition, the university groups expect to involve three other physicists, six engineers, three draftsmen, and twelve technicians during various phases of the experiment. In addition, the universities will supply at least two full-time people stationed at Fermilab during the testing and installation period of the drift chambers and gamma ray detectors at Fermilab.

3. R.K. Yamamoto was chosen to be Project Manager to direct all aspects of the design, construction, installation, testing, and initial operation of the drift chamber and gamma ray detector.

4. The scientific spokesman for this Experiment is I.A. Pless.

5. The presently assigned Fermilab liaison physicist is L. Voyvodic

B. Equipment and Beam:

1. The instrumentation and experiment will be done using the N3 beam to the 30-inch hybrid bubble chamber facility located in the neutrino area.

2. The beam will be equipped with appropriate quadrupoles, bending magnets, collimators, and with additional instrumentation as described herein.

3. Fermilab will provide:

a. The secondary beam and beam enclosures ----

b. Instrumentation for tuning and controlling the beam, including Čerenkov counters (30.0K)

c. The 30-inch Fermilab bubble chamber with manpower for bubble chamber operation and beam line technicians. It is understood that the experimenters will assist in these efforts. ----

d.	The film and film processing will be provided by Fermilab. Test strip developing facilities will be available for use during the exposure.	
e.	Proportional wire planes with 2" radius active area	$(14.6K)
f.	Upstream system and interfaces	(23.3K)
g.	Cables, power supplies, etc.	(13.0K)
h.	Proportional wire planes with 6" radius active area for downstream system	(19.4K)
i.	Downstream systems and interfaces	(10.0K)
j.	Cables and power supplies for downstream system	(15.0K)
k.	Enclosure for detectors	(2.0K)
l.	Data tagging computer - existing PDP-11	(80.0K)
m.	The experimenters request the use of an existing computer in Lab A for debugging equipment. Cables and serial read-out equipment must be installed to Enclosure 114.	6.0K
n.	Space in bubble chamber high bay area for downstream detecting equipment	-
o.	Standard PREP electronics, CAMAC crate and modules (see Appendix II)	78.7K
	PREP equipment presently assigned to E154	(1.3K)
p.	Cables from bubble chamber high bay area to Laboratory A	(5.0K)
q.	Lead glass photo tubes - 48 pieces (existing)	(15.0K)
r.	Rigging	5.0K
s.	Fast turn around CDC 6600 time (50 hours)	-
	New Costs	$ 89.7K
	Existing Value	$(228.6K)
	Total	$ 318.3K

4. The University experimenters and Oak Ridge National Laboratory will provide:

a. Drift chamber with 1.2 meter diameter active area and read out system	40.0
b. Lead glass gamma ray detector with .75 meter x .75 meter active area and read out system	80.0
Total New Equipment	$120.

5. The Fermilab Physics Department will provide:

a. Computing time on IBM 370/195 (10 hours)	3.
b. Three (3) scanner/measurer-months on Film Analysis Facility with PDP-10. To be decided later.	--- ---
c. Funds towards item 4. above	5.0
Total Cost	8.5

C. Funding

1. Fermilab funds are available in FY 76 and FY77 for items in Category B3. The Fermilab Neutrino Department budget codes for this experiment are ENU (operating) and EAH (equipment).

2. The budget codes of the university experimenters at Fermilab are ___ (operating) and ___ (equipment). The budget codes for the Fermilab experimenters through the Physics Department are ___ (operating) and ___ (equipment).

3. Each university will approach its funding agency (ERDA, NSF) for an incremental increase of at least $10K. This will provide a base of $90K or greater to fund this experiment. R.K. Yamamoto was chosen to be the treasurer to monitor the university funds. (ORNL will provide $30K to augment the university funds which will be spent mainly on item B. 4a).

D. Special Considerations:

1. It is recognized that the physics under investigation in Experiment #299 has been expressed in two phases. It is understood that Phase II of this investigation is contingent on completion of Phase I and on the approval of a separate proposal by Fermilab.

   a. Phase I - 600 x 10^3 pictures: (approved)

      i. 500 x 10^3 pictures with a mixture of π^+ and p at 150 GeV/c (158 x 10^3 pictures already have been taken as of the signing of this document)

      ii. 100 x 10^3 pictures of π^- at 150 GeV/c

   b. Phase II - 600 x 10^3 pictures: (requiring a new proposal)

      1. 400 x 10^3 pictures with a mixture of π^+ and p at 150 GeV/c

      ii. 200 x 10^3 pictures of π^- at 150 GeV/c

2. As part of the ongoing program to improve the Fermilab 30-inch hybrid bubble chamber system, the experimenters will design, construct and bring into operation a large drift chamber and a gamma ray detector. These two devices will increase the acceptance of the hybrid system for charged particles and give information on the direction and energy of gamma rays. The experimenters will furnish the equipment described in the body of this document and when the devices are installed, documented and operational, they will be turned over to Fermilab to be operated as a part of the Fermilab bubble chamber spectrometer system.

3. Beam characteristics and bubble chamber operation.

   a. Beam will use the available filter to optimize the π^+/p ratio. This will nominally be 1/3 or greater.

   b. The nominal beam spill to the bubble chamber should be 100 microseconds or longer.

   c. The experimenters will be provided with 35 mm film. The bubble chamber will be operated in a multi-pulse mode during each accelerator cycle.

   d. The 30-inch magnet will be operated at approximately 25

   e. The film is the property of the Fermi National Accelerator Laboratory and is on loan to the experimenters for an eighteen (18) month period starting with the date of exposure. Following this period the film is to be returned to Fermilab for possible reassignment to other approved research groups unless an extension of the loan has been arranged.

   f. The picture count is to be determined by the frame counter. Reasonable care will be taken by the beam line technicians and bubble chamber crews to provide quality pictures.

4. Testing time

   a. Experimenters estimate that the installation of the gamma ray detector and drift chamber will take one month. On site testing of the system will require two months. A beam spill of 100 microseconds or longer is

required. Beam will be available on a parasitic basis only.

b. A short test run with 5,000 correlated bubble chamber pictures will be required to fully certify the installation.

5. The experimenters will provide all programs, magnetic tapes and consumable items for the on-line computer system.

6. Six (6) copies of all publications or preprints for work done at Fermilab will be sent by the Scientific Spokesman for this experiment to the Director of Fermilab.

E. Experimental Planning Milestones (tentative)

	Relative Time	Estimated Date
1. Construction of prototype lead glass hodoscope	t_o-10 mos.	1 Sept, 197
2. Beam testing of prototype lead glass system (requiring about 1 week of prime running in N3 hadron beam at 50 GeV)	t_o-9 mos.	1 Oct, 1975
3. Construction of prototype drift chamber	t_o-7 mos.	1 Dec, 1975
4. Test prototype drift chamber (requiring parasitic use of N3 hadron beam)	t_o-6 mos.	1 Jan, 1976
5. Construction of drift chambers	t_o-4 mos.	1 Mar, 1976
6. Construction of gamma ray detector	t_o-4 mos.	1 Mar, 1976
7. Installation of equipment	t_o-3 mos.	1 Apr, 1976

8.	Test of equipment	t_o-2 mos.	1 May, 19
9.	Data collection	t_o	1 July, 1
10.	Completion of experiment	t_o+6 mos.	1 Jan, 19

This Agreement is mutually acceptable to both the experimenters and Fermilab. Circumstances and needs will change as the experimental program develops. This Agreement will be amended when necessary.

James R. Sanford 9/29/75
James R. Sanford (Date)
Fermi National Accelerator Laboratory

Irwin A. Pless 10/10/75
I. A. Pless (Date)
Massachusetts Institute of Technology

Appendix I

Current One-Page Summary of Physics Objectives and Experimental Techniques for Experiment 299

Precision Study of High Energy Collisions Induced by Incident 150 GeV/c Pions and Protons

The experiment will be performed using the Fermilab Proportional Wire Hybrid 30" Bubble Chamber System. A total of 600,000 pictures will be taken of which 500,000 will be with π^+ and protons on hydrogen at 150 GeV/c, and 100,000 with π^- on hydrogen, also at 150 GeV/c.

The objective of the experiment is the study of the following topics:

1) Charged particle multiplicity moments
2) Production spectra for charged and neutral particles
3) Leading particle and diffraction phenomena
4) Correlating in momentum and rapidly among the produced particles
5) Factorization of production amplitudes with respect to the quantum numbers of the incident particle.

In addition, we expect to make a preliminary study of $K^{\pm}p$ and $\bar{p}p$ interactions.

Appendix II

New PREP Equipment for Experiment #299

PREP REQUEST FILE/ SORT BY AFFILIATION

AFFILIATION E299

TYPE CODE	QTY	MFGR	MODEL #	DESCRIPTION	UNIT COST	TOTAL COST
AA	2	ORTEC	401A	NIM BIN	182	364
AB	2	BL PACK	1011	NIM BIN PWR SUPPLY	362	724
AD	5	LECROY	621AL	QUAD DISCRIMINATOR	795	3975
AE	3	LECROY	364AL	4-FOLD LOGIC UNIT	675	2025
AF	2	LECROY	429	LOGIC FAN-IN/FANOUT	545	1090
CA	13	STD ENGR	KCS	CAMAC CRATE	695	9035
CB	13	STD ENGR	1410	CAMAC PWR SUPPLY	850	11050
CC	10	LECROY	2249	CAMAC ADC	2000	20000
CI	13	JORWAY	70A	CRATE CONTROLLER	855	11115
CI	3	GEC-ELL	CBF6501	CAMAC B-H EXTENDER	1000	3000
CJ	3	STD ENGR	MM816C	CAMAC MEMORY CORE	2795	8385
FB	5	POW DES	1570	H V POWER SUPPLY	595	2975
FD	5	FERMILAB	FS-7092	HV DISTRIBUTION BOX	1000	5000

TOTAL QUANTITY IS 79 ITEMS AT A TOTAL COST OF $ 78738

TOTALS:

ALL ITEMS	$ 78738	ALL DELIV ITEMS	$ 0
ALL 'A' ITEMS	$ 7975	ALL ORED ITEMS	$ 78738

Exploratory discussion for setting up a beam line test for the 299 lead glass hodoscope

The following is a suggested outline for determining the important energy and special characteristics of the lead glass hodoscope suggested for the 299 gamma ray detector. This outline is meant to be a reference point of discussion and not a firm commitment on any party.

1. Beam line - Fermilab

   a) Flux density of e^- up to 100 cts/mm^2 in a "few hours" at most.

   b) $\frac{\Delta p}{p} \sim 0.3\%$

   c) $25 < p < 200$ GeV/c

   d) PDP-11 computer plus scope

   e) NIM LOGIC - borrowed

   f) beam counters

2. Remote CAMAC System - Fermilab

   a) CAMAC CRATE

   b) serial crate controller system

   c) parallel to serial converter

   d) 12 channel A to D converter (borrowed or bought)

3. 5 element x, 5 element y 2 dimensional lead glass hodoscope - Fermilab

   a) glass and photo tubes

   b) box

   c) movable carriage

   d) calibration tubes and pulser

   e) cross slide

4. Calibration system and data - PHSC

   a) similar to that described in FGD and PHSC - Fermilab agreement

   b) provide phototube + source + neutral density filter and mount.

   c) use Fermilab neon tube and pulser

5. Binary glass system - Fermilab

   a) glass 12" x 12" by $\frac{1}{4}$", $\frac{1}{2}$", 1", 1"

   b) mount for above

6. Hole counter system - PHSC

   a) two counters

      i) 1" diameter
      ii) $1\frac{1}{2}$" diameter with 3.6 mm diameter hole in center

   b) photo tubes - 56 AVP

   c) bases - 5 nanosecond pulse

   d) two-dimensional cross slides with 4" travel

7. Software - PHSC

   a) data gathering

   b) histograms

8. Off-line computer time - Fermilab-PHSC

As noted above, the outline is not meant to be an agreement but rather the basis for discussion so that an agreement can be reached. The enclosed sketch is just a rough idea of how the test might go.

M. Johnson
I. A. Pless

11 February 1975

Outline for the Joint Construction between the European FGD Collaboration and the American PHSC-Fermilab of a Forward Gamma Detector

The following outline is the result of discussions between Gigi Ventura and Irwin Pless. These discussions followed presentations to the whole PHSC-Fermilab and a subgroup of the PHSC-Fermilab.

The purpose of this outline is to delineate construction ideas and preliminary responsibilities for accomplishing two objectives. The first objective is a preliminary study of the critical parameters of the system. This will involve a test period in the Fermilab beams with a prototype representing a minimal configuration. The second is the construction, installation, and operation of a full-size Forward Gamma Detector in the Fermilab 30" Hybrid Bubble Chamber System, to be used for physics experiments. It is anticipated that the equipment will remain at Fermilab through 1 January 1977.

I. Preliminary Test

A. Size:

1. Full-size along beam direction

2. One quarter area perpendicular to beam direction

B. Components:

1. 4 block 15 x 15 x 60 cm^3

a. Responsibility

i. FGD

2. 30 x 30 cm^2 two coordinate scintillation hodoscope

a. Responsibility

i. FGD

3. 31.5 x 31.5 cm^2 two coordinate lead glass hodoscope

a. Responsibility

i. PHSC-Fermilab

I. B. 4. 30 x 30 cm^2 three coordinate PWC hodoscope

a. Responsibility

i. PHSC-Fermilab

5. 64 Channel ADC - 10 bit

a. Responsibility

i. FDG - borrowed

ii. PHSC-Fermilab - borrowed

6. NIM Logic

a. Responsibility

i. PHSC-Fermilab

7. Calibration phototubes - 2 each

a. Responsibility

i. FGD

8. Movable Carriage

a. Responsibility

i. PHSC-Fermilab

II. Operational Hardware

A. Size:

1. 30 radiation lengths along beam direction

2. 60 x 60 cm^2 perpendicular to beam direction

B. Components

1. Lead glass counter

i. 16 blocks 15 x 15 x 60 cm^3

a. Responsibility

i. FGD

ii. PHSC-Fermilab

2̄. Calibration tube and two-dimensional remote control [1]

a. Responsibility

i. FGD

ii. PHSC-Fermilab

3̄. Nitrogen box

a. Responsibility

i. PHSC-Fermilab

2. Vertex hodoscope

1̄. 60 x 60 cm^2 three coordinate scintillation hodoscope

a. Responsibility

i. FGD

b. Calibration tube and remote control system [1]

a. Responsibility

i. FGD

2̄. Nitrogen box

a. Responsibility

i. FGD

3. Lead glass hodoscope

1̄. 62.5 x 62.5 cm^2 two coordinate lead glass hodoscope

a. Responsibility

i. PHSC-Fermilab

2̄. Calibration tube and one-dimensional remote control [4]

a. Responsibility

i. FGD

ii. PHSC-Fermilab

3̄. Nitrogen box

a. Responsibility

i. PHSC-Fermilab

4. Drift chamber

   I. 120 x 120 cm^2 drift chamber

      a. Responsibility

         i. PHSC-Fermilab

5. Mechanical mount

   I. Two-dimensional remote control mechanical mount for items 1, 2, 3, 4, and 5.

      a. Responsibility

         i. PHSC-Fermilab

6. Calibration device [6 each]

   I. Tubes - nuclear services - ADC - Self Trigger - LED

      a. Responsibility

         i. FGD

This document just records, as mentioned above, informal discussions between Drs. Ventura and Pless. This document is not meant to be a binding commitment but, rather, a basis for discussion before any final commitments are made. In particular, the attached rough sketch is only that; much effort must be expended before these crude ideas become a working scheme.

G. Ventura

I. Pless

30 January, 1975

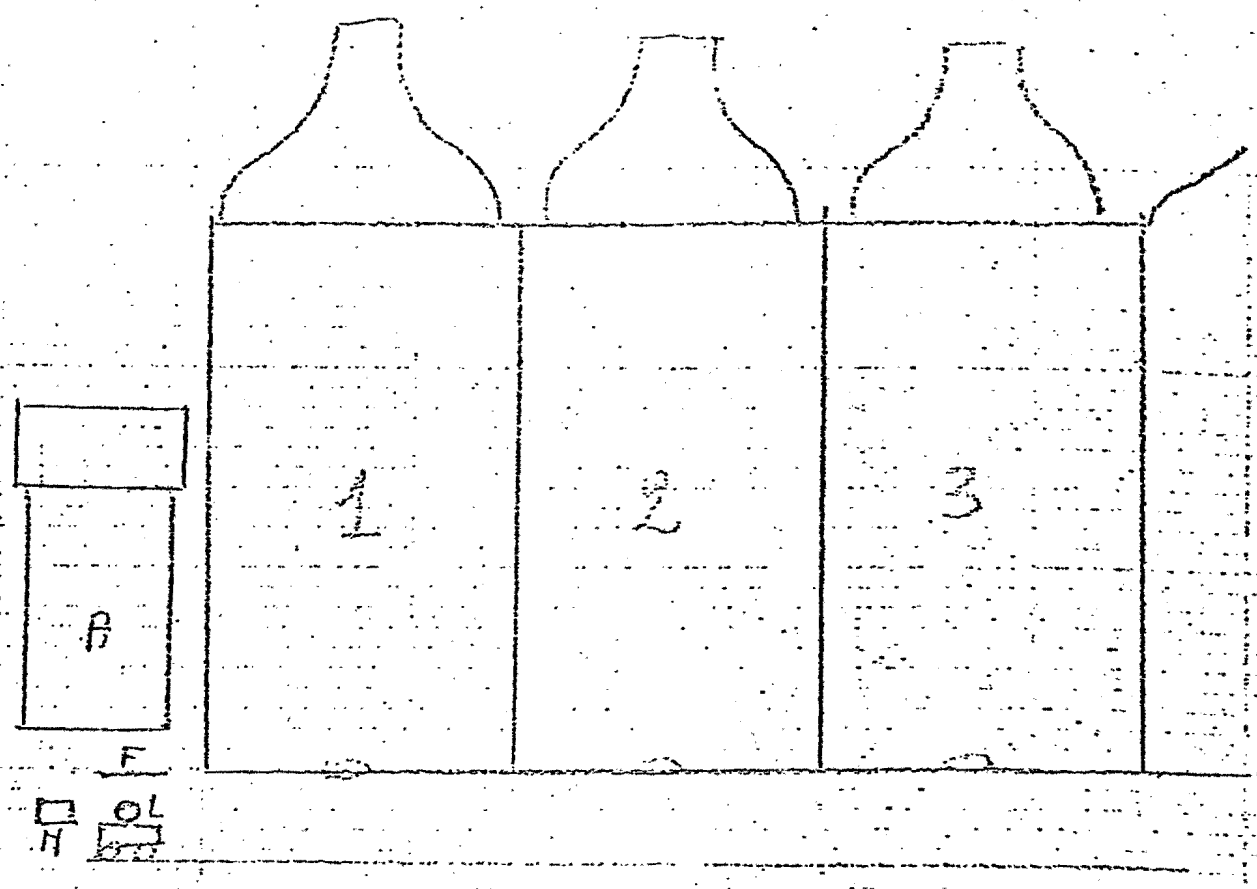

A is a reference PM, whose gain is kept constant by monitoring the light pulses from the NaI (Am 241 doped) source N. The LED L can be moved, by computer control, over the central region of the faces of lead glass blocks 1, 2, 3, etc. to control the stability of their gains, and over A to check for shifts in the light output of L itself. Since for the lead glass counters a pulse intensity is needed equivalent to the light from a shower of several tens GeV, while the pulses from N correspond to or ~ 1 GeV shower, an attenuating filter F is set between L and the photocathode of A, so as to roughly equalize its outputs for L and N.